The Thesis Committee for Emad Abbad Alabbad
Certifies that this is the approved version of the following thesis:

Experimental Investigation of Geomechanical Aspects of Hydraulic Fracturing Unconventional Formations

APPROVED BY
SUPERVISING COMMITTEE:

Supervisor:

Jon E. Olson

Mukul M. Sharma

Jon T. Holder

Experimental Investigation of Geomechanical Aspects of Hydraulic Fracturing Unconventional Formations

by

Emad Abbad Alabbad, B.S.Pet.E.

Thesis

Presented to the Faculty of the Graduate School of
The University of Texas at Austin
in Partial Fulfillment
of the Requirements
for the Degree of

Master of Science in Engineering

The University of Texas at Austin
August 2014

Acknowledgements

This research work and its author have received input, help, and encouragement from multiple individuals, groups, and organizations whose contributions must be acknowledged. Therefore, I would like firstly to give credits to a few individuals who had direct input to this work, secondly to acknowledge some groups and organizations for their essential and supplemental contributions to my graduate career, and thirdly to thank some people whose support and encouragement have been vital to my success in this endeavor.

Firstly, I would like to give credit to my thesis's supervising committee, a few fellow graduate researchers at the University of Texas at Austin's Petroleum and Geosystems Engineering Department (UT-Austin's PGE), and the research sponsors for their respective contributions to this research. The credit of this work is shared with my supervising professor Dr. Jon Olson for providing me with the opportunity to work on such a project and for the continuous guidance and valuable inputs offered throughout the various stages of the work. I am also thankful for his cheerful character and friendly manners during our interactions the past two years. I am happy to have had Jon as a mentor and have him now as a colleague in the discipline and a friend. Similarly, I would like to give credit to Dr. Mukul Sharma for his revision and inputs. The remarks he shared added more value to this work. Also, I would like to give credit to Dr. Jon Holder for his supervision and assistance in the laboratory and for his revisions and edits to the thesis write-up. I appreciate his experience, continuous support, and humble character inside and outside the laboratory. Moreover, some credits go to Kan Wu for her collaboration in performing numerical simulations to analyze some results and to the previous works of Benjamin Bahorich and Seyed Hosseini for setting up parts of the experimental work. This work, at-large, has been sponsored by UT-Austin's Fracture Research and Application Consortium (FRAC) and Saudi Aramco's Advanced Degree Program (ADP).

Secondly, I would like to express my appreciation to those who contributed to the success of my graduate studies and research. Many thanks go to the staff members of the PGE Department at UT-Austin Dori Coy for her secretarial assistance, Frankie Hart for her coordination and support in graduate affairs, Glen Baum for his support in obtaining porosity measurements, Gary Miscoe for his support in coring rock samples and obtaining permeability measurements, and Daryl Nygaard for his vital help and support in providing machine-shop services and operating the core saw machinery. Also, I would like to thank my office mates at CPE 3.142 and my fellow Saudi Aramco ADP scholars for the pleasant relationships we had on and off campus. Moreover, much appreciation goes to OPEC's Petroleum Studies Department in Vienna for their rewarding summer research fellowship, Saudi Aramco's Gas Production Engineering for the rich on-the-job experiences, and the University of Oklahoma for the fine undergraduate education, all of which have made my graduate studies and research more fruitful.

Thirdly, I must express my sincere appreciation to the individuals whose support and encouragement have been essential to the successes of my graduate career. I thank my friends Murtadha AlTammar and Abdulaziz Altubayyeb for their camaraderie during this endeavor and support inside and outside the classroom. Also, I thank my relatives and friends who have exchanged contacts or visits during my stay in Austin; the memories created are valued dearly. Moreover, my sincere appreciation goes to my family; I deeply thank my brothers Ahmed, Maitham, and Ali, sister Fedaa, sister in-law Maram, nephew Mustafa, niece Sarah, future wife Noor, grandmother Fatimah, and parents Najat and Abbad for their love, prayers, and encouragement. My family has been an irreplaceable source of motivation in all of my endeavors, for which I am immensely grateful. Finally, I thank god for the countless blessings he endowed me, the most recent of which is the successful completion of this thesis and the M.S.E. degree.

Abstract

Experimental Investigation of Geomechanical Aspects of Hydraulic Fracturing Unconventional Formations

Emad Abbad Alabbad, M.S.E.

The University of Texas at Austin, 2014

Supervisor: Jon E. Olson

Understanding the mechanisms that govern hydraulic fracturing applications in unconventional formations, such as gas-bearing shales, is of increasing interest to the petroleum upstream industry. Among such mechanisms, the geomechanical interactions between hydraulic fractures and pre-existing fractures on one hand, and simultaneous multiple hydraulic fractures on the other hand are seen of high importance. Although the petroleum engineering and related literature contains a number of studies that discusses such topics of hydraulic fracture interactions, there still remain some aspects that require answers, validations, or further supporting data. Particularly, experimental evidence is fairly scarce and keenly needed to solidify the understanding of such complex applications. In this work, the investigation methodology uses a series of hydraulic fracturing laboratory tests performed on synthetic rocks made of gypsum-based cements such as hydrostone and plaster in various experimental set ups. Those laboratory tests aim to closely investigate hydraulic fracture intersection with pre-existing fractures by assessing some factors that govern its outcomes. Specifically, the roles of the pre-existing fracture cementation, aperture, and relative height on the intersection mode are examined. The results show dominant effect of the cement-fill type relative to the host-rock matrix in determining whether hydraulic fracture crossing the pre-existing interface may occur. Similarly, hydraulic fracture height relative to the height of the pre-existing fracture may dictate the intersection results. However, the intersection mode seems to be insensitive of the pre-existing fracture aperture. Moreover, simultaneous multi-fracture propagation is examined and found to be impacted by the interference of the stresses induced from each fracturing source on neighboring fracturing sources. Such stress interference increases as the number of the propagating hydraulic fractures increase. While hydraulic fractures initiating from fracturing sources located in the middle of the fracturing stage seem to have inhibited propagation, outer hydraulic fractures may continue propagating with outward curvatures. Overall, the experimental results and analyses offer more insights for understanding hydraulic fracture complexity in unconventional formations.

Table of Contents

List of Tables

List of Figures

Chapter 1: Introduction

1.1 RESEARCH OBJECTIVES

This research addresses two main topics related to the geomechanical processes of hydraulic fracturing unconventional formations: Hydraulic fracture interactions with pre-existing fractures and the interactions between simultaneous multiple hydraulic fractures. By discussing both topics, the research aims to achieve the following goals:

- Provide sets of laboratory experimental data that can be used to test, calibrate, or further enhance the reliability of hydraulic fracturing numerical simulators.
- Identify fracturing pressure responses that may be indicative of unique fracture processes.
- Provide insights to understanding the factors affecting hydraulic fracture crossing of orthogonal pre-existing fractures including the roles of:
    - Pre-existing fracture's cementation.
    - Pre-existing fracture aperture.
    - Hydraulic fracture height bypass of pre-existing fractures.
- Provide insights to understanding the complex mechanisms that take place when a hydraulic fracture intersects pre-existing fractures including:
    - Mixed mode I and II fractures.
    - Mixed mode I and III fractures.
- Provide insights to understanding the factors affecting simultaneous multiple hydraulic fracture propagation.

1.2 RESEARCH MOTIVATIONS

The successful exploitation of unconventional formations such as shale and tight sand for energy production of natural gas, oil, or geothermal has been strongly tied to the increasing technological developments in hydraulic fracturing treatments. Hence, there is a continuous need to better understand the complex technical factors that govern such hydraulic fracturing applications in order to optimize fracturing treatments. The following list summarizes the main items that motivated this work:

- The poor (or partial) understanding of the mechanics that govern the outcome of hydraulic fracture intersections with pre-existing fractures, which are commonly present in unconventional formations.
- The influence of the interaction between simultaneous multiple hydraulic fractures (i.e. perf-and-plug hydraulic fracturing techniques) on the cost and productivity of multistage fracturing treatments that are commonly used in formations with very low permeability.
- The lack of proper understanding of the geometry and trajectory complex patterns of some hydraulic fracturing treatments, the indications of which have been recorded commonly when fracturing unconventional formations.

1.3 DEVELOPING UNCONVENTIONAL FORMATIONS OVERVIEW

In recent years, high successes have been achieved in North America in obtaining economical hydrocarbon recoveries from unconventional resources, particularly gas shale. Natural gas production reports from U.S. shale formations in Barnett, Haynesville, Woodford, among other basins show very successful results. These successes have motivated other countries to begin exploring and assessing their unconventional resources. For example, Saudi Arabia, Russia, China, and Argentina have begun evaluating their unconventional plays with varying predictions of production success (Holditch 2014). It has been evident that horizontal drilling and hydraulic fracturing technologies have been crucial in the development of such unconventional resources.

Overcoming the very-low-permeability nature of unconventional formations such as shale has been a key objective of utilizing such fracturing applications. An increasingly successful approach to tight formation development uses extended-reach horizontal laterals that are completed with multiple hydraulic-fracturing stages aimed to create multiple fractures, which provide conductive paths in tight reservoirs that permit the flow of hydrocarbons into the wellbore. Such multistage fracturing approach usually consists of multiple fracturing stages that span the pay zone, each stage of which is often designed with multiple perforation clusters. The injection of the hydraulic fracturing fluids is applied into each stage sequentially using some common well completion techniques such as “perf-and-plug” or sliding sleeve. While the hydraulic multistage fracturing treatment’s main objective is increasing the productivity of the well, it is always a key operational target to carry out the treatment with a reduced cost. Achieving such economic and operational goals necessitates optimizing the design of each hydraulic fracturing stage. Such stage design optimization requires proper understanding of the relevant geomechanical mechanisms that govern hydraulic fracture propagation. Since each stage often requires multiple perforation clusters, it is critical to understand the mechanisms controlling simultaneous multiple hydraulic fractures, which are likely to generate given the currently practiced fracturing stage designs. Such an understanding would help avoiding unproductive, or sometimes destructive, costly segments of the hydraulic fracturing treatment design. Moreover, given the common occurrence of natural fractures in unconventional formations, understanding the mechanisms and impacts of intersected natural fractures on hydraulic fracture propagation and geometry becomes highly important. Fracture diagnostics commonly show that such fracturing treatments often result in fracture networks, which remain a poorly understood topic. Therefore, current research works have found high interests in examining this topic, and its related subjects, in a variety of methods. This work addresses some aspects related to hydraulic fracture propagation in unconventional formations and provides experimentally-supported conclusions.

1.4 ROCK AND FRACTURE MECHANICS BACKGROUND

The Earth's underground rocks are always subjected to stresses, which are described by the ratios of the acting forces to the elementary surface areas (Valko and Economides 1995). The stress conditions underground are often reported by the values of the stresses applied in the three principal directions: One vertical and two horizontals that are perpendicular to each other. The vertical stress is mainly driven by the Earth's overburden while the horizontal stresses are often dictated by the Earth's tectonics. The Andersonian scheme classification of stress regimes explains the relative magnitudes of these stresses by describing three possible faulting regimes: Normal, strike-slip, or reverse (Zoback 2007). Most petroleum engineering applications, especially in deep reservoirs, commonly fall under normal-faulting-regime stress conditions, where the maximum principal stress acts vertically.

Like all underground rocks, the mechanical properties of the reservoir rocks characterize their strengths and stress-strain relationships. Fracturing is one form of brittle failure that can be induced by hydraulic means in order to enhance well productivity. Fracture orientation and trajectory are controlled by the principal stresses; opening-mode fractures' planes are oriented perpendicular to the minimum principal stress. For example, in a normal-faulting stress regime, a vertical fracture striking parallel to the direction of the maximum horizontal stress, $S_{h\ max}$, would be expected, which is the orientation perpendicular to the direction of the minimum horizontal stress, $S_{h\ min}$.

The rock's breakdown pressure is commonly used in reference to the pressure at which tensile failure, i.e. fracture, is initiated around the wellbore and is highly controlled by the rock's tensile strength and confining stresses. During fracturing injection, a fracture may grow in length, height, and width. Two classical 2-dimesional propagation models, which depict fracture geometry during propagation, were developed by Perkins and Kern (1961) and Nordgren (1972)—the PKN model—and Khristianovic and Zheltov (1955) and Geertsma and de Klerk (1969)—the KGD model. Both models have been standard references in the petroleum engineering literature.

1.5 THESIS DESCRIPTION

The next chapters of this thesis address in more details the two topics of interest: Hydraulic fracture interaction with pre-existing orthogonal fractures and the interaction between simultaneous multiple hydraulic fractures. Both topics are first reviewed based on some of the published work available in the petroleum engineering and related literature. A summary of the literature review is given in Chapter 2. Next, a full description of the experimental methodology used to investigate some of the key objectives is given in Chapter 3 along with laboratorial procedures, list of tests, measurements, and assumptions. After that, a summary of all the experimental data and results is outlined in Chapter 4. Finally, some data analyses and discussions of the results are offered in Chapter 5 followed by a summary of key conclusions in Chapter 6.

Chapter 2: Literature Review

Numerous works available in the petroleum engineering and related literature discuss the two main topics addressed in this thesis: Hydraulic fracture interaction with pre-existing natural fractures and the interaction between simultaneous multiple hydraulic fractures. The method of investigation found in the literature for each topic can be categorized into three areas: Field work, theoretical modeling, and laboratory experiment. This chapter reviews some of the most relevant works from each of the areas, overviews their approaches, and summarizes their major findings.

2.1 HYDRAULIC FRACTURE INTERACTION WITH PRE-EXISTING FRACTURES

The study of how hydraulic fractures geomechanically interact with pre-existing natural fractures requires an understanding of the interaction of hydraulic fractures with all forms of discontinuity such as lithologic boundaries, bedding planes, and other interfaces that may exist underground. Therefore, the scope of work discussed in the subsequent sections may include examining hydraulic fracture interaction with various interfaces and forms of discontinuity, which are useful analogues to the interaction with pre-existing natural fractures.

2.1.1 Field Work

2.1.1.1 Mineback Observations

Observations and measurements obtained from hydraulic-fracturing mineback projects provide a fundamental understanding of the interaction between hydraulic fractures and pre-existing natural fractures. Warpinski and Teufel (1987, 1991) studied the effects of geologic discontinuities such as joints, faults, and bedding planes on hydraulic fracture propagation during a mineback project at the Nevada Test Site. In their work, it was observed that when a hydraulic fracture crosses a joint, the hydraulic fracture propagation past the joint is often found at an offset distance to its original location and is sometimes divided into multiple strands of smaller hydraulic fractures (Warpinski and Teufel 1987). Similarly, hydraulic fractures may or may not cross other geologic interfaces such as faults or bedding planes based on the magnitudes of the interfacial friction and the stress contrast across the interface (Warpinski and Teufel 1987). When the friction on bedding planes is sufficient, hydraulic fractures may propagate across those planes without parting the planes (Warpinski and Teufel 1987). However, when the stress contrast across interfaces such as bedding planes or faults is significantly large, the propagation of hydraulic fractures tend to terminate at or within short distances from those interfaces (Warpinski and Teufel 1987). Further in-situ measurements suggest that stress changes within the stimulated region are common especially near geologic interfaces (Warpinski and Teufel 1991). Therefore, stress variability due to the presence of some geological features is an important factor in controlling the behaviors of hydraulic fractures when intersecting discontinuities. Warpinski and Teufel (1987) measured around 400 psi stress contrast across a fault shortly past which the propagation of a hydraulic fracture terminated. Stress orientation may also change across horizontal interfaces and was measured as high as 45º (Warpinski and Teufel 1991).

2.1.1.2 Data from Hydraulic Fracturing Treatments

Another source of field data comes from applications of hydraulic fracturing treatments in naturally-fractured formations. Kresse et al. (2013) examined the effects of the fracturing fluid viscosity and flow rate on hydraulic fractures interaction with natural fractures. In their study, Kresse et al. (2013) used the responses of microseismic events recorded during hydraulic fracturing treatments as an indicator of natural fracture activation. Two sets of microseismic data were recorded in the study: One set was recorded during the pumping of a hydraulic fracturing treatment using cross-linked gel at a rate of 70 bpm and another set was recorded during a refracturing treatment using slickwater at an average rate of 128 bpm on the same well in Barnett Shale (Kresse et al. 2013). It was concluded from the results that the more-viscous fracturing fluid achieved only moderate activation of natural fractures with a limited stimulated network, indicating limited penetration of the fracturing fluids into the natural fractures. On the other hand, the lower-viscosity fracturing fluid achieved a larger stimulated network indicating the penetration of fracturing fluids through a wider network of natural fractures (Kresse et al. 2013). Figure 2.1 shows the areal location of the microseismic events recorded on both treatments. Hence, Kresse et al. (2013) used these results to support their hypothesis, which was further analyzed experimentally and numerically, that higher values for flow rate and viscosity of the fracturing fluids increase the chances of hydraulic fractures crossing natural fractures due to increased pressurization rate. Conversely, lower treatment flow rate and fracturing fluid viscosity increase the chances of hydraulic fracturing fluids leaking into natural fractures in spite of fluid pressure (Kresse et al. 2013).

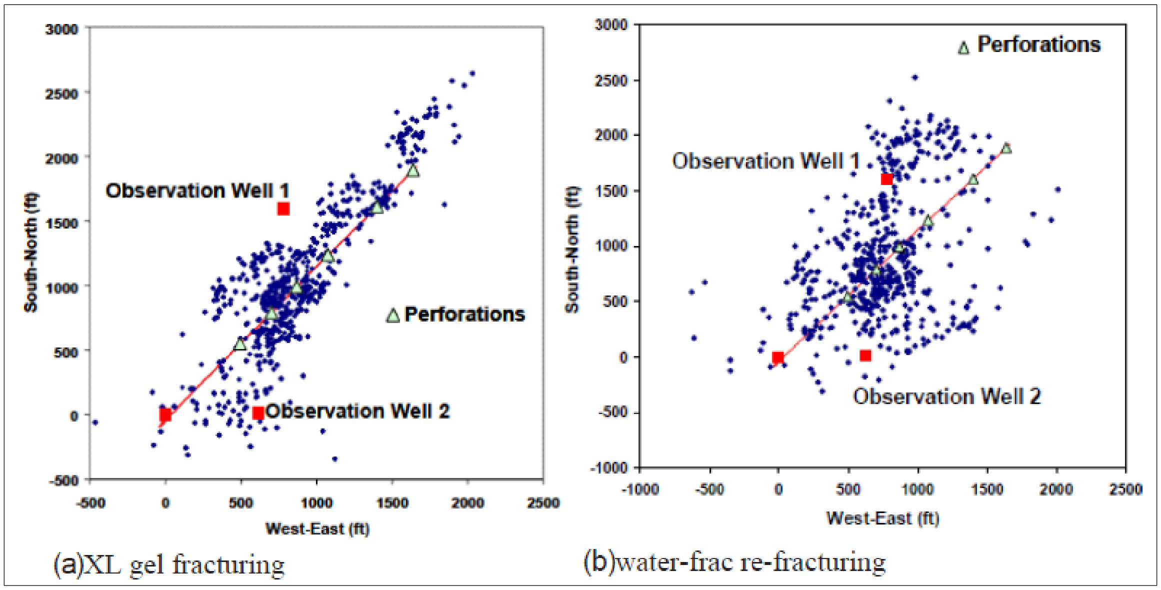

Figure 2.1: A plot of the locations of microseismic events recorded on a well during hydraulic fracturing treatment using cross-linked gel (on the left) is compared to another plot of microseismic events recorded on the same well during re-fracturing treatment using slickwater in Barnett Shale (from Kresse et al. 2013)

2.1.2 Theoretical Modeling

2.1.2.1 Analytical Approach

Renshaw and Pollard (1995) studied fluid-pressurized fractures crossing natural fractures at a right intersection angle using an analytical model. Based on their work, a mathematical criterion for compressional crossing of a fracture tip to orthogonal interfaces was developed. The derivation of this crossing criterion uses brittle, linear elastic materials as fracture propagation medium and unbounded, perpendicular frictional surfaces as interfaces. (Renshaw and Pollard 1995). The theory that explains the compressional crossing processes state that a fracture tip crosses a frictional interface when the compressive stresses acting perpendicularly on the interface are sufficient to prevent slip at the time the stresses ahead of the fracture tip are sufficient to initiate a fracture across the interface (Renshaw and Pollard 1995). In other words, the slip or opening of the interface reduces the stress concentration ahead of the fracture tip which may hinder or terminate fracture crossing of the interface. Thus, sufficient bonding or compressive stresses on the interface are required to inhibit its slip or opening and allow fracture propagation past the interface (Renshaw and Pollard 1995). In addition to slip inhibition, the stress singularity at the fracture tip is another factor which enables fracture propagation past interfaces. However, when a fracture contacts an interface, the stress singularity at the tip is often lost, which limits the fracture ability to reinitiate across the interface. Therefore, fracture reinitiation across an interface is more likely to happen when the stress singularity still exists prior to the fracture contacting the interface (Renshaw and Pollard 1995). Equation 2.1 and Figure 2.2 illustrate the mathematical and graphical expressions of the compressional crossing criterion (Renshaw and Pollard 1995).

$$\frac{-\sigma_{xx}^{r}}{T_o - \sigma_{yy}^{r}} = \frac{0.35 + \frac{0.35}{\mu}}{1.06} \tag{2.1}$$

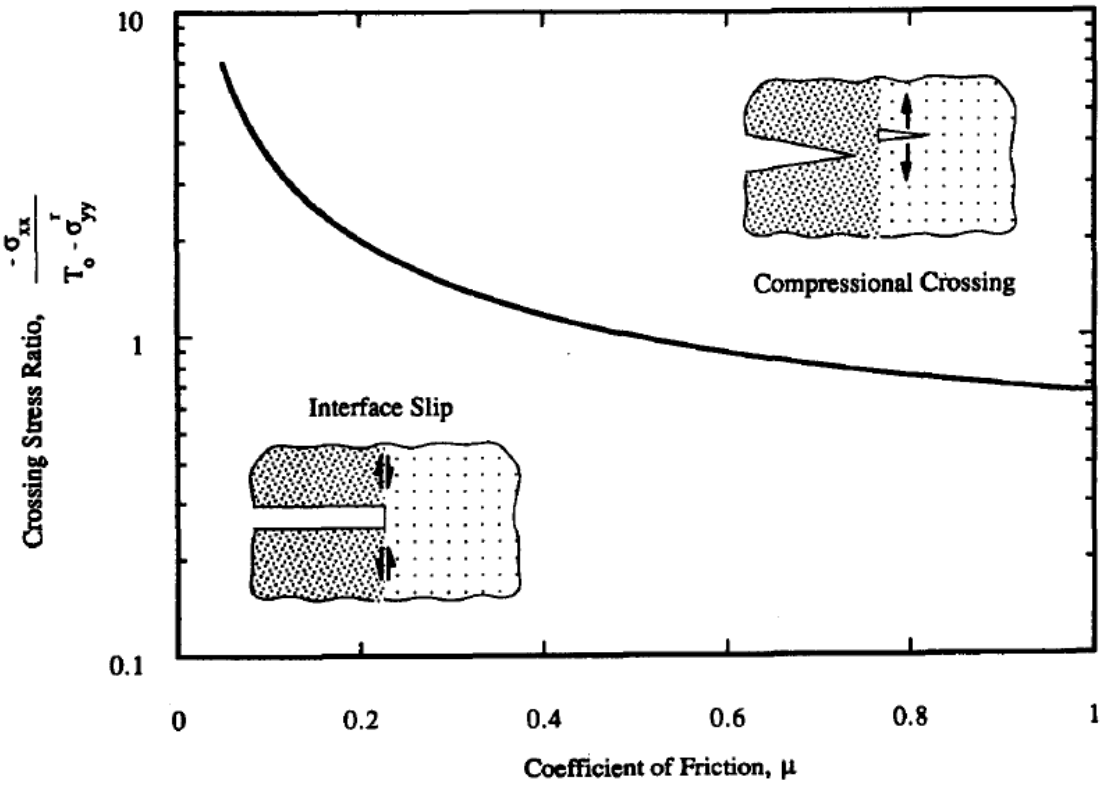

Figure 2.2: Compressional crossing threshold line defines two regions based on the value of the crossing stress ratio for a given interface friction coefficient: Above the line is a compressional crossing region where the fracture crosses the interface and below the line is an interface slip region where the fracture terminates at the slip of the interface (from Renshaw and Pollard 1995)

Gu and Weng (2010) and Gu et al. (2012) extended the fracture crossing criterion to non-orthogonal interfaces. Their work concluded that the more oblique the fracture-interface intersection angle is, the more difficult crossing becomes (Gu and Weng 2010, Gu et al. 2012). Hence, at very oblique intersection angles, fracture propagation often dilates along the interface (Gu and Weng 2010).

2.1.2.2 Numerical Approach

Numerous numerical modeling studies have been carried out to investigate the effect of natural fractures on hydraulic fractures. It was found that the presence of natural fractures clearly affects hydraulic fracture geometry and propagation patterns (Taleghani and Olson 2013). Taleghani (2009) and Taleghani and Olson (2013) used finite-element modeling to study some aspects of the hydraulic-fracture-natural-fracture interaction. Some of the outcomes of their work suggest that bigger horizontal stress difference results in magnified effects of natural fractures on vertical hydraulic fractures (Taleghani and Olson 2013). For example, natural fracture diversion of hydraulic fracture propagation becomes an arrest under larger stress differences (Taleghani and Olson 2013). Similarly, hydraulic fracture width reduction due to the interaction with natural fractures is amplified under greater differential stresses (Taleghani and Olson 2013). Furthermore, the conditions under which hydraulic fracture crossing may occur were examined and the results were highly sensitive to the orientation of natural fractures (Taleghani and Olson 2013). Crossing is more likely to occur when the natural fractures are oriented orthogonally to the propagation path of the hydraulic fracture (Taleghani and Olson 2013). Additionally, crossing is also sensitive to the contrast in fracture toughness between the host rock and the material composing the natural fracture (Taleghani and Olson 2013). Natural fractures composed of material whose fracture toughness is higher than a quarter of the toughness of the host rock are more favorable for crossing (Taleghani and Olson 2013).

Kresse et al. (2013) and Kresse and Weng (2013) also used finite-element modeling to study the effects of fracturing fluid properties and leakoff on the interaction between hydraulic and natural fractures. It was found that higher fracturing fluid viscosity and injection flow rate correspond to a higher propensity to crossing (Kresse et al. 2013). The increased viscosity reduces the size of shear failure while the increased injection flow rate increases the amount of tensile failure, which altogether makes the hydraulic fracture more likely to cross and the natural fracture less likely to slip (Kresse et al. 2013, Gil et al. 2011, Nagel 2011). Furthermore, permeable natural fractures add more complexity to the fracturing problem due to their added leakoff component. Although this component is yet to be fully modeled, it is thought that it enhances fluid leakoff into the reservoir and is highly sensitive to natural fracture permeability, which is a function of normal stresses, shear stresses and pore pressure (Kresse and Weng 2013). Moreover, fracturing fluid pressure can be a critical factor shaping the interaction with natural fractures. The fracturing fluid of a hydraulic fracture can open and invade the natural fracture when the fracturing fluid pressure at the intersection point exceeds the compressive stresses acting on the natural fracture (Kresse and Weng 2013). However, the fracturing fluid may only penetrate the natural fracture without opening when its pressure at the intersection point is higher than the pore pressure in the natural fracture but lower than the fracture closure stress (Kresse and Weng 2013).

2.1.3 Laboratory Experiment

2.1.3.1 Fluid-Driven Cracks

Among others, Blanton (1982), Warpinski and Teufel (1987), and Bahorich (2012) have experimentally examined hydraulic fracturing interaction with pre-existing fractures in real and synthetic rocks. Blanton (1982) used shale and hydrostone samples while Warpinski and Teufel (1987) used sandstone samples to investigate the effects of differential stress magnitudes and pre-existing fracture orientations on the interaction between hydraulic fractures and permeable natural fractures. The experimental results illustrated in Figure 2.3 showed that higher differential stresses and more orthogonal angles are likely to yield hydraulic fracture crossing especially when its pressure is insufficient to open the pre-existing fracture (Blanton 1982, Warpinski and Teufel 1987). On the other hand, low differential stresses and more oblique angles are likely to cause the hydraulic fracture to dilate into the pre-existing fracture with fracturing fluid flowing along it (Blanton 1982, Warpinski and Teufel 1987). The chances for hydraulic fracture arrest increases at oblique angles and with increasing differential stress magnitudes (Blanton 1982, Warpinski and Teufel 1987). Hanson et al. (1981) explained hydraulic fracture arrest at the opening of an unbounded interface by closely examining the stress state at the intersection region (Blanton 1982). It was found that for an opening-mode hydraulic fracture, as the fracture approaches the interface, the stress intensity factor at the tip normalized about the stress intensity factor in absence of the interface tends to infinity (Hanson et al. 1981, Blanton 1982). Therefore, the material ahead of the fracture tip will be drawn towards the tip under tension, which reduces the normal stresses acting on the interface as the fracture propagates closer to it (Hanson et al. 1981, Blanton 1982). Hence, the reduction of the normal stresses on the interface at some point would allow the interface to open and consequently cause the fracture to arrest when intersecting the open interface (Hanson et al. 1981, Blanton 1982).

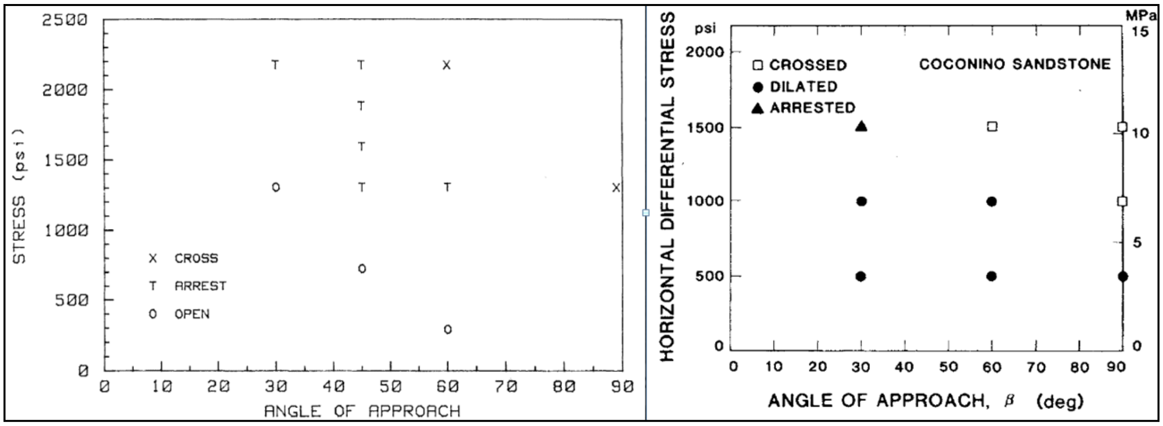

Figure 2.3: Experimental results obtained by Blanton (on the left) and Warpinski and Teufel (on the right) for hydraulic fracture behaviors when intersecting pre-existing fractures at different orientations and differential stresses (from Blanton 1987 and Warpinski and Teufel 1987)

Similarly, Bahorich (2012) and Olson et al. (2012) studied hydraulic fracture interaction with impermeable, strong natural fractures experimentally using hydrostone and plaster specimens with embedded glass interfaces as cemented pre-existing fractures. It was observed that the hydraulic fracture is likely to divert into the direction of the pre-existing fracture especially at non-orthogonal intersection angles (Bahorich 2012, Olson et al. 2012). As the intersection angle is more orthogonal, the hydraulic fracture propagation pattern is found either one or a combination of three scenarios: Arrest, branch out, or height bypass (Bahorich 2012, Olson et al. 2012). Hydraulic fracture arrest possibility increases as the intersection angle tends towards perpendicularity. However, weak bonds between the pre-existing cemented fractures and the host rock may lead the hydraulic fracture to divert along the pre-existing fracture and branch out at the end points by kicking off (Bahorich 2012, Olson et al. 2012). Similarly, hydraulic-fracture-to-pre-existing-fracture height ratio may lead the hydraulic fracture to bypass the pre-existing fracture via height growth (Bahorich 2012, Olson et al. 2012).

2.1.3.2 Mechanical-Driven Cracks

Renshaw and Pollard (1995) conducted several experimental tests to verify the compressional crossing criterion. They used multiple brittle layers and mechanically-induced cracks to test for compressional crossing at various conditions of compressive stress acting on the interface and friction coefficient of the interface surface (Renshaw and Pollard 1995). The results obtained from the experiments were in agreement with the analytical criterion discussed previously. Similarly, Wang et al. (2013) performed a series of semi-circular bending tests to examine the interaction between mechanically-induced fractures with pre-existing interfaces. The tests used multiple sets of interfaces with various orientations, compositions, and thicknesses (Wang et al. 2013). It was found that crossing is highly influenced by the intersection angle with a crossing percentage as low as 0% at 30-degree angles and as high as 90-100% at 90-degree angles (Wang et al. 2013). Moreover, the interface composition is another factor which may affect crossing. The properties of the material that compose the interface control the degree of sufficiency of the frictional resistance or cohesion available to prevent slip and allow crossing (Wang et al. 2013). Nevertheless, the thickness of the interface showed only a minor effect on fracture crossing. Fracture crossing of thicker orthogonal interfaces exhibited a jog distance along the interface (Wang et al. 2013).

2.2 THE INTERACTION BETWEEN SIMULTANEOUS MULTIPLE HYDRAULIC FRACTURES

Many references available in the petroleum engineering and related literature report studies of the geomechanical interaction between simultaneous multiple hydraulic fractures using different methodologies. The subsequent sections review some of the published works that addressed this topic using field, theoretical, or experimental approaches.

2.2.1 Field Work

Various observations and data obtained from oil and gas field applications have been valuable in investigating the interaction between simultaneous multiple hydraulic fractures. Fisher et al. (2004) and Ketter et al. (2006) used data from Barnett Shale to analyze the effects of the perforation design and the induced stresses on the propagation of simultaneous multiple hydraulic fractures. Results from microseismic fracture mapping showed that as the number of perforation clusters in a fracturing stage increases, the induced stresses increase as well (Fisher et al. 2004). As a consequence, fewer than three perforation clusters per stage are preferable in order to avoid excessive induced stresses (Fisher et al. 2004). In addition to the number of perforation clusters, the spacing between the clusters is another factor that also has an effect on the amount of induced stresses. It was found that a perforation-cluster spacing that is 50% larger than the height of the propagating hydraulic fractures reduces the amount of the induced stress interference between the fractures (Ketter et al. 2006). As hydraulic fractures propagate, the opening of each fracture causes the compressive stresses acting perpendicularly on the faces of neighboring fractures to increase (Fisher et al. 2004). Thus, this induced increase in stresses leads to stress interference between simultaneous hydraulic fractures, which is commonly referred to as stress shadow.

Miller et al. (2011) diagnosed the effectiveness of multistage hydraulic fracturing treatments by examining production-log data collected from 100 horizontal wells located in six shale basins in the United States. A major finding drawn from this study was that a significant number of perforation clusters did not sufficiently contribute to gas production. In all six basins, one third of the logged perforation clusters were not producing. Figure 2.4 summarizes the fracturing stage production rate in the logged wells as expressed in terms of a percentage of a theoretical value obtained by dividing the well’s total production rate by the number of the fracturing stages per well. The majority of the fracturing stages are underperforming due to limited production from the stages’ perforation clusters. Furthermore, in some basins, two thirds of the gas production came from only one third of the perforation clusters (Miller et al. 2011). Nevertheless, it was found that only one out of every five wells had all perforation clusters producing. In other words, the observed trend showed that as the number of perforation clusters per fracturing stage increases, the number of non-producing clusters increases. Thus, fracturing stages with more than six perforation clusters had almost half of the clusters not producing. This clear lack of productivity found in some perforation clusters is most probably attributed to the absence or ineffectiveness of the designed hydraulic fractures along those clusters mainly due to stress shadow effects. Hence, stress shadow increases the local minimum principal stress and often restricts or inhibits the growth of middle hydraulic fractures (Fisher et al. 2004). This analysis explains why as the number of perforation clusters in a stage increases, more clusters are likely to be underperforming due to decreased spacing between the clusters decreases which leads to excessive induced stresses. Miller et al. (2004) concluded that an optimum spacing between perforation clusters in a hydraulic fracturing stage ranges from 75 to 175 ft.

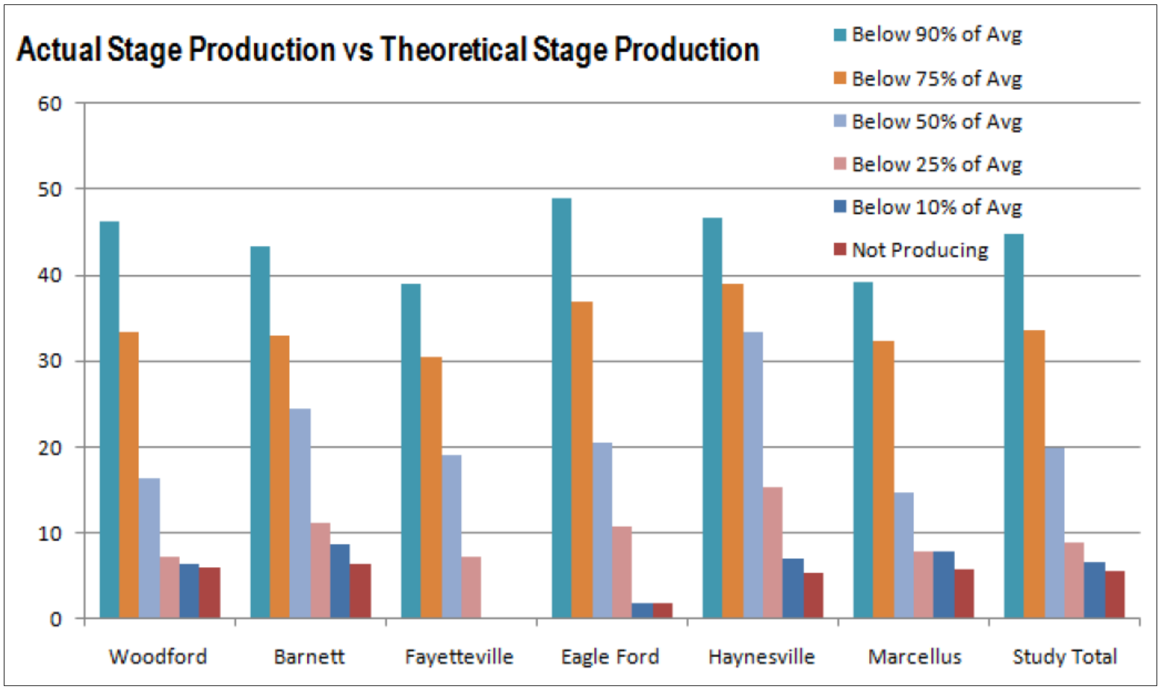

Figure 2.4: A fracturing stage production-rate summary of wells in six US shale basins compares actual production rates and theoretical rates obtained by dividing each well's total production rate by the number of fracturing stages per well (from Miller et al. 2011)

Holley et al. (2010), Molenaar et al. (2012), and Koskella et al. (2014) used data from real-time downhole monitoring devices to investigate hydraulic fractures in multistage fracturing applications. Among others, fiberoptic data such as distributed temperature sensing (DTS) and distributed acoustic sensing (DAS) were used to profile the distribution of fracturing fluids through cooling-warming sequence and assess injection rates and volumes (Molenaar et al. 2012). Preliminary analyses of these data clearly showed some restrictions in hydraulic fracture growth along the middle perforation clusters (Molenaar et al. 2012, Koskella et al. 2014). One of the mechanisms responsible for such fracture behaviors was explained by the uneven distribution of the fracturing fluids in a fracturing stage with multiple perforation clusters (Holley et al. 2010, Molenaar et al. 2012). Data from distributed sensing devices during fracturing treatments showed that outer hydraulic fractures often dominate while inner hydraulic fractures screenout (Holley et al. 2010, Molenaar et al. 2012).

2.2.2 Theoretical Modeling

Soliman et al. (2004) studied multiple hydraulic fractures analytically and examined several geomechanical aspects including fracture reorientation, non-planar fracture geometry, stress interference, and the effects of the perforation interval length. Their results highlighted multiple findings one of which is the reduction in hydraulic fractures widths due to reorientation, which is directly proportional to the wellbore diameter, inversely proportional to the length of the perforated interval, and highly controlled by the wellbore trajectory with respect to the direction of the second principal stress (Soliman et al. 2004). The radius of reorientation was found to increase with larger pumping rates and decrease with higher differential in-situ stresses (Veeken 1989, Soliman et al. 2004). Another finding was the role of the length of perforation intervals or clusters in inducing multiple hydraulic fractures. Perforation clusters with an interval longer than four times the size of the wellbore diameter are likely to yield multiple hydraulic fractures which often lead to an increased fracturing treatment pressure and reduced treatment rate per fracture (Soliman et al. 2004, Ketter et al. 2006).

Bunger et al. (2012) and Lolon et al. (2009) investigated multiple hydraulic fracturing using numerical simulations. Fracture geometry of closely-spaced hydraulic fractures was found highly dependent on the treatment injection rate, fracturing fluid viscosity, frictional properties of proppants, and the spacing between the fractures (Bunger et al. 2012). Moreover, the relationship between the number of fracturing stages and productivity increases was assessed using parametric reservoir simulation of the Bakken formations (Lolon et al. 2009). Although it is generally expected that more fracturing stages per well increases well productivity, a threshold exists for the number of fracturing stages above which productivity increase diminishes and was found highly sensitive to reservoir permeability and lateral length (Lolon et al. 2009). For example, for higher-permeability formations with a horizontal permeability around 0.04 mD, the optimum number of fracturing stages was identified between 10 and 12 stages (Lolon et al. 2009).

Olson (2008), Olson and Wu (2012), Shin and Sharma (2014) and Nagel et al. (2014) investigated the interaction between simultaneous multiple hydraulic fractures using numerical modeling. Stress shadow effects on the in-situ stress state and their interference on hydraulic fracture propagation were closely examined. Analyses of a propagating hydraulic fracture tip showed that stress shadow increases the local principal stresses everywhere around the hydraulic fracture except at the tip (Nagel et al. 2014). In particular, maximum increase in principal stresses was found across the hydraulic fracture face in the direction of the minimum principal stress (Nagel et al. 2014). Figure 2.5 illustrates the induced in-situ stress changes in a vertical hydraulic fracture. Additionally, the stress shadow also decreases the shear stress behind the tip (Nagel et al.

2014). Altogether, those stress changes are induced due to some physical processes including fracturing fluid leakoff into the reservoir and mechanical opening of the hydraulic fracture (Shin and Sharma 2014). For example, fluid leakoff increases reservoir pore pressure which drives up the stresses in vicinity of the hydraulic fracture (Shin and Sharma 2014). Similarly, the opening of a hydraulic fracture increases the closure pressure on neighboring fractures (Shin and Sharma 2014). As a result of such stress changes, simultaneously propagating hydraulic fractures may have limited fracture growth and altered geometry (Shin and Sharma 2014, Olson and Wu 2012). Outer hydraulic fractures, located closer to the toe or the heel of the horizontal lateral, were found to curve away from the wellbore. On the other hand, inner hydraulic fractures, located in the middle of the horizontal lateral, were found to have limited propagation and sometimes complex patterns due to turning directions as driven by the altered local stresses (Shin and Sharma 2014, Olson and Wu 2012, Olson 2008). In addition to the alteration in fracture propagation patterns and the reduction in fracture penetration, stress shadow was found to also cause the treatment net pressure to increase. Further analyses of stress shadow effects showed larger effects with shorter spacing between perforation clusters, larger number of perforation clusters per stage, higher fracturing fluid viscosity, higher hydraulic fracture height, and greater Young's modulus for the stimulated formation (Shin and Sharma 2014, Olson and Wu 2012). Inversely, stress shadow effects decrease with higher treatment injection rate (Shin and Sharma 2014, Olson and Wu 2012). Figure 2.6 illustrates the trend of stress shadow effects for simultaneous hydraulic fractures as the cluster spacing decreases using a numerical simulation.

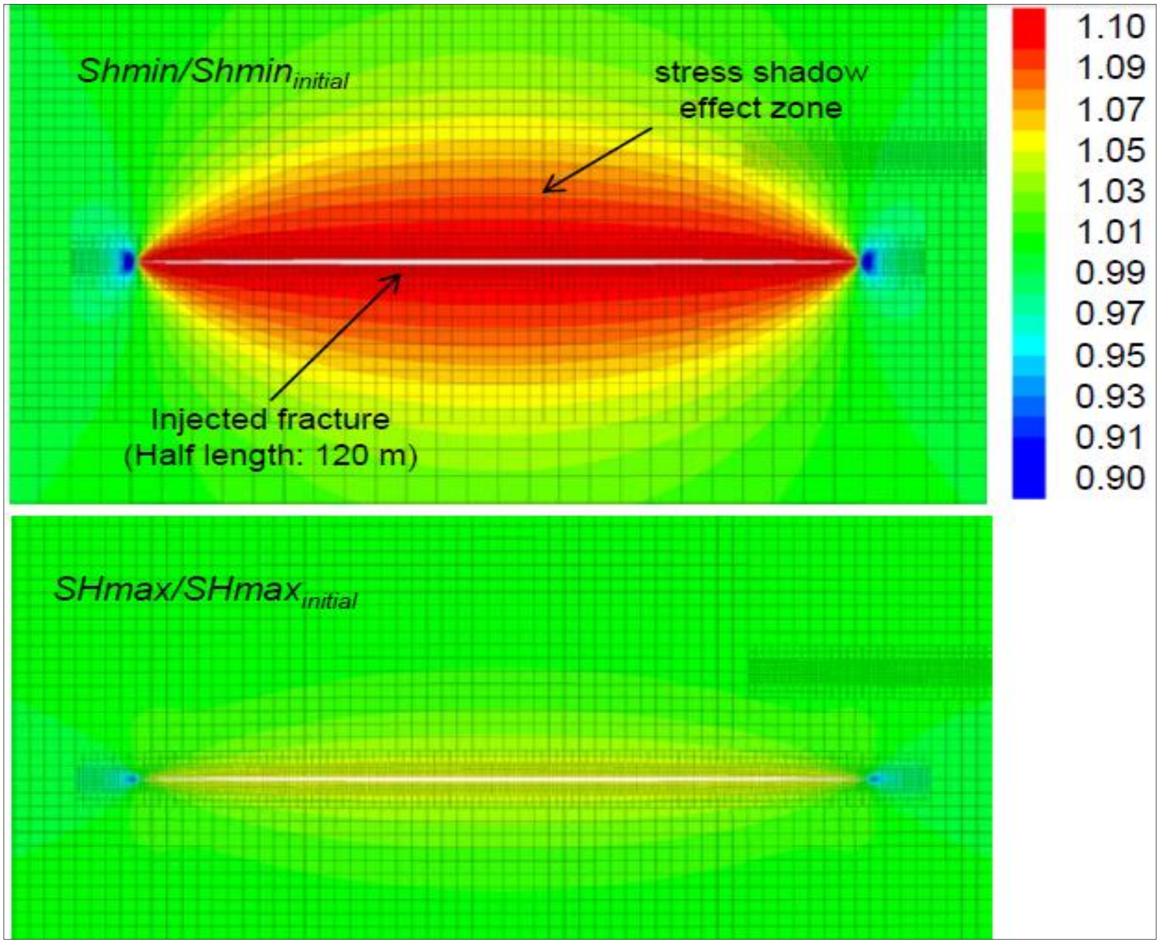

Figure 2.5: Numerical simulation of in-situ local stress for a vertical hydraulic fracture shows maximum stress increase in the direction of the remote minimum horizontal stress and moderate increase in the direction of the remote maximum horizontal stress (from Nagel et al. 2014)

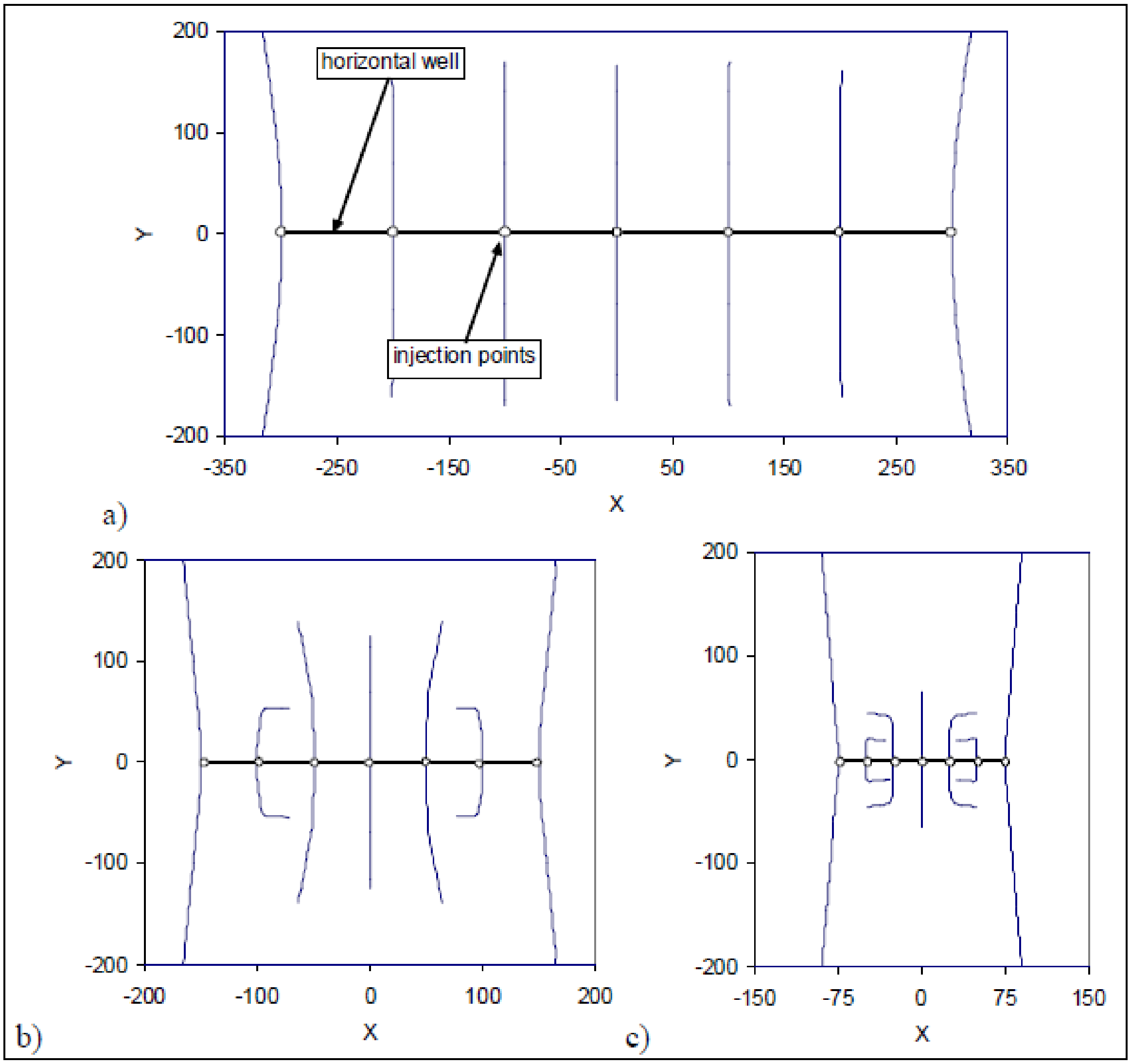

Figure 2.6: A top-view display of numerical simulations shows increasing stress shadow effects on simultaneous hydraulic fractures with decreasing fracture spacing from (a) to (b) in a horizontal lateral (from Olson 2008)

2.2.3 Laboratory Experiment

A limited amount of experimental work addresses the interaction between simultaneous multiple hydraulic fractures. El Rabaa (1989), Abass et al. (1996), and Brumley and Abass (1996) performed hydraulic fracturing tests using hydrostone blocks and provided useful insights to understand multiple hydraulic fractures. One of the findings was the importance of the role of perforation cluster design in controlling the number of hydraulic fractures developing from each cluster. Both the length of the perforation interval and the spacing between clusters were highlighted as important parameters in the perforation design. It was determined that a cluster with a perforation interval shorter than four times the wellbore diameter is likely to produce only one hydraulic fracture (El Rabaa 1989). However, longer perforation intervals are likely to have multiple hydraulic fractures propagating simultaneously (El Rabaa 1989). Similarly, the spacing between perforation clusters that is sufficient to ensure that the propagating hydraulic fractures may not connect was found longer than the fracture length (El Rabaa 1989). On the other hand, a distance between perforation intervals equal to the wellbore diameter was defined as the lower limit below which hydraulic fractures will connect regardless of wellbore trajectory with respect to in-situ stresses (El Rabaa 1989). Another finding highlighted by those experimental studies was related to non-planar propagation of hydraulic fractures. Wellbore orientation relative to the minimum principal stress was identified to have a main responsibility in causing non-planar behaviors in hydraulic fractures (Brumley and Abass 1996). For example, for vertical hydraulic fractures, based on the wellbore trajectory relative to the minimum horizontal stress, the fractures may reorient their paths as they propagate away from the wellbore. Consequently, fracture width reduction and treatment pressure increase were found to be common occurrences in non-planar hydraulic fractures (Brumley and Abass 1996). Explanations for those consequences of non-planar behaviors were also offered. One reason for width reduction in parallel reoriented fractures is that they share the same rock material (Abass et al. 1996). Since there is only limited rock material, fracture width becomes smaller as hydraulic fractures reorient and more fractures propagate in-parallel (Abass et al. 1996). As for the increase in treatment pressure, it was mostly attributed to the increased fluid leakoff and friction due to an increase in fracture wall waviness, which often occurs in non-planar hydraulic fractures. Nonetheless, non-planar propagation was highlighted as a mechanism for simultaneous hydraulic fractures to combine away from the wellbore (Brumley and Abass 1996).

2.3 CONCLUDING REMARKS

The petroleum engineering and related literature has discussed various aspects pertaining to hydraulic fracture interaction with pre-existing natural fractures and the interaction between simultaneous multiple hydraulic fractures. There have been multiple theories and findings that were derived from field observations, theoretical modeling, and laboratory work with varying degrees of validation. Most importantly to the objectives of this work, it has been widely accepted that for a hydraulic fracture intersecting a pre-existing fracture, a right intersection angle gives the highest tendency for hydraulic fracture crossing. Also, it has been clearly indicated that the presence of pre-existing forms of discontinuities such as natural fractures often yields complex hydraulic fracture propagation and geometry. However, there remain some uncertainties concerning the understanding of some mechanisms and factors related to hydraulic fracture crossing pre-existing fractures despite the numerous discussions offered in the literature. For example, the roles of the pre-existing fracture cementation, the pre-existing fracture aperture, and the hydraulic fracture height growth on the intersection mode require further investigation.

Similarly, for simultaneous multiple hydraulic fractures, it is strongly evident that the closer the fracturing sources to one another, the higher the interaction between the fractures is, namely higher geomechanical effect induced by the propagation of a hydraulic fracture on neighboring fractures. However, the type and the degree of the interaction have not yet been fully and quantifiably understood. Therefore, this work is motivated to address in the next chapters some aspects of such poorly understood topics in order to reduce relevant sources of uncertainties, increase the understanding of such complex topics, and offer validation to some existing findings.

Chapter 3: Methodology—Laboratory Testing

This research mainly uses an experimental approach to investigate the geomechanical topics at hand: The interaction between hydraulic fractures and orthogonal pre-existing discontinuities, designed to represent natural fractures, and the interaction between simultaneous multiple hydraulic fractures. A series of laboratory experiments and measurements were made en-route to achieving the research objectives. Therefore, this chapter details some important laboratorial and experimental components that were used in this work.

3.1 HYDRAULIC FRACTURING EXPERIMENTS

3.1.1 Experimental Approach

The laboratory experiments performed in this work were designed to simulate hydraulic fracturing treatments that are applied in oil and gas wells in the petroleum upstream sector. Mimicking such hydraulic fracturing field applications in the laboratory required simplifying and downsizing the geological system and the well completion and fracturing designs to manageable forms. Thus, synthetic rock materials such as hydrostone and plaster were used to create the geological system in the form of 1-foot cubic blocks. The block samples comprised of three horizontal layers overlaying one another; two boundary layers represented seal rocks and one middle layer represented the reservoir. Perforated aluminum pipes were molded in the synthetic blocks to act as cased wellbores. This cubic system was subjected to three principal stresses, one vertical and two horizontals, aimed to create a stress field similar to that induced by the Earth's overburden and tectonics at the reservoir level. Dyed gel-based fluids were used as the fracturing fluids in the hydraulic fracturing tests. During these tests, the fracturing fluids were injected down the pipes into the blocks using a syringe pump, which controlled injection rates. At the conclusion of every fracturing test, the block was saw-cut open in order to observe and record the test's outcomes. More detailed descriptions of the various parts of this overall approach are given in the next section.

3.1.2 Experimental Description

3.1.2.1 General Hydraulic-Fracturing Test Set-Up

The hydraulic fracturing tests can be divided into three parts: Block preparation, hydraulic-fracture testing, and block opening.

<u>First Part: Block Preparation</u>

The experimental procedures started by a series of steps aimed to produce the cubic block sample used for the fracturing test. These block-making steps included designing and placing the tubular pipe, i.e. the wellbore, and casting the synthetic-rock layers that composed the block sample, i.e. seal and reservoir layers. The following list describes in details the steps taken in this part of the experimental procedures:

1. 1-foot cubic Plexiglas box was used to cast the block sample (Figure 3.1).
2. The wellbore was designed using $3/8^{th}$ inch outer diameter, 0.035 inch thickness, aluminum tube. The wellbore was plugged from the bottom, drilled at the lower end to create perforation holes, configured, and placed in the casting box as displayed in Figure 3.2. Hence, most tests had two perforation holes with roughly 0.08-inch diameter, 180-degree phasing, and parallel-to-the-maximum-horizontal-stress orientations. Also, most tests used vertical wellbores placed at the center of the box but curved horizontally towards the upper portion of the box to allow the pipe to exit the box smoothly from an upper corner.
3. A nylon string was inserted into the wellbore pipe for every perforation hole to mold perforation penetrations. One end of each nylon string was left to stick out

the perforation hole inside the casting box for no more than two wellbore diameters in length. The other end of the nylon string came out of the pipe from the outside-the-box end to allow the string to be pulled out after the cement materials were cast in the box; removing the strings after the cement hardened left behind a penetration cavity, which acted as a perforation channel between the wellbore and the casted layer. Also, in order to avoid cement leaking into the wellbore through the perforation holes during casting the layers as well as allow for easy removal of the string after the cement is cast, the nylon strings were coated with silicon vacuum grease, which properly seals around the nylon strings at the perforation-hole end and reduces the strings' adherences to the cement (Figure 3.3).

4. After the wellbore was positioned in the casting box with the nylon strings inserted, three synthetic-rock layers were made by consecutively casting cementing materials in the box to form the block sample. Table 3.1 contains cement mixing and casting details used for each layer in a typical sample (Figure 3.4).
5. Once the block sample was fully cast in the Plexiglas box, it was left to harden for about 24 hours. Then, the box sides were removed to allow the sample to fully cure and dry out for no less than 7 days (Figure 3.5). A previous study has found that hydrostone and plaster cements require about 5-day curing time to obtain sufficient mechanical properties (Bahorich 2012).

Table 3.1: Preparation details of the cementing materials used in making the layers of a typical synthetic-rock sample that was used in the hydraulic fracturing tests in the laboratory

Step #	**Layer Type**	**Cementing Material**	**Cement-to-Water Mixing Ratio (lb)**	**Cement Curing Time Before Casting Next Layers (minutes)**
1	Bottom Seal	Hydrostone	35.0/11.4	7
2	Reservoir	Plaster	25.3/14.5	4
3	Upper Seal	Hydrostone	35.0/11.4	—

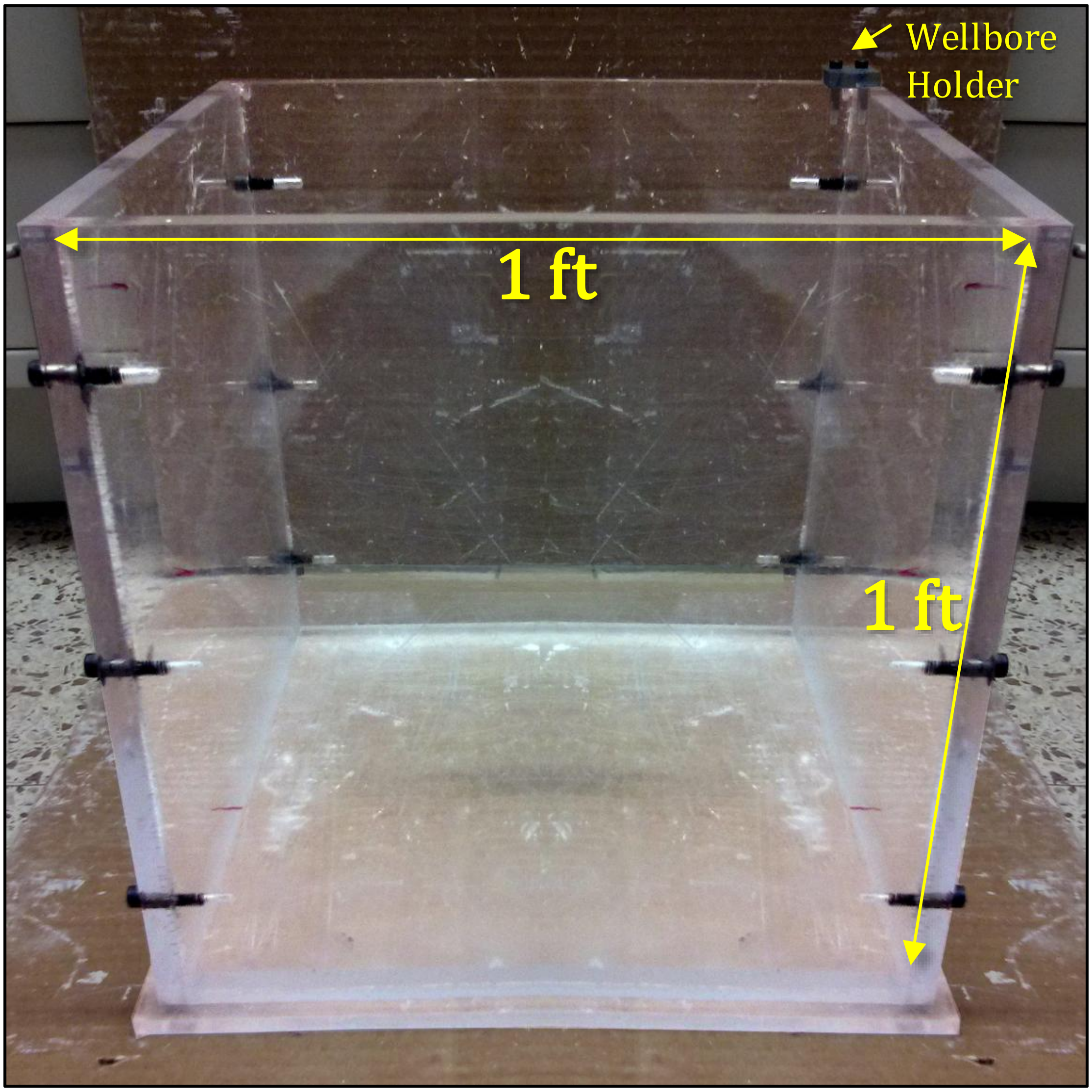

Figure 3.1: Plexiglas box used to cast the synthetic-rock block sample used in the hydraulic fracturing laboratory tests

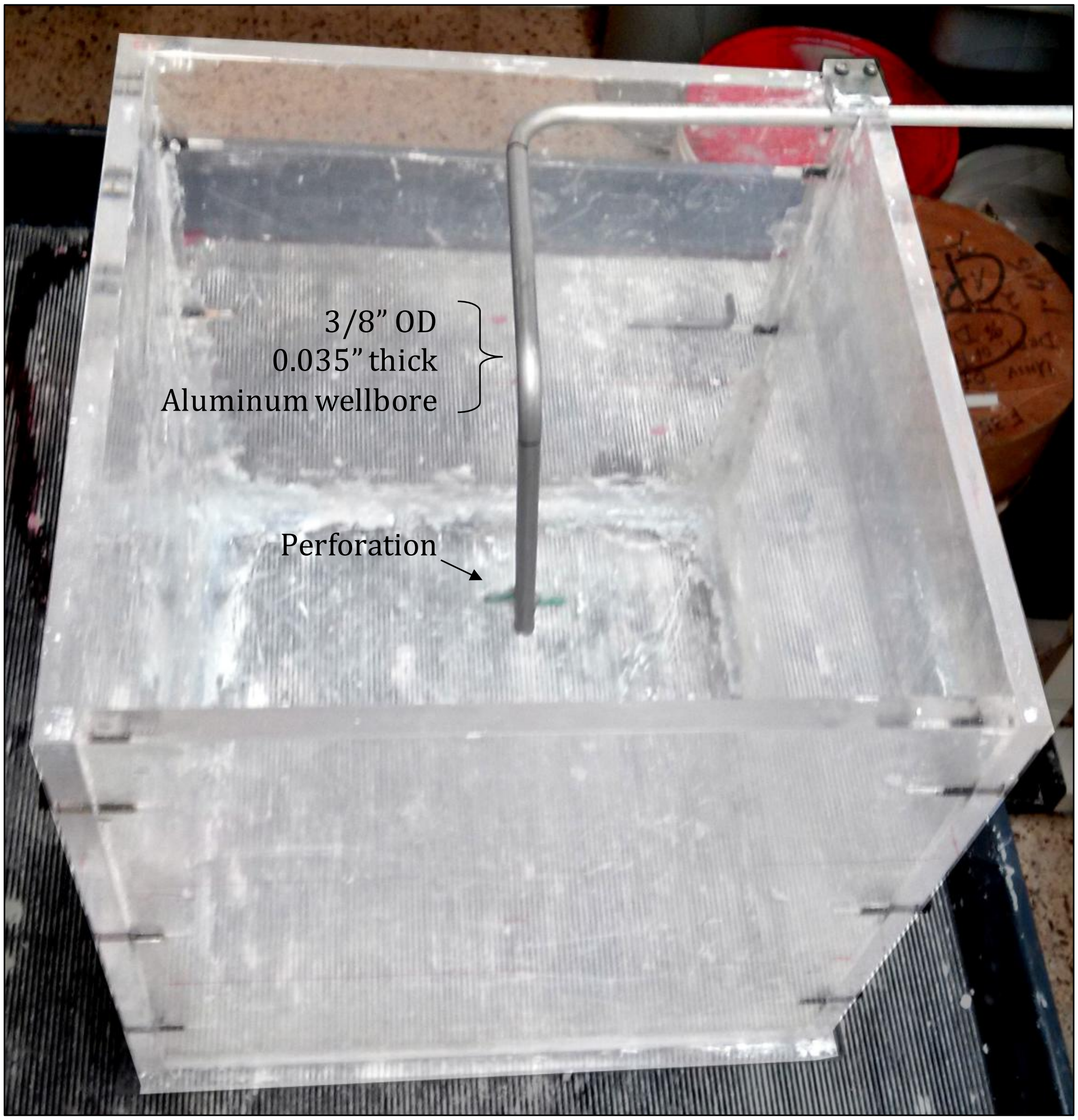

Figure 3.2: Typical wellbore design and placement inside the Plexiglas box

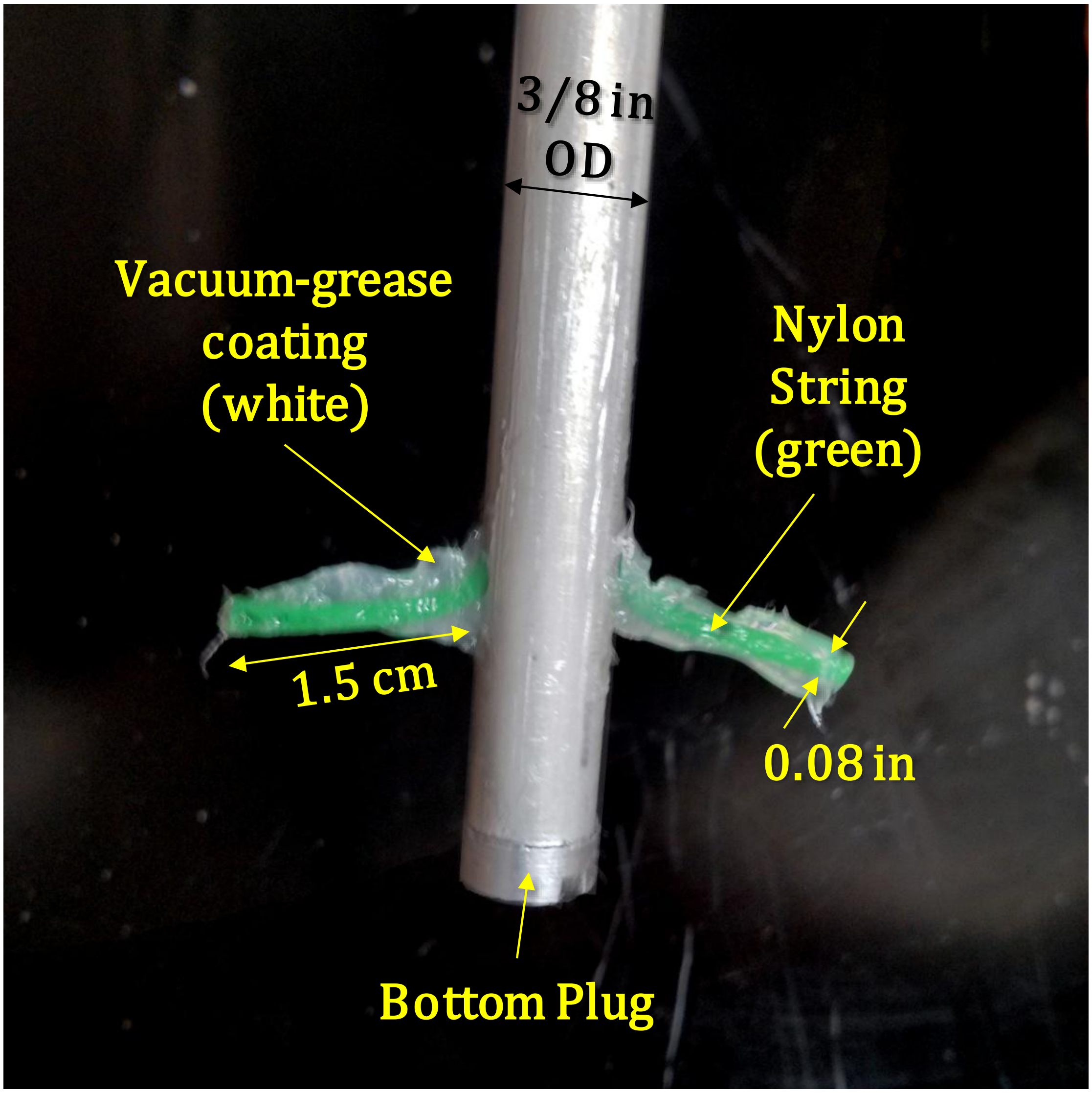

Figure 3.3: A typical perforation design used in the hydraulic fracturing tests

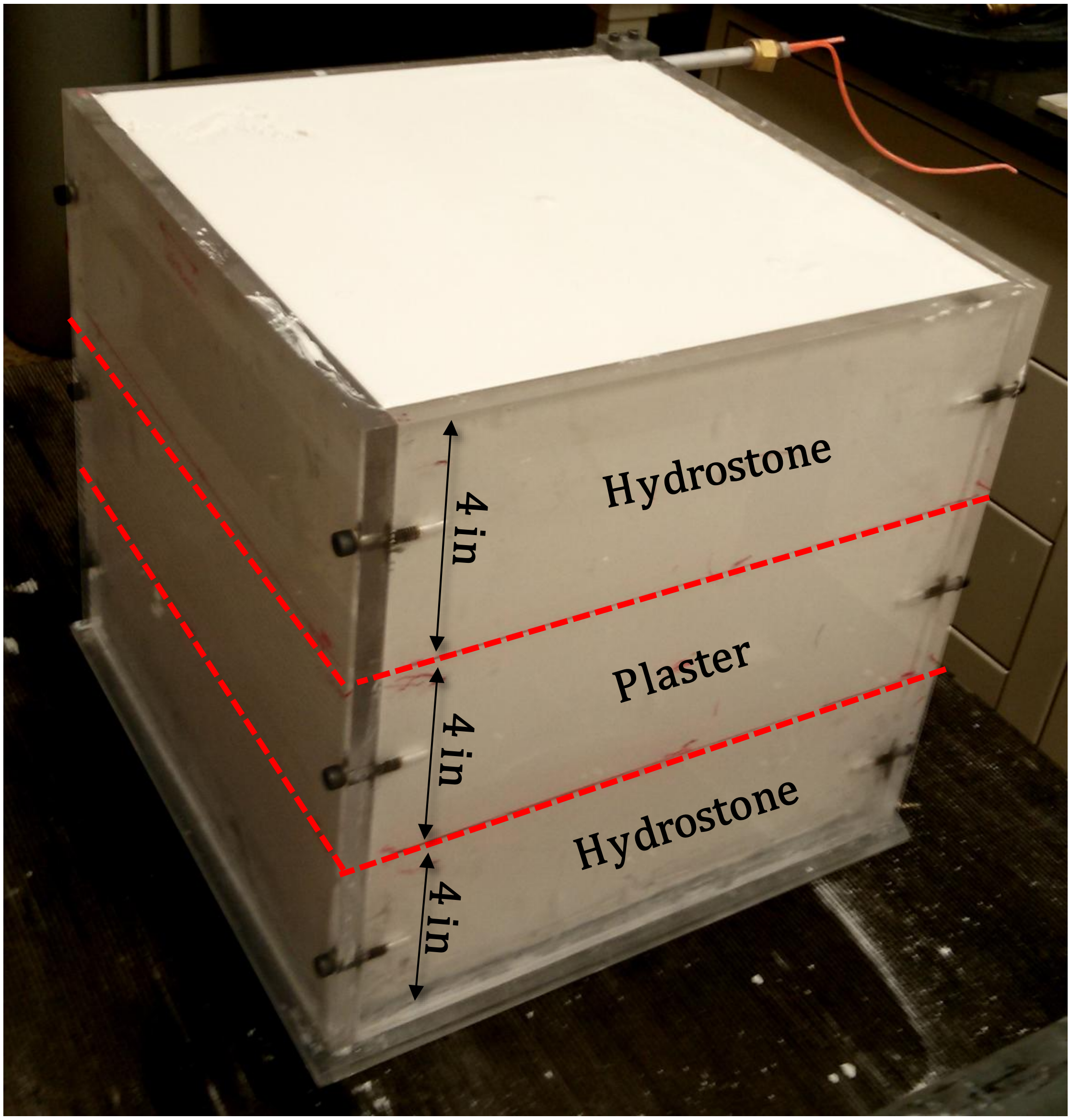

Figure 3.4: A typical synthetic-rock block sample immediately after its layers were poured into the casting Plexiglas box

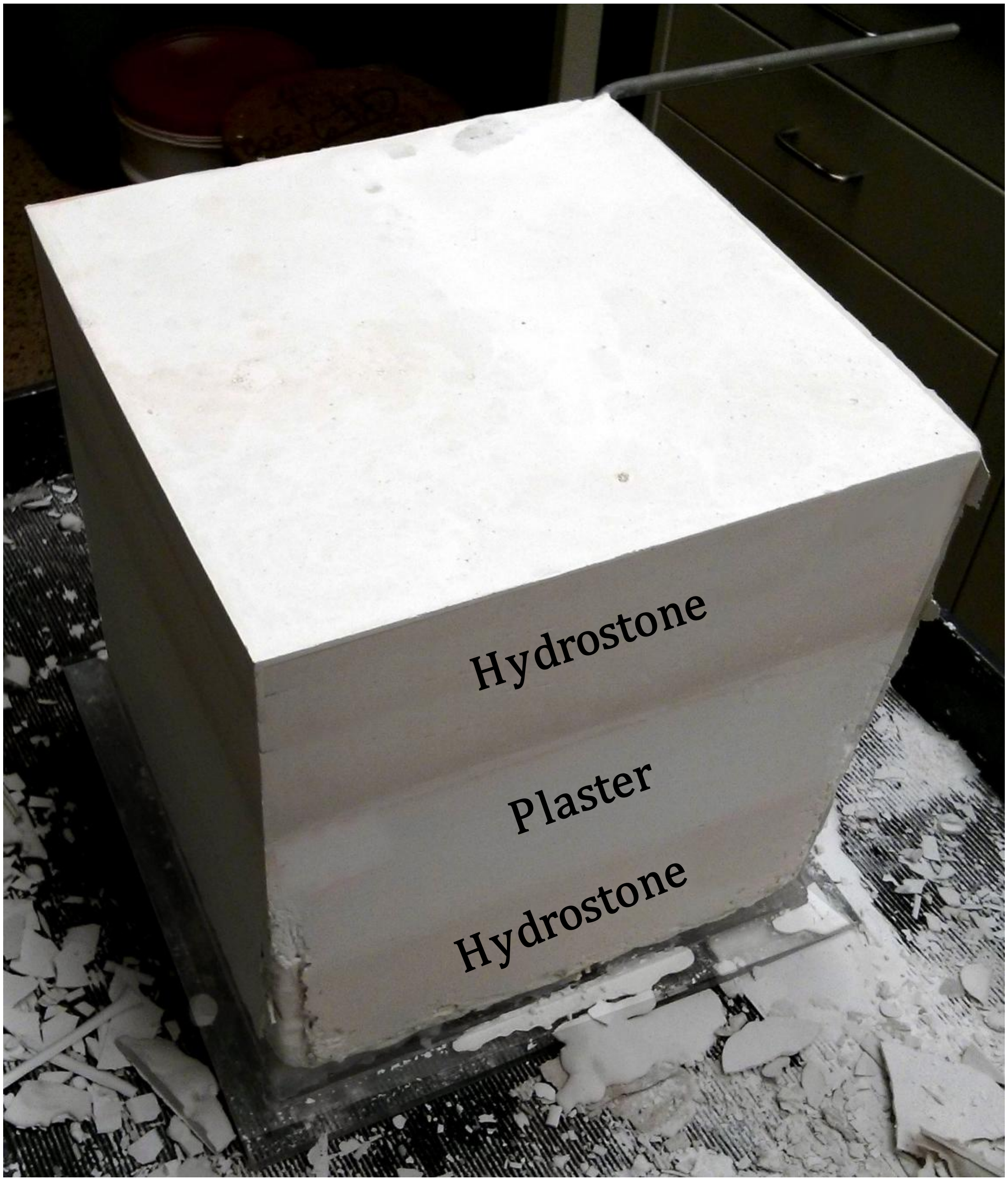

Figure 3.5: A typical synthetic-rock block sample after 24-hour curing time

Second Part: Hydraulic-Fracture Testing

After the block sample was made and cured, another series of steps were followed in order to carry out the hydraulic fracturing test on the sample. The sequence of steps in this part of the procedures consisted of applying principal stresses on the sample, preparing fracturing fluids, and fracturing the sample by high-rate injection of the fracturing fluids. The following list describes these experimental steps in more detail:

6. A specially designed testing apparatus was used for hydraulic-fracture testing the block sample. The apparatus consisted of an aluminum box to house the sample, gas-pressured flat jacks to apply boundary stresses on the sample, a Teledyne ISCO 1000D syringe pump to inject fracturing fluids, and pressure transducers connected to a computer system to monitor and store injection pressure and flow rate data (Figures 3.6 and 3.7).
7. Once the 1-foot cubic block sample was fully cured, it was placed inside the 1.08-foot cubic, aluminum testing box. Three inflatable rubber flat jacks were placed in the spacing between the box walls and the sides of the block sample; one flat jack sat horizontally on the top between the sample's top face and the box's lid and two flat jacks were placed vertically against two adjacent faces of the block sample and the respective box's walls. The other faces of the block sample were left against the box's walls. In other words, each pair of opposite faces of the sample, which represented a principal direction, had one face against a flat jack and the other face against an aluminum wall (Figure 3.8, 3.9, and 3.10).
8. When the sample and the flat jacks were properly positioned inside the aluminum box, the box was securely closed using metal bolts. Then, the flat jacks were connected to gas sources and pressured to exert boundary stresses in the three principal directions: A vertical stress of 100 psi, a maximum horizontal stress of 75 psi, and a minimum horizontal stress of 25 psi. The sample was usually left under stress for one to three days to allow the block to adjust to the stress field.

9. One liter of linear-gel based fracturing fluid was usually prepared for every test. The recipe and mixing details used for fracturing fluids preparation are detailed in Table 3.2.
10. The fracturing fluid was then poured into the pump chamber and the pump was connected to the wellbore inlet by a flexible metal hose.
11. Once all components of the apparatus were properly inspected and confirmed functional, the hydraulic fracturing test was begun. At first, a low injection rate of 80 milliliter per minute was used until the fracturing fluid had reached the perforations and steady pressure build-up was exhibited. Then, a high injection rate of 200 milliliter per minute was applied and held throughout the duration of the test. Meanwhile, pressure response was monitored through live recordings of two pressure transducers at the pump chamber and at the wellbore inlet.
12. Upon the conclusion of the fracturing test, the injection was stopped, the pump hose was disconnected from the wellbore inlet, the flat jacks were depressurized, the aluminum box was opened, and the block sample was removed from the fracturing apparatus station. Also, the injection pressure and flow rate data of the hydraulic fracturing test were measured and stored.

Table 3.2: The recipe and mixing details used to prepare the fracturing fluids used for hydraulic-fracture testing in the laboratory

Step #	**Component Added**	**Amount**	**Mixing Time (minutes)**
1	Water	1 (Liter)	—
2	BJ Services Guar-Based Gel (GW-38)	4.2 (lb)	30
3	Potassium Chloride (NaCl)	20 (lb)	5-10
4	Red Dye	Few drops	2

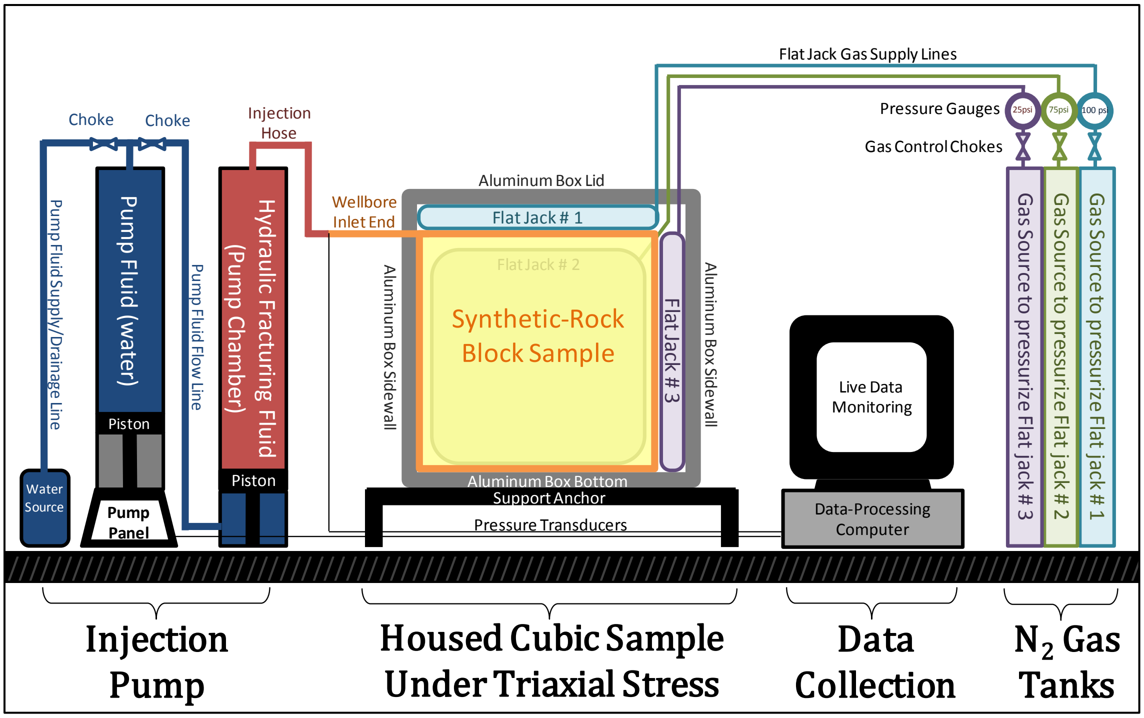

Figure 3.1: Schematic illustration of the hydraulic-fracture testing apparatus used in the laboratory testing

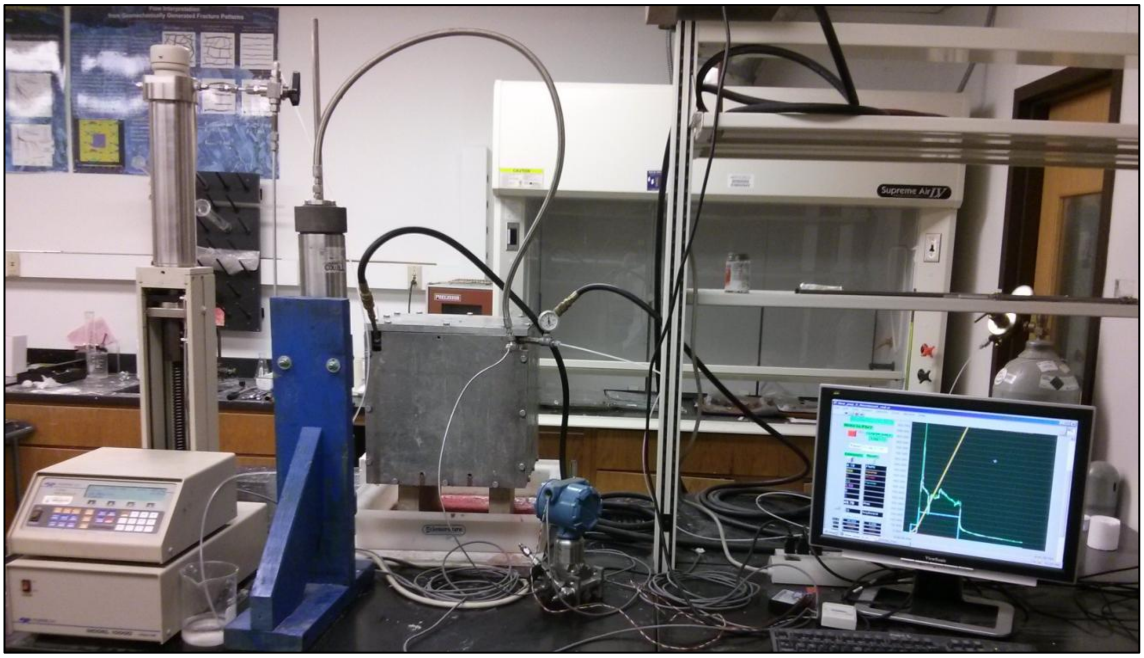

Figure 3.7: Photo of the hydraulic-fracture testing apparatus used in the laboratory

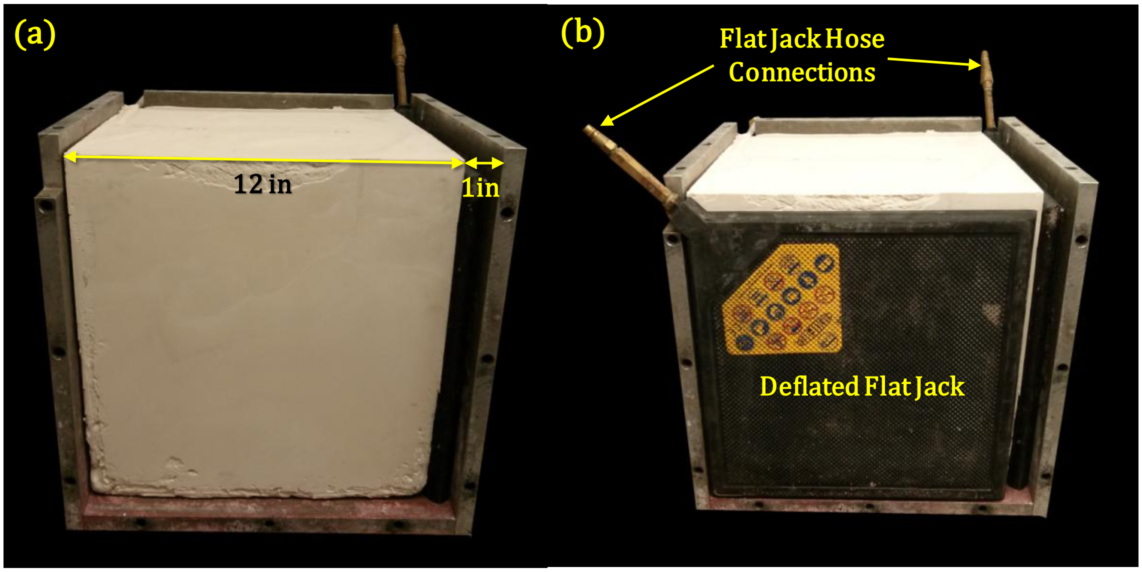

Figure 3.8: Side view of the sample placement inside the aluminum housing box that was partially assembled to allow proper visibility

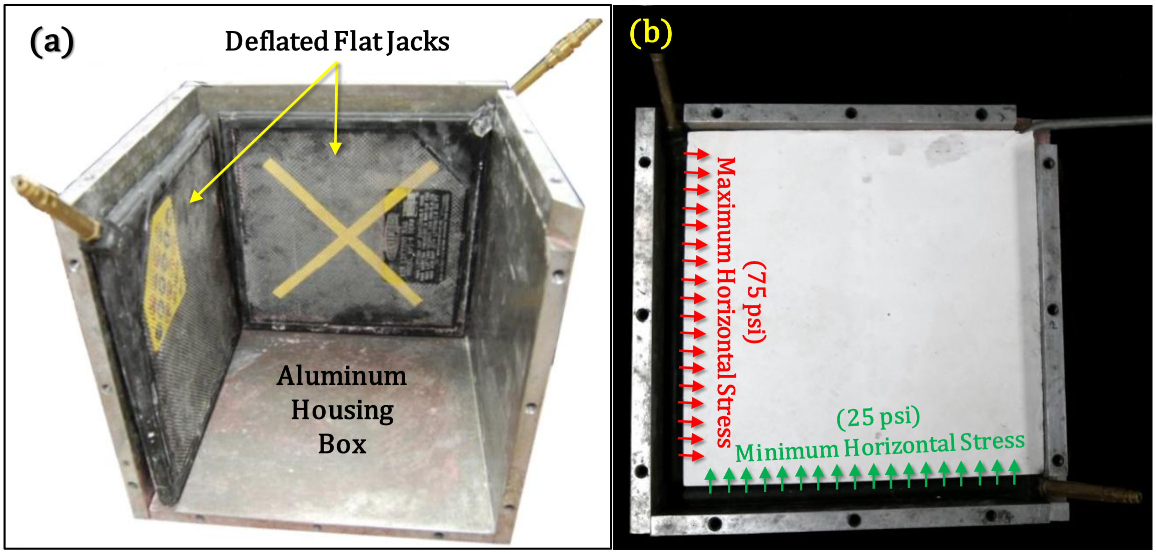

Figure 3.9: (a) Another side view showing the aluminum housing box and two flat jacks partially assembled prior to sample placement (edited from Bahorich 2012) (b) Top view of a typical set up of the block sample inside the aluminum box where the rubber flat jacks exert stresses in the principal directions (top flat jack and aluminum lid where removed to allow proper visibility)

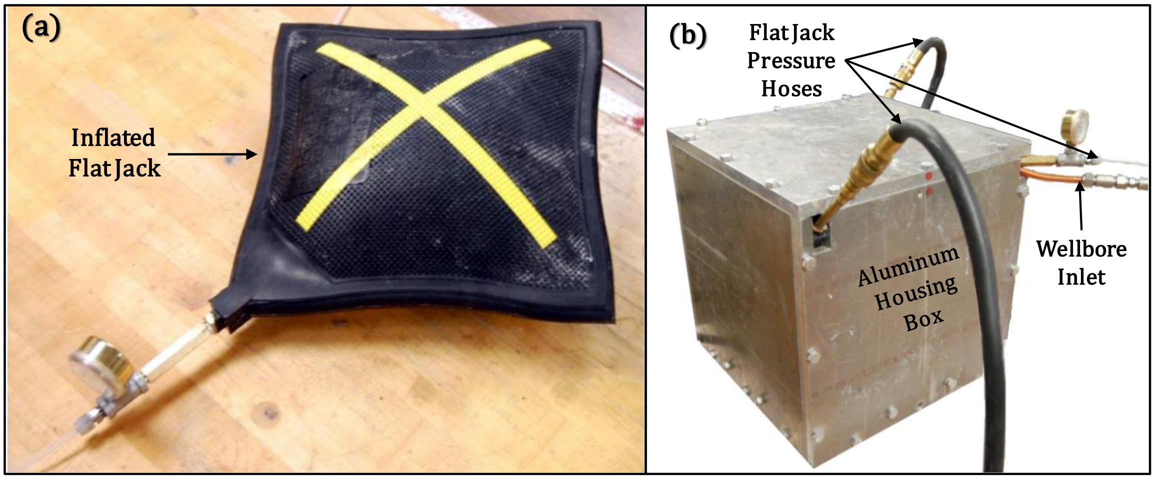

Figure 3.10: (a) Inflated flat jack (edited from Hosseini 2012), (b) Fully assembled aluminum box housing a block sample under stress for a hydraulic fracturing test (edited from Bahorich 2012)

Third Part: Block Opening

The last part of the experimental procedures was to open the block sample and trace the resultant hydraulic fracture. The following list provides detailed description of the steps taken in this part of the procedures:

13. The rock-cutting machinery used to open the block sample consisted mainly of an electric, rotary core saw with a circular lapidary diamond blade that is approximately 1 foot in diameter and 0.25 cm in thickness. Attached to the saw is a moving base where the sample was placed (Figure 3.11).
14. Typically, the first saw cut was done horizontally in the middle of the central layer (i.e. the saw-cut plane was parallel to the layers' bedding planes), which resulted in splitting the block into two halves (Figure 3.12). This initial saw-cut allowed accessing top and bottom views of the synthetic-rock layer hosting the vertical hydraulic fracture. As a result, the hydraulic fracture propagation path was usually fully captured in this saw-cut plane in the form of a red-dyed crack

line; the crack line viewed in this saw-cut plane represented the hydraulic-fracture length (Figure 3.13).

15. Subsequent saw-cutting and chiseling was then done on both halves of the block sample as required until cross-sectional views of the hydraulic fracture faces were obtained.

Figure 3.11: The core saw with lapidary diamond blade used to cut-open the hydraulic-fracture tested samples

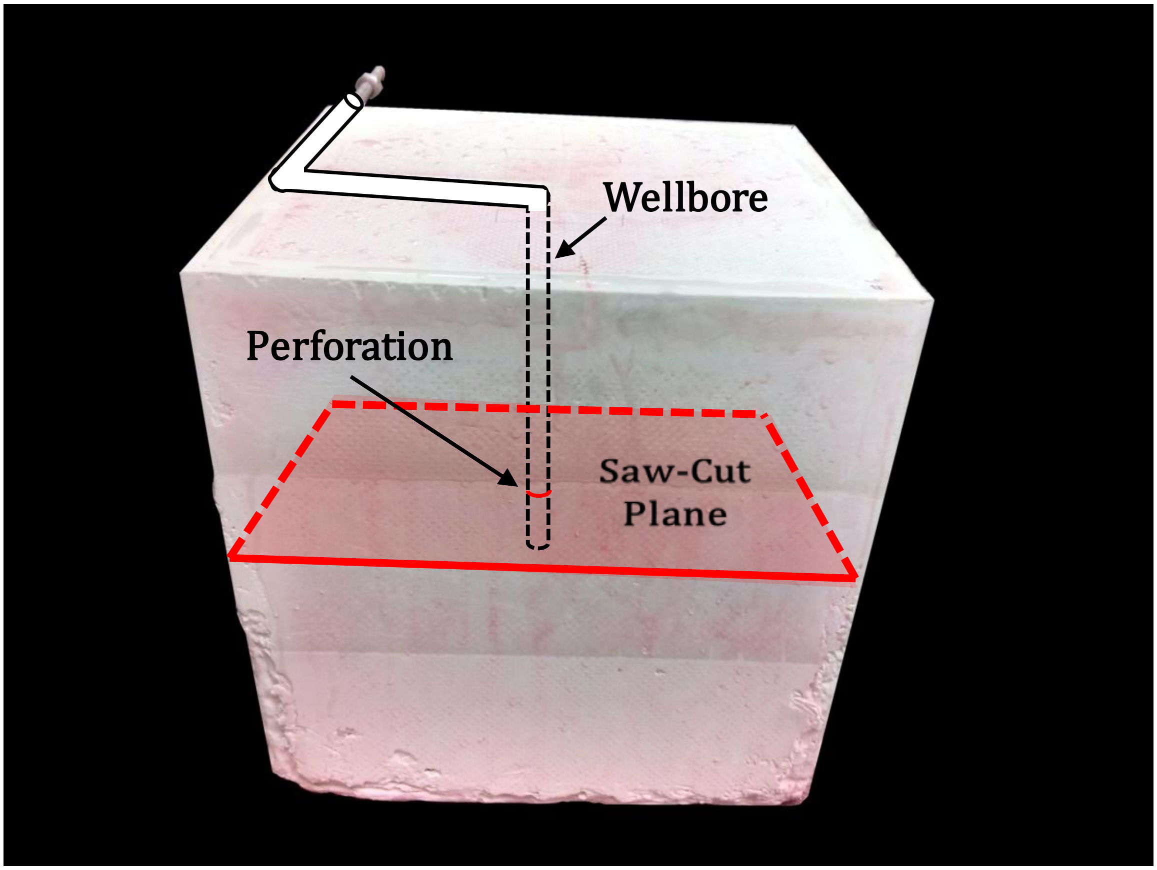

Figure 3.12: A block sample marked with the initial saw-cut plane during the block opening procedure after the hydraulic fracturing test

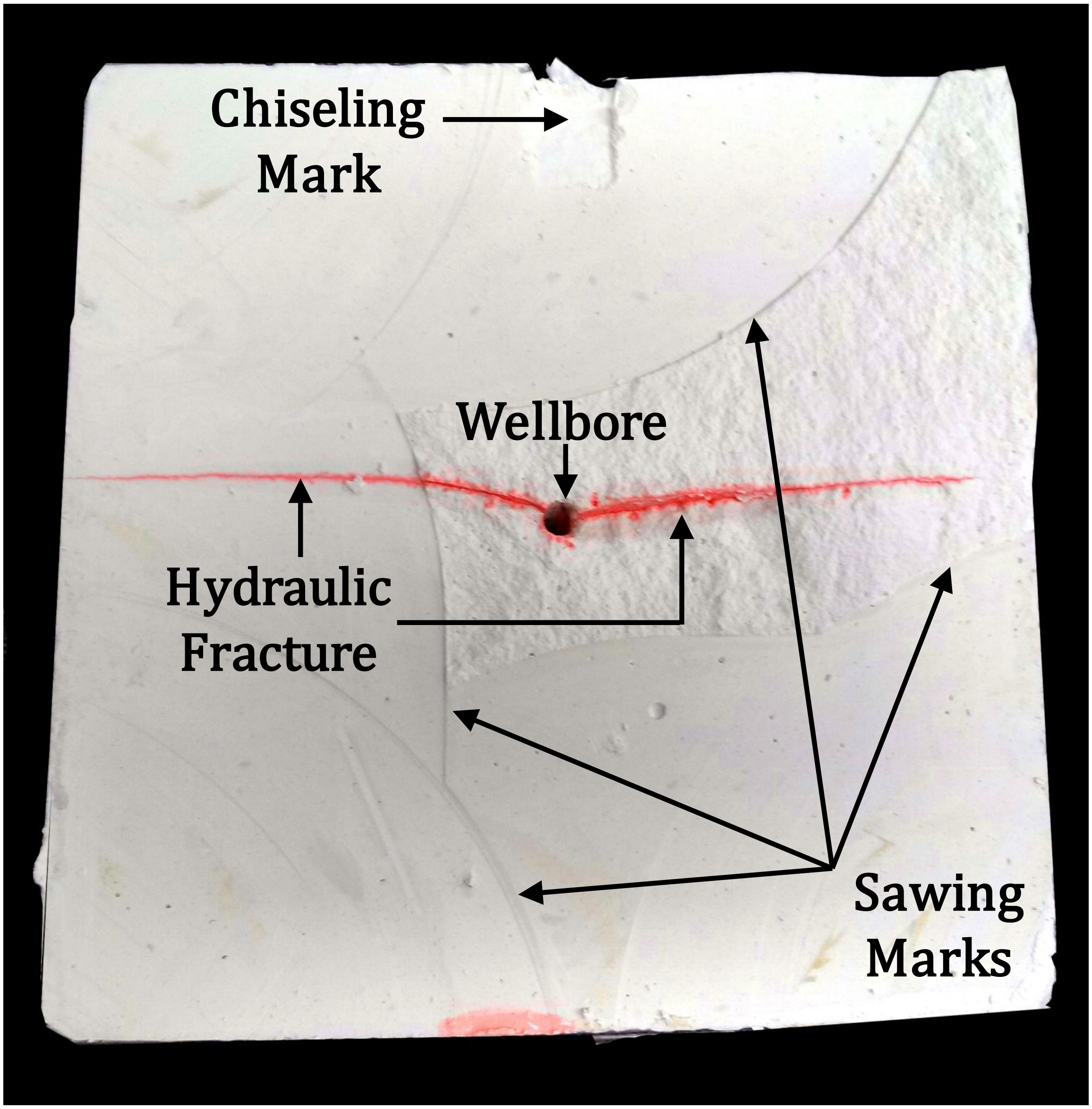

Figure 3.13: Top view of the saw-cut surface of a block sample clearly shows a hydraulic fracture trace (i.e. the red line extending away from the wellbore represents hydraulic fracture length), smooth surfaces indicating areas of saw-cutting, and a small portion of rough surface due to break-opening the block using a chisel and a hammer after making a number of saw cuts

3.1.2.2 Test for Interaction with Pre-Existing Fractures

The general hydraulic fracturing test set-up and procedures, which were described in details in the previous section, were also followed when testing for hydraulic fracture interaction with pre-existing fractures. However, additional steps were added to the second part of the procedures, i.e. block preparation, in order to account for pre-existing fractures. The way these pre-existing fractures were included in the block sample was by preparing solid slices, usually either cured hydrostone or plaster, to represent cemented natural fractures and then inserting them into the middle layer of the block sample. These additional steps are described in the following list:

1. A cuboid of the selected pre-existing fracture material was made in a special casting box similar to the method used in casting the block sample. Once casted, the cuboid was left to cure for a period no less than 7 days.
2. After the cuboid was fully cured, it was sliced into multiple slices with the desired dimensions using an electric rotary saw as illustrated in Figure 3.14.
3. For each test, two equally-dimensioned slices were inserted into the middle layer of the block sample. Slice insertion took place immediately after the middle layer was poured into the Plexiglas casting box. Each slice was vertically placed across the perforation hole, which was always aligned to the direction of the maximum horizontal stress, midway between the wellbore and the edge of the block. The orientation of the slice inclusion was always orthogonal to the direction of the maximum horizontal stress; the slice height-by-length interface was always perpendicular to the directional plane of the maximum horizontal stress (Figure 3.15).

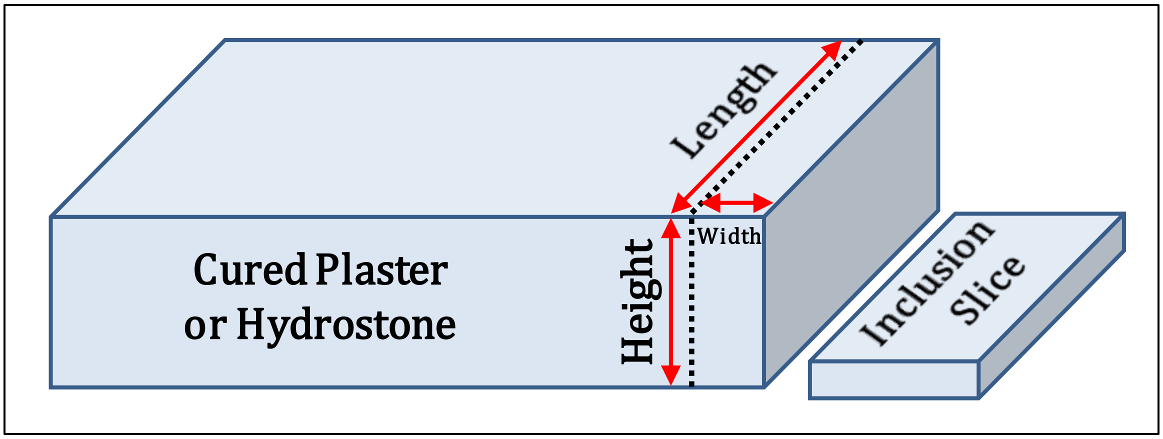

Figure 3.14: A cuboid of fully cured cementing material is sliced using an electric saw to create multiple inclusion slices used as natural fractures (the dashed black lines mark saw cut orientation)

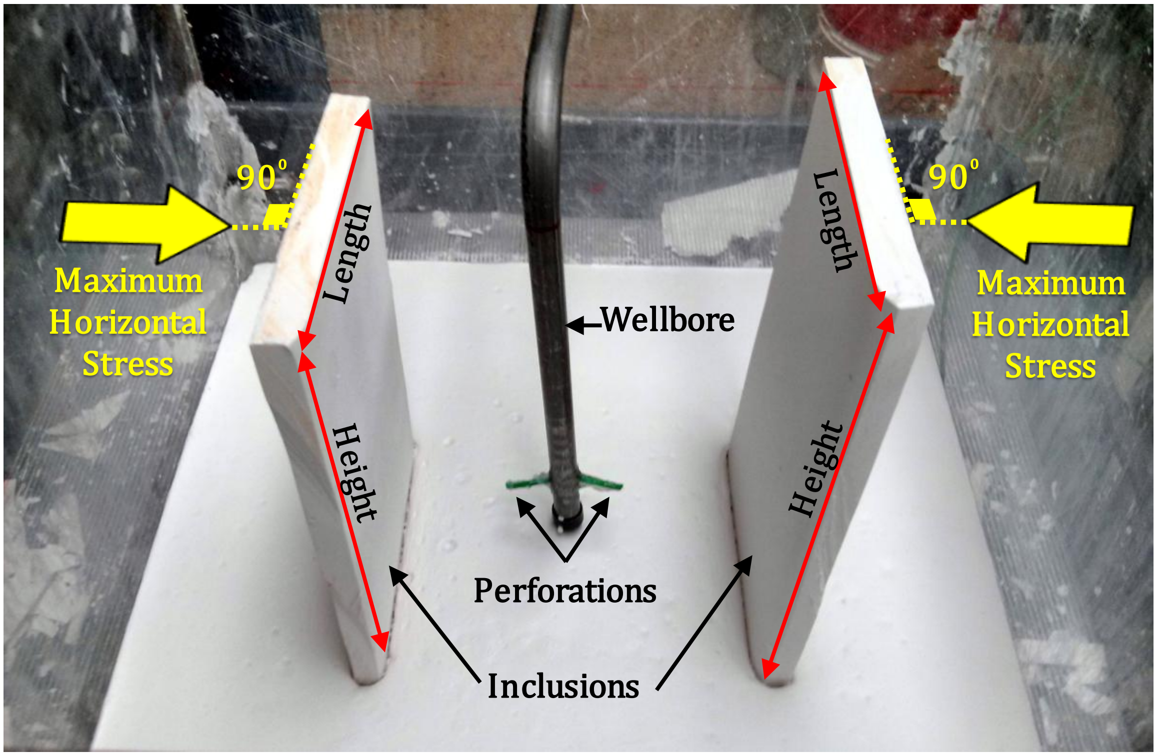

Figure 3.15: A typical inclusion orientation representing orthogonal cemented natural fractures used in the block samples tested for hydraulic-fracture-natural-fracture interaction (these particular inclusions from Test 8 represented discontinuities with exaggerated height)

3.1.2.3 Test for Interaction between Simultaneous Multiple Hydraulic Fractures

For investigating the interaction between simultaneous multiple hydraulic fractures, the general testing set up and procedures applied but with some modifications to the wellbore and perforation designs, i.e. the second part of the general testing procedures. Multiple hydraulic fracturing sources, i.e. perforation clusters, needed to be included in the wellbore design in order to simultaneously generate multiple hydraulic fractures. Therefore, there had been three types of attempts to achieve this objective: Horizontal wellbore with multiple perforation clusters, pseudo-horizontal wellbore with multiple perforation clusters, and pseudo-horizontal wellbore with limited-entry perforation clusters.

First Attempt: Horizontal Wellbore with Multiple Perforation Clusters

The block sample design in this attmept used a horizontal wellbore geometry with multiple, equally-spaced, equally-sized perforation clusters. The horizontal wellbore was oriented in a parallel direction to the direction of the minimum horizontal stress in order to promote initiating transverse hydraulic fractures, which was a primary requirement for the test. However, initiating proper transverse hydraulic fractures from a horizontal wellbore using the tools available in this laboratory failed. Despite the repeated attempts and the various design modifications that were tried, all eight testing attempts were not successful. Hence, some diagnostic work was carried out on those failed attempts and concluded that the various penetration designs used in making the perforation clusters along the horizontal wellbore were insufficient to overcome the near-wellbore stresses and fracturing-fluid leakage along the wellbore, which repeatedly drove the hydraulic fractures to initiate longitudinally along the axis of the wellbore as illustrated in Figure 3.16. Further investigation of such hydraulic fracture initiation problems was done by Chang et al. (2014). Their observations and analyses suggested that in order to produce hydraulic fractures that are transversely oriented to the wellbore axis in the laboratory, the perforation clusters should be a circular notch with a diameter equal to at least twice the length of the wellbore's outer diameter (Chang et al. 2014). Such notches are usually made using specially designed jetting tools, which were not available for this work.

Figure 3.16: Examples of various horizontal wellbore designs attempted in multiple tests that had unsuccessful outcomes due to the observed tendency of such testing set up to generate longitudinal hydraulic fractures instead of the requisite transverse fractures.

Second Attempt: Pseudo-Horizontal Wellbore with Multiple Perforation Clusters

Since hydraulic fracture initiations were limited to longitudinal orientations along the wellbore axis, a different wellbore geometry was attempted. The new wellbore design was based on constructing multiple, equally-spaced, equally-sized vertical wellbores connected from the top through an injection manifold that provided flow communication between the wellbores. The injection manifold extended from one end outside the block sample acting as the wellbore inlet. The vertical wellbores were placed along a directional line parallel to the minimum horizontal stress direction, i.e. pseudo-horizontal-wellbore axis, and each wellbore had a single perforation cluster aligned towards the direction of the maximum horizontal stress direction. Perforation design was exactly as described previously in the general test set-up and identical in all vertical wellbores. In other words, each vertical wellbore played the role of a single perforation cluster in a horizontal fracturing stage. Figure3.17 shows the wellbore configuration inside the casting Plexiglas box for this testing set up. Unfortunately, only partial successful fracture initiation was achieved, probably due to uneven distribution of injection pressure and flow rate away from the manifold inlet.

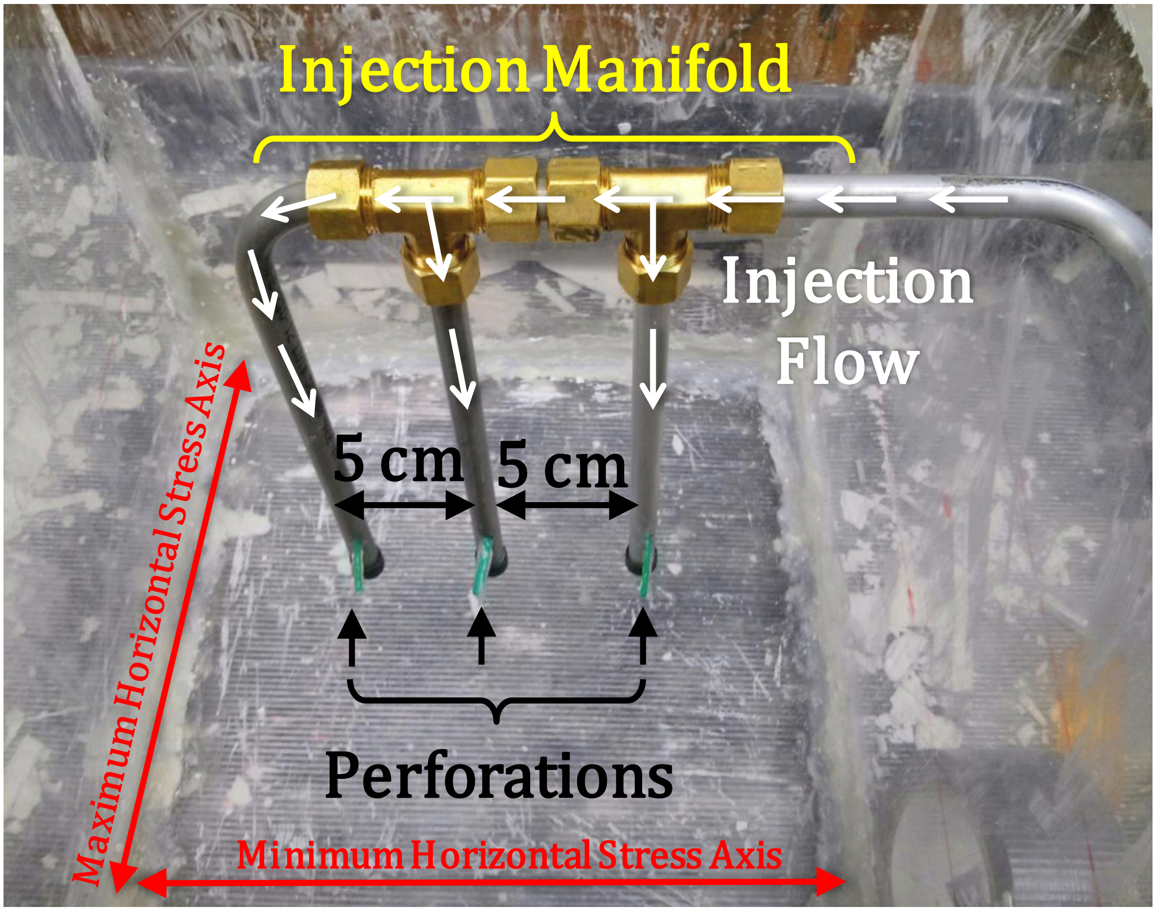

Figure 3.17: Pseudo-horizontal wellbore configuration attempted in Test 9 for testing the interaction between simultaneous multiple hydraulic fractures

<u>Third Attempt: Pseudo-Horizontal Wellbore with Multiple Perforation Clusters of Increasing Sizes</u>

Similar to the approach used in the second attempt, this attempt also used an injection manifold with multiple perforated vertical wellbores. The only modification to this configuration was to the sizes of the vertical wellbores and their respective perforation clusters. Hence, as the vertical wellbore location was farther away from the injection source, i.e. the injection manifold inlet, the wellbore outer diameter and the perforation holes diameters and penetration lengths increased accordingly. The purpose of this increase in geometric sizes away from the injection source was to overcome uneven flow and pressure distribution along the wellbores, which was suspected to be the major cause of producing a single fracture in the previous attempt. Figure 3.18 illustrates the wellbore configuration inside the casting Plexiglas box for this testing set up. However, this attempt also resulted in partial success due to the limited improvement to the distribution of injection flow rate and pressure as well as some experimental problems that lead to plugging one perforation cluster.

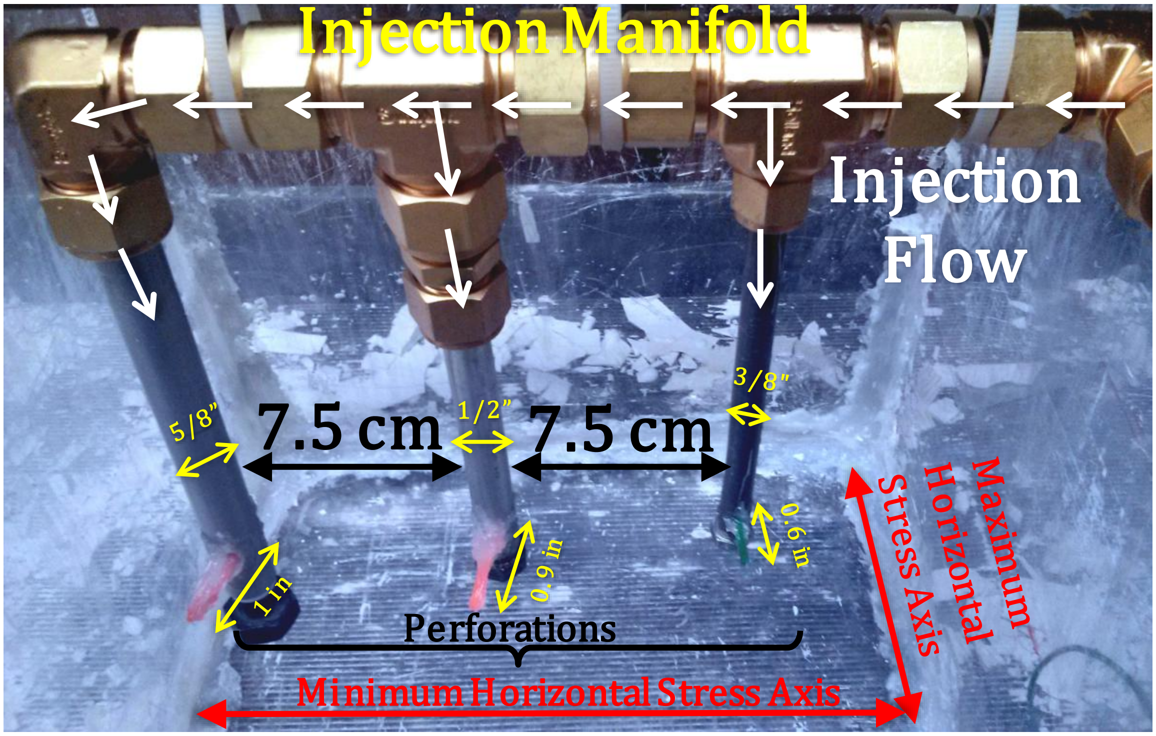

Figure 3.18: Pseudo-horizontal wellbore configuration with multiple perforation clusters of increasing sizes attempted in Test 10 for testing the interaction between simultaneous multiple hydraulic fractures

<u>Fourth Attempt: Pseudo-Horizontal Wellbore with Limited-Entry Perforation Clusters</u>

Having only obtained partial successes from the previous attempts, further analyses were called for in order to evaluate the major factors controlling multiple-fracture initiations using a pseudo-horizontal wellbore configuration. Therefore, fracturing fluid rheology, pressure drop inside circular pipes, and pressure drop across perforation holes were all examined as functions of flow rate. Preliminary results based on theoretical analysis showed that pressure drop inside circular pipes had a dominant effect on the overall pressure drop inside the pseudo-horizontal wellbore system, especially when using more viscous fluids at higher flow rates. Moreover, it was noted that the previous attempts lacked the presence of considerable pressure drops inside the vertical wellbores, which was needed in order to restrict the tendency for uneven flow distribution between the vertical wellbores. In other words, when the first hydraulic fracture occurred, the flow inside the corresponding vertical wellbore increased consequently, which left the other wellbores without significant flow to develop sufficient pressure to create fractures. Hence, it was decided to add a flow-rate-sensitive pressure drop to the wellbore design calculation whereby the pressure losses along the vertical wellbores increase considerably with increased flow rates, which provides a mechanism that inhibits injection flow being dominated by a single wellbore. This mechanism mimics the effects of the limited-entry perforation designs often used in field applications of fracturing stage completions. Pressure-drop calculations and laboratory measurements were made to test for pressure-drop increases per increased flow rates using various wellbore sizes and fluid types. The following correlations (Equations 3.1 through 3.9) govern the mimicked limited-entry effect described previously:

1. Fracturing fluid shear rate (Darby 2001 and Hosseini 2012)

$$\left(\frac{\partial u}{\partial y}\right) = \frac{4\,q}{\pi\,r^2} \tag{3.1}$$

2. Non-Newtonian, power-law fracturing fluid viscosity (Morrell and de Waele 1920 and Hosseini 2012)

$$\mu_v = K_v \left(\frac{\partial u}{\partial y}\right)^{n-1} \tag{3.2}$$

3. Reynold's Number (Economides et al. 1994)

$$N_{Re} = \frac{4\, q\, \rho}{\pi\, D\, \mu_v} \tag{3.3}$$

$$N_{Re} < \ 2{,}300 \ \Rightarrow \ Laminar\ flow \tag{3.4}$$

$$N_{Re} \geq \ 2{,}300 \ \Rightarrow \ Turbulant\ flow \tag{3.5}$$

4. Fanning friction factor for fluid flow in a pipe (Economides et al. 1994 and Chen 1979)

$$Laminar\ flow \ \Rightarrow \ f_f = \frac{16}{N_{Re}} \tag{3.6}$$

$$Turbulant\ flow \ \Rightarrow \ f_f = -4\ \log\left\{\frac{\in}{3.7065} - \frac{5.0452}{N_{Re}}\ \log\left[\frac{\in^{1.1098}}{2.8257} + \left(\frac{7.149}{N_{Re}}\right)^{0.8981}\right]\right\} \tag{3.7}$$

5. Pressure drop for flow in a circular pipe (edited from Economides et al. 1994)

$$\Delta P = \frac{2\, f_f\, \rho\, u^2\, L}{D} \tag{3.8}$$

6. Pressure drop for flow through a perforation hole (Jennings 2008)

$$\Delta P = \frac{\rho\, q^2}{D^4\, C^2} \tag{3.9}$$

As a result of the theoretical and empirical assessment of the pressure drop required to add a limited-entry-like effect to the pseudo-horizontal wellbore design, it was determined that the best selection for vertical wellbores that was feasibly available was stainless steel pipes with 0.125 inch outer-diameter and 0.028 inch wall thickness. In addition to this small-sized pipe selection, a more viscous fracturing fluid using cross-linked gel was required (Figure 3.19). Although this attempt also had limited success with respect to propagating multiple, full-size hydraulic fractures, it was the only approach that had all three fracture-injection sources initiating cracks of various sizes.

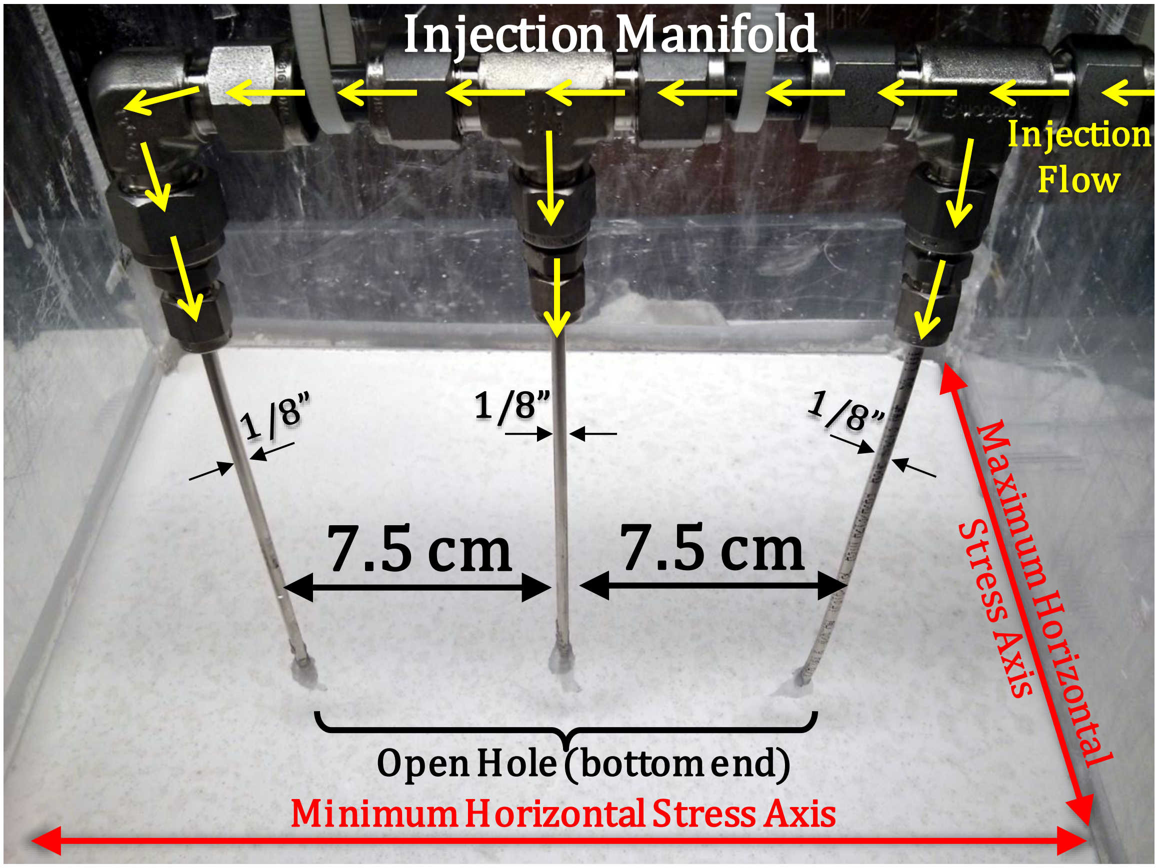

Figure 3.19: Pseudo-horizontal wellbore configuration with limited-entry perforation clusters (in the form of open hole sections) used in Test 11 for testing the interaction between simultaneous multiple hydraulic fractures

3.1.3 List of Hydraulic-Fracturing Tests

A total of 21 hydraulic-fracturing tests were carried out during this research work. However, only 11 tests were included in this thesis and the remaining 10 were disqualified for either having experimental failures or producing un-useful results for the objectives at hand. Table 3.3 contains full details regarding the test set-ups of all the reported 11 tests.

Table 3.3: List of all the hydraulic fracturing experiments included in this work and their set-up details (Continue Next Page)

Component	**Parameter**	**General Test**	**Test for Interaction with Pre-Existing Fractures**							**Test for Interaction between Simultaneous Multiple Hydraulic Fractures**		
		Test 1	**Test 2**	**Test 3**	**Test 4**	**Test 5**	**Test 6**	**Test 7**	**Test 8**	**Test 9**	**Test 10**	**Test 11**
System	1. Top Layer 2. Middle Layer 3. Bottom Layer	Hydrostone Plaster Hydrostone	Hydrostone Plaster Hydrostone	Plaster Hydrostone Plaster	Hydrostone Plaster Hydrostone	Hydrostone Hydrostone Hydrostone	Hydrostone Plaster Hydrostone	Hydrostone Plaster Hydrostone	Hydrostone Plaster Hydrostone	Hydrostone Plaster Hydrostone	Hydrostone Plaster Hydrostone	Hydrostone Plaster Hydrostone
	Layers Dimensions (L x W x H, in each)	12 x 12 x 4	12 x 12 x 4	12 x 12 x 4	12 x 12 x 4	12 x 12 x 4	12 x 12 x 4	12 x 12 x 4	12 x 12 x 4	12 x 12 x 4	12 x 12 x 4	12 x 12 x 4
	Curing Time (days)	7	8	7	6	8	7	8	21	9	7	7
Wellbore	Orientation	Vertical	Vertical	Vertical	Vertical	Vertical	Vertical	Vertical	Vertical	Pseudo-Horizontal	Pseudo-Horizontal	Pseudo-Horizontal
	Material	Aluminum	Aluminum	Aluminum	Aluminum	Aluminum	Aluminum	Aluminum	Aluminum	Aluminum	Aluminum	Aluminum
	Outer Diameter (in)	0.375	0.375	0.375	0.375	0.375	0.375	0.375	0.375	0.375	3/8, 1/2, 5/8	1/8, 1/8, 1/8
	Thickness (in)	0.035	0.035	0.035	0.035	0.035	0.035	0.035	0.035	0.035	0.035	0.028
Perforation	Number of Perforations	1	1	1	1	1	1	1	1	3	3	3
	Number of Openings	2	2	2	2	2	2	2	2	2	2	Open hole
	Perforation Diameter (in)	0.08	0.08	0.08	0.08	0.08	0.08	0.08	0.08	0.08	0.08, 0.095, 0.1	0.04, 0.04, 0.04
	Penetration Length (in)	0.6	0.6	0.6	0.6	0.6	0.6	0.6	0.6	0.6	0.6, 0.9, 1.0	0.4, 0.4, 0.4
	Perforation Spacing (in)	—	—	—	—	—	—	—	—	1.97	2.95	2.95
Inclusion	Inclusion Material	—	Plaster	Hydrostone	Plaster	Hydrostone	Ice (i.e. Void)	Hydrostone	Plaster	—	—	—
	Inclusion Interface Dimensions (L x H, in)	—	3.9 x 1.9	3.9 x 2.0	3.8 x 1.8	3.9 x 2	3.9 x 2	3.9 x 2.2	3.9 x 9.1	—	—	—
	Inclusion Thickness (in)	—	0.11	0.08	0.93	1.38	0.39	0.12	0.39	—	—	—
	Number of Inclusions	—	2	2	2	2	2	2	2	—	—	—
	Distance to Wellbore (in)	—	3	3	3	3	3	3	3	—	—	—
	Areal Orientation from the Maximum Horizontal Stress Direction (degrees)	—	90	90	90	90	90	90	90	—	—	—
	Vertical Orientation from the Vertical Stress Direction (degrees)	—	0	0	0	0	0	0	0	—	—	—

Table 3.3: List of all the hydraulic fracturing experiments included in this work and their set-up details (Continued)

Component	Parameter	General Test	Test for Interaction with Pre-Existing Fractures							Test for Interaction between Simultaneous Multiple Hydraulic Fractures		
		Test 1	Test 2	Test 3	Test 4	Test 5	Test 6	Test 7	Test 8	Test 9	Test 10	Test 11
Stress State	Vertical Stress (psi)	100	100	100	100	100	100	100	100	100	100	100
	Maximum Horizontal Stress (psi)	75	75	75	75	75	75	75	75	75	75	75
	Minimum Horizontal Stress (psi)	25	25	25	25	25	25	25	25	25	25	25
	System Under Stress Time (hr)	22	43	68	72	70	45	47	71	70	83	90
Fracturing Test	Fracturing Fluid	Linear Gel	Linear Gel	Linear Gel	Linear Gel	Linear Gel	Linear Gel	Linear Gel	Linear Gel	Linear Gel	Linear Gel	Cross-Linked Gel
	Injection Flow rate (mL/min)	200	200	200	200	200	200	200	200	200	200	200
	Volume of Total Fracturing Fluid Injected (mL)	830	907	991	929	843	948	951	951	951	986	996
	Breakdown Pressure (psi)	636	674	1050	603	1050	616	559	482	473	526	1012

3.2 LABORATORY MEASUREMENTS

A few properties of the material used in the hydraulic fracturing experiments were measured in the laboratory. The general approach on acquiring such properties was a combination of making several laboratory measurements on some samples and using previously-reported measurements available in the literature. Once the measurement data were obtained and reviewed, an average value for each property was calculated. Subsequently, these property values were used to calculate other relevant parameters using mathematical correlations. The final results of these laboratory measurements and calculations are summarized in the next chapter. Table 3.4 provides a summary of the major measurements and the laboratory methodologies used in obtaining them.

Table 3.4: Summary of the major laboratory measurements conducted in order to obtain key property values for the different components used in the hydraulic fracturing experiments

Category	**Property**	**Methodology**	**Measured Samples**
Petrophysical Properties	Porosity	Helium Porosimeter	Cured Hydrostone and Plaster
	Permeability	Nitrogen Permeameter	
	Bulk Density	Measure mass and volume	
Mechanical Properties	Young's Modulus	Triaxial Compression Test	Cured Hydrostone and Plaster
	Tensile Strength	Brazilian Test	
	Fracture Toughness	Semi-Circular Bending Test	
	Apparent Fracture Toughness	Semi-Circular Bending Test	Bonded Interfaces
Fluid Properties	Viscosity	Viscometer	Guar- Gel Fracturing Fluid
	Shear Rate	Viscometer	
	Density	Measure mass and volume	

3.3 EXPERIMENTAL LIMITATIONS

Some limitations apply to the results of this laboratory work, especially when used to draw conclusions for field-scale hydraulic fracturing applications. The following list summarizes the major assumptions and constraints related to the various components of the laboratory work:

- The hydraulic fracturing laboratory tests were done under room temperature conditions.
- The magnitudes of the principal stresses applied during the hydraulic fracturing tests (i.e. 25, 75, 100 psi) were relatively low, which may have imposed stress-field errors. Additionally, each principal stress was induced by pressurizing the block in the desired direction using one rubber flat jack on one side and aluminum box wall on the other side, which may have been a source of disturbance to the targeted constant-stress boundary conditions.
- The possibility of synthetic-rock cements (i.e. hydrostone and plaster) marginal property inconsistencies due to either cement brand changes or water-cement ratio inaccuracies.
- Outcome alterations of the hydraulic fracturing tests due to boundary effects related to the block-sample size, geometry, and the testing set up.
- Only a limited number of the research laboratory testing scope was carried out due to the lengthy nature of each test and the time constraints of the academic-degree program, of which this work is a part.
- Lack of digital hydraulic fracture propagation monitoring systems in the hydraulic fracturing tests (i.e. seismic, acoustic).
- Hydraulic fracture geometry and propagation is determined on the basis of visible traces of dyed fracturing fluids after the block sample is broken-open.

- Hydraulic fracturing injection used only fracturing fluids (i.e. gelled water) without proppants
- The hydraulic fracture orientation with respect to the wellbore in all the hydraulic fracturing tests was limited to longitudinal fractures due to the design's inability to overcome the near-wellbore stresses and the tendency of the fracturing fluid to leak along the wellbore.

3.4 EXPERIMENTAL QUALITY ASSURANCE AND QUALITY CONTROL (QAQC)

In order to mitigate the degree of errors and uncertainties due to the experimental limitations described previously, a set of QAQC steps were followed and are listed below:

- The block samples were left under stress for more than 48 hours in order to ensure the stress-field was properly developed prior to starting the hydraulic fracturing tests.
- Synthetic-rock cement mixing and curing methods were standardized for all the hydraulic fracturing tests in order to increase the degree of consistency of their material properties across all tests.
- Laboratory measurements for the petrophysical, mechanical, and fluid properties were taken multiple times from multiple samples and averaged accordingly in order to account for variation differences.
- Two reading points for injection pressure were used in order to increase data reliability.
- Detailed observations during the hydraulic fracturing tests and after the block samples were broken-open were recorded for better assessment of the quality of the test outcomes.

- The outcomes of each hydraulic fracturing test were evaluated against research objectives and qualified or disqualified accordingly. Hence, out of 21 hydraulic fracturing tests carried out in the laboratory, the outcomes of only 11 tests qualified and were used in this work.

Chapter 4: Data and Results

This chapter summarizes the major data and results obtained from the various laboratory experiments and measurements conducted throughout this research work. These results and data include fracture geometry visual illustrations, fracturing fluid injection pressure profiles, cementing material petrophysical and mechanical properties, and fracturing fluid properties.

4.1 HYDRAULIC FRACTURING EXPERIMENTAL RESULTS

The results from eleven hydraulic fracturing tests are summarized in Tables 4.1 and 4.2 and are presented in more details in the figures shown in the subsequent subsections.

Table 4.1: Hydraulic fracture summary of geometry and propagation outcomes from the eleven hydraulic fracturing laboratory tests

Test Type	**Test #**	**Average Fracture Total Length (cm)**	**Average Fracture Height (cm)**	**Fracture Initiation Pressure (psi)**	**HF Propagation Modes**
General	1	29	6	636	Planar HF
Interaction with Pre-Existing Fractures (PEF)	2	~ 30	10	674	Planar and non-planar HF-PEF crossings
	3	15-18	~ 28	1,050	Planar HF-PEF crossings
	4	~ 58	6-23	603	Mixed HF-PEF crossing and deflection
	5	30	17-23	1,050	Planar HF-PEF crossings
	6	48	~ 10	616	HF-PEF deflections
	7	68	≤ 9	559	HF-PEF deflections
	8	70	11	482	HF-PEF deflections
Interaction between Simultaneous Multiple Hydraulic Fractures	9	23, 0, 0	~ 10, 0, 0	473	Slightly non-planar HF
	10	0, 4, 18	0, 2, 9	526	Moderately non-planar HF
	11	2, 1, 16	3, 2, 8	1,012	Highly angled HF

Table 4.2: A summary of the experimental observations recorded during the eleven hydraulic fracturing laboratory tests

Test #	Event	Event-Like Pressure Response	Time of Event-Like Pressure Response (min:sec)	Event-Like Laboratory Observation	Time of Event-Like Laboratory Observation (min:sec)	Comment
1	HF broke out of block	HF extension pressure increased decline	5:02	—	—	—
2	HF broke out of block	HF extension pressure sharp fall	3:36	Fracturing fluid leaked outside the aluminum box	< 6:00	HF marks were visible at the block side wall
3	HF broke out of block	—	—	Fracturing fluid leaked outside the aluminum box	< 2:43	—
4	HF broke out of block	HF extension pressure sharp fall	3:48	—	—	HF marks were visible at the block side wall
5	HF broke out of block	HF extension pressure sharp fall	2:41	Fracturing fluid leaked outside the aluminum box	< 4:17	HF marks were visible at the block side and top walls
6	HF contained inside block	—	—	No fracturing fluid leaked outside the aluminum box	—	Fracturing fluid leakoff marks were visible on block side wall
7	HF contained inside block	—	—	No fracturing fluid leaked outside the aluminum box	—	—
8	HF contained inside block	HF extension pressure increased decline	4:35	Fracturing fluid leaked outside the aluminum box	4:25	fluid leaked from around the wellbore inlet outside the box
9	HF broke out of block	HF extension pressure increased decline	2:55	Fracturing fluid leaked outside the aluminum box	< 4:29	HF marks were visible at the block side wall
10	HF broke out of block	—	—	Fracturing fluid leaked outside the aluminum box	3:10	—
11	HF broke out of block			Fracturing fluid leaked outside the aluminum box	<3:15	HF marks were visible at the block side wall

4.1.1 Test 1

Test 1 corresponds to a baseline fracturing test. The test set up of in-situ principal stresses of 100, 75, and 25 psi, injection rate of 200 milliliter per minute, and of linear gel fracturing fluid provide a standard for the following tests. Test 1 resulted in a single, planar, well-contained hydraulic fracture (Figures 4.1-4.4).

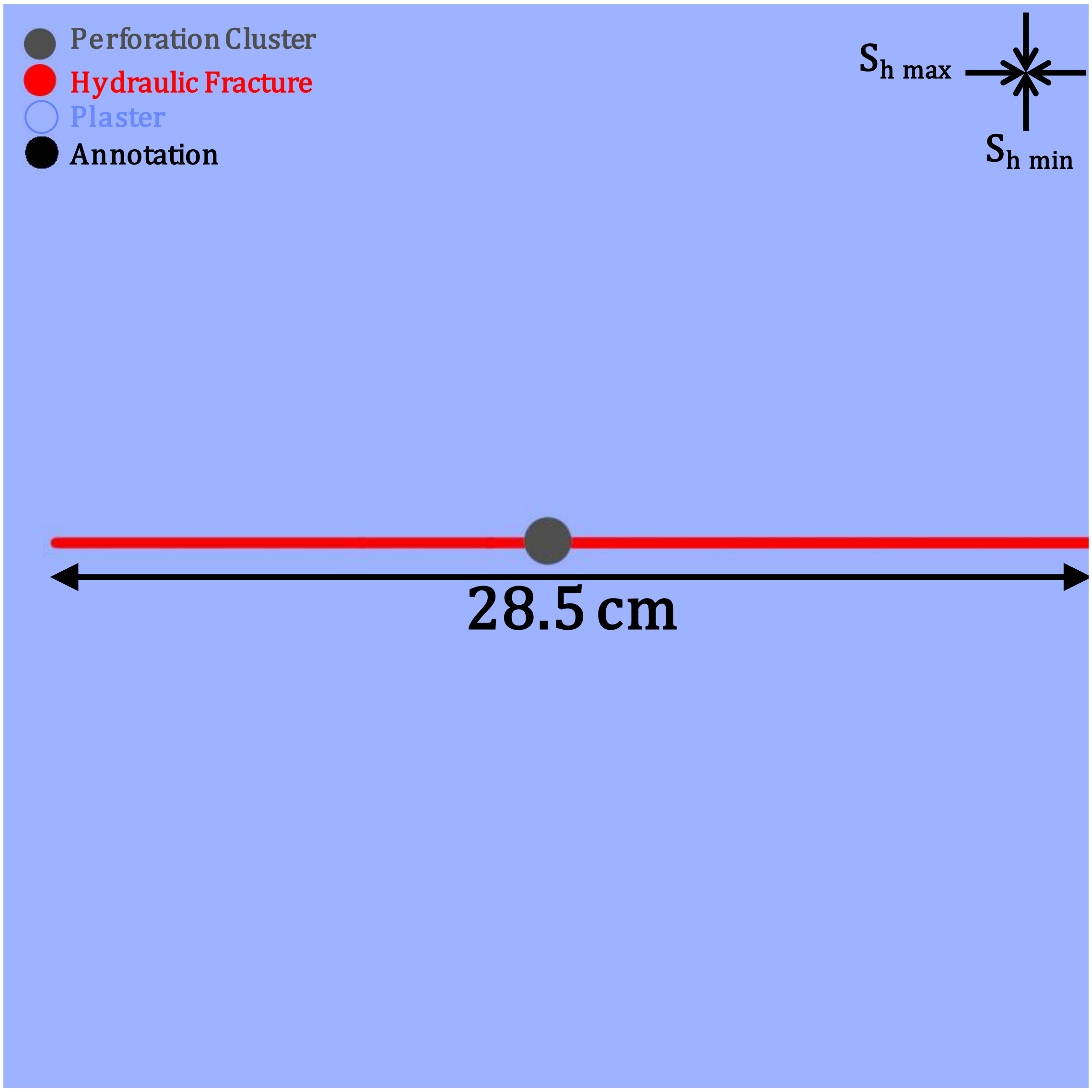

Figure 4.1: Top view illustration of the middle section of the block sample in test 1

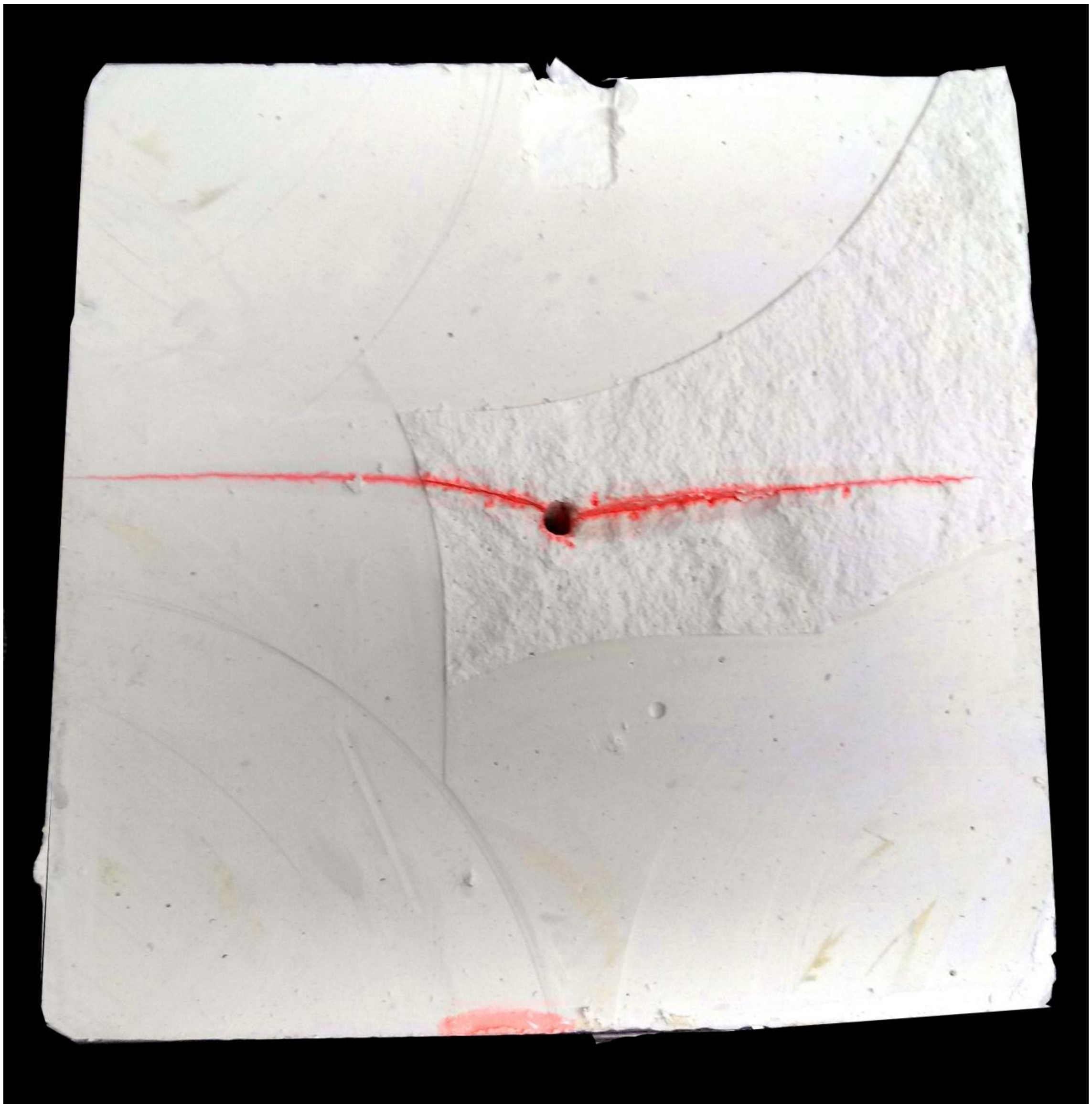

Figure 4.2: Top view photo of the middle section of the block sample in test 1 shows planar hydraulic fracture in red dye

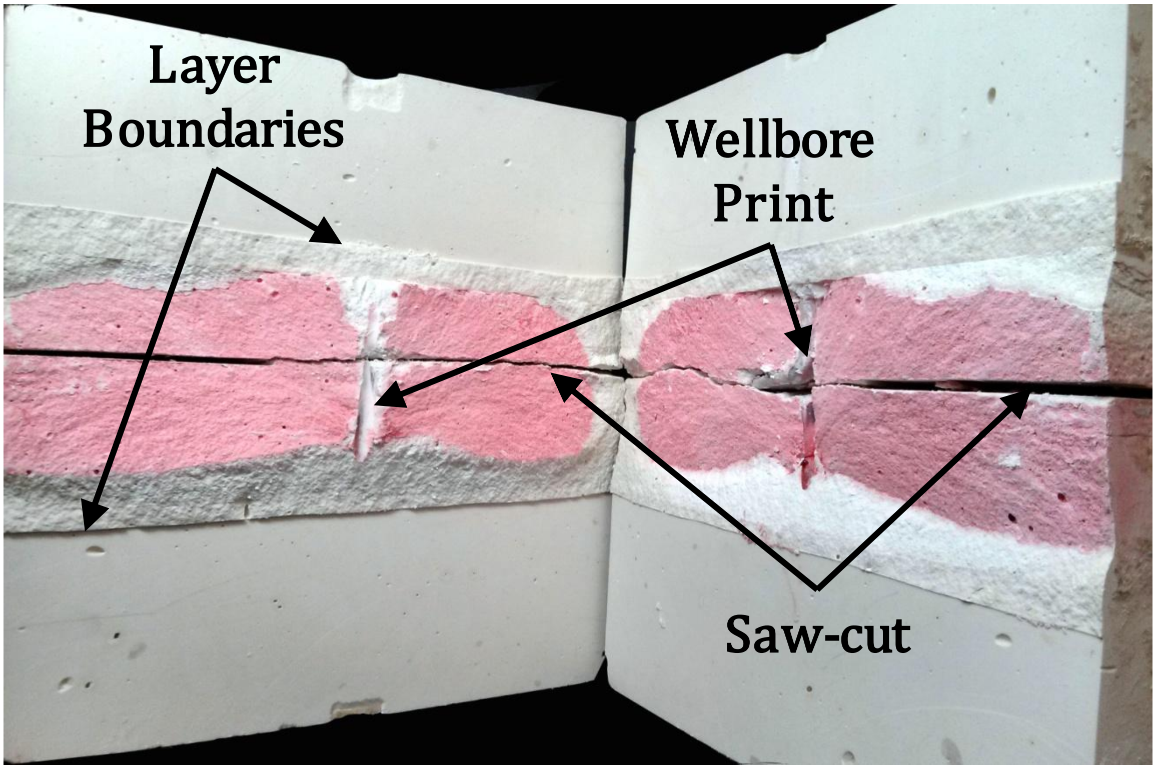

Figure 4.3: Cross-sectional view photo of the block sample in test 1 shows a well-contained planar hydraulic fracture in red dye

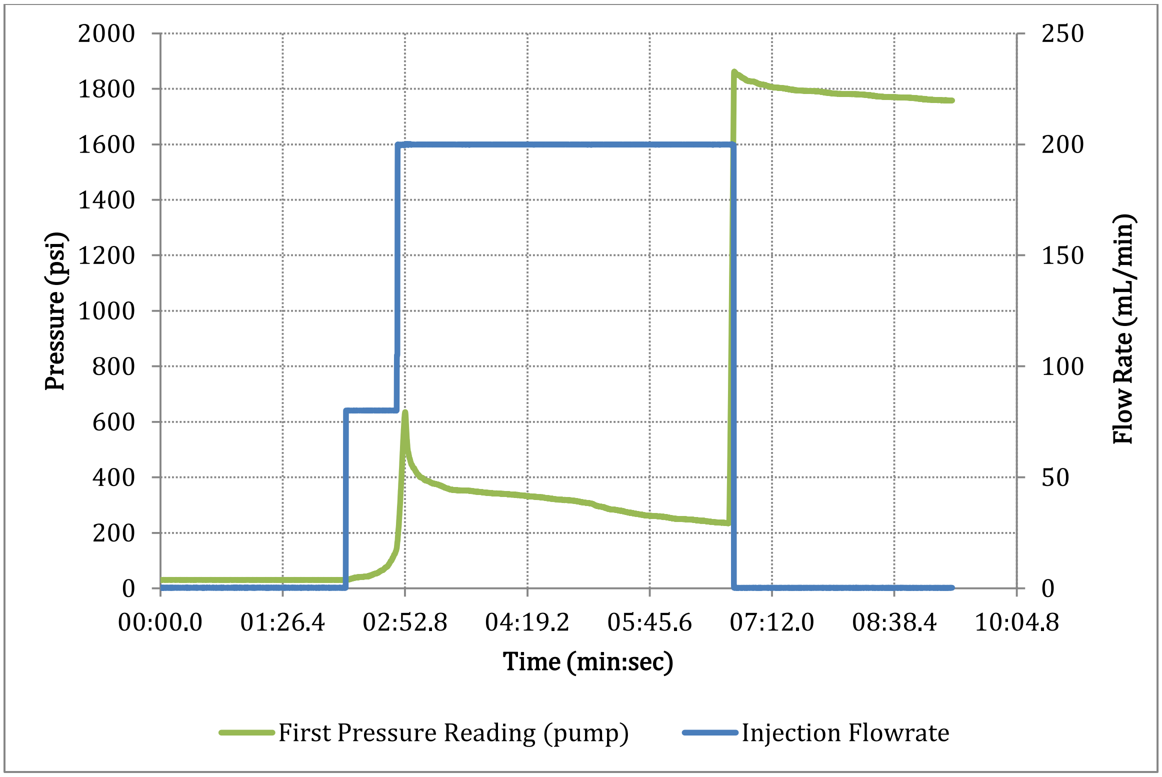

Figure 4.4: Injection pressure and flow rate profiles for hydraulic fracturing test 1 (the jump in pressure towards the end of the test was due to reaching stroke limits of the pump before it was shut off)

4.1.2 Test 2

Test 2 used regularly-sized, orthogonal pre-existing inclusions of the same type as the host layer, which was plaster. This test primarily tests the effect of PEF cementation on HF-PEF intersection outcomes. Test 2 resulted in HF crossing the pre-existing inclusions with signs of partial deflections along the pre-existing inclusions (Figures 4.5-4.9).

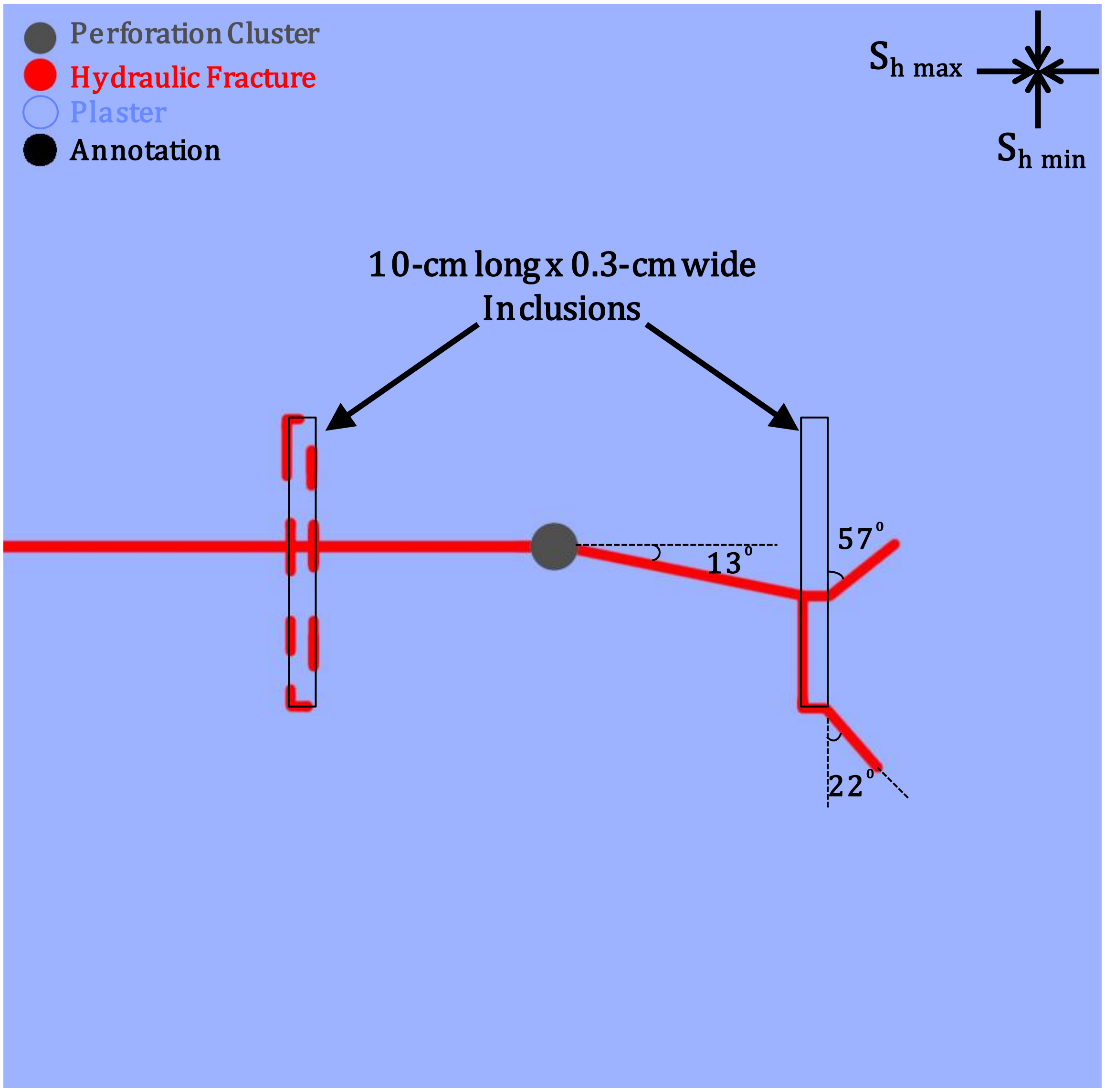

Figure 4.5: Top view illustration of the middle section of the block sample in test 2

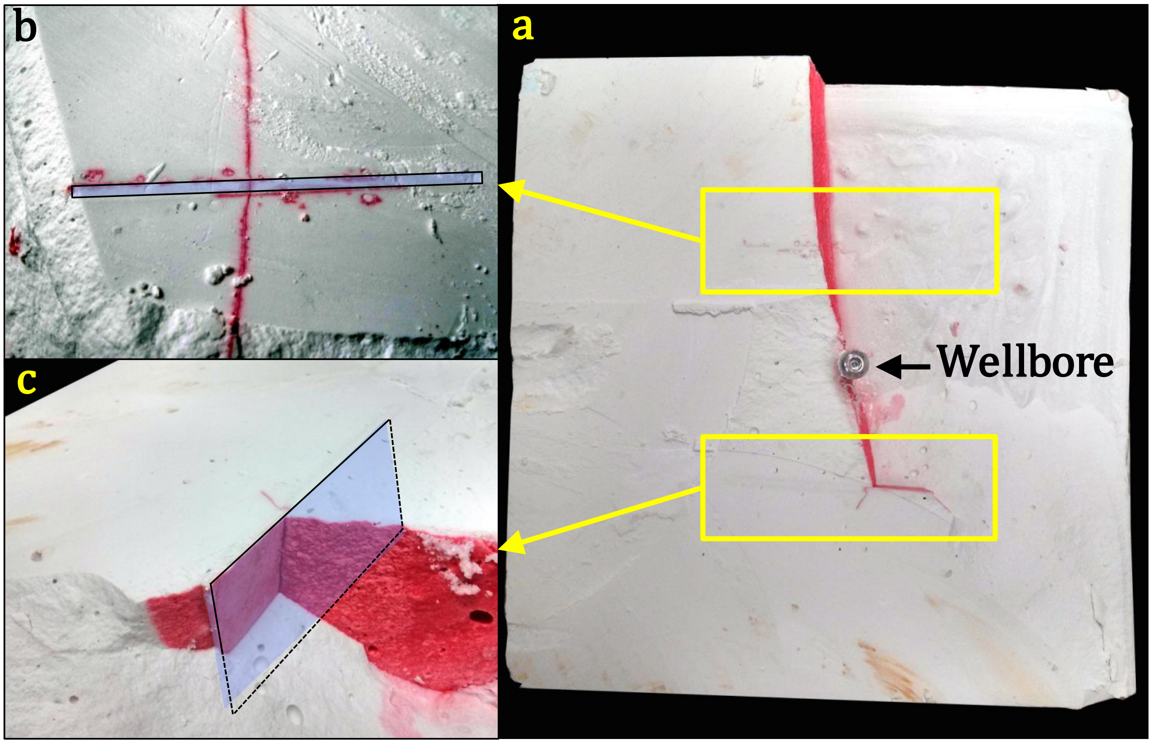

Figure 4.6: a) Bottom view photo of the middle section of the block sample in test 2 shows crossings and a deflection of hydraulic fracture propagation in red dye, b) Close-up top view photo of an embedded discontinuity (marked in blue shade) shows planar hydraulic fracture crossing with some fracturing fluid leakage along the discontinuity interface, and c) Close-up side view photo of an embedded discontinuity (marked in blue shade) shows crossing and deflection of hydraulic fracture propagation

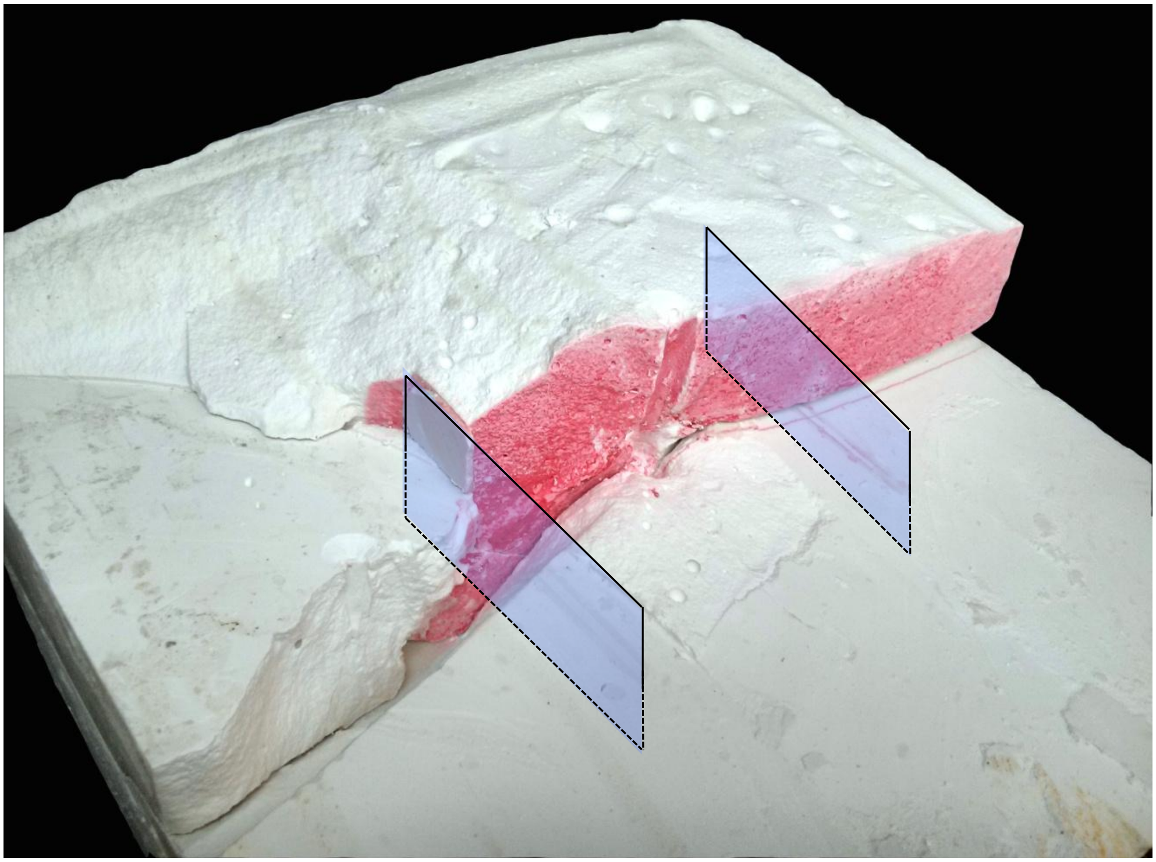

Figure 4.7: Side view photo of the block sample in test 2 shows hydraulic fracture (in red dye) crossing the embedded discontinuity (marked with blue shade) on the right side and deflecting with a downwards height bypass on the left side

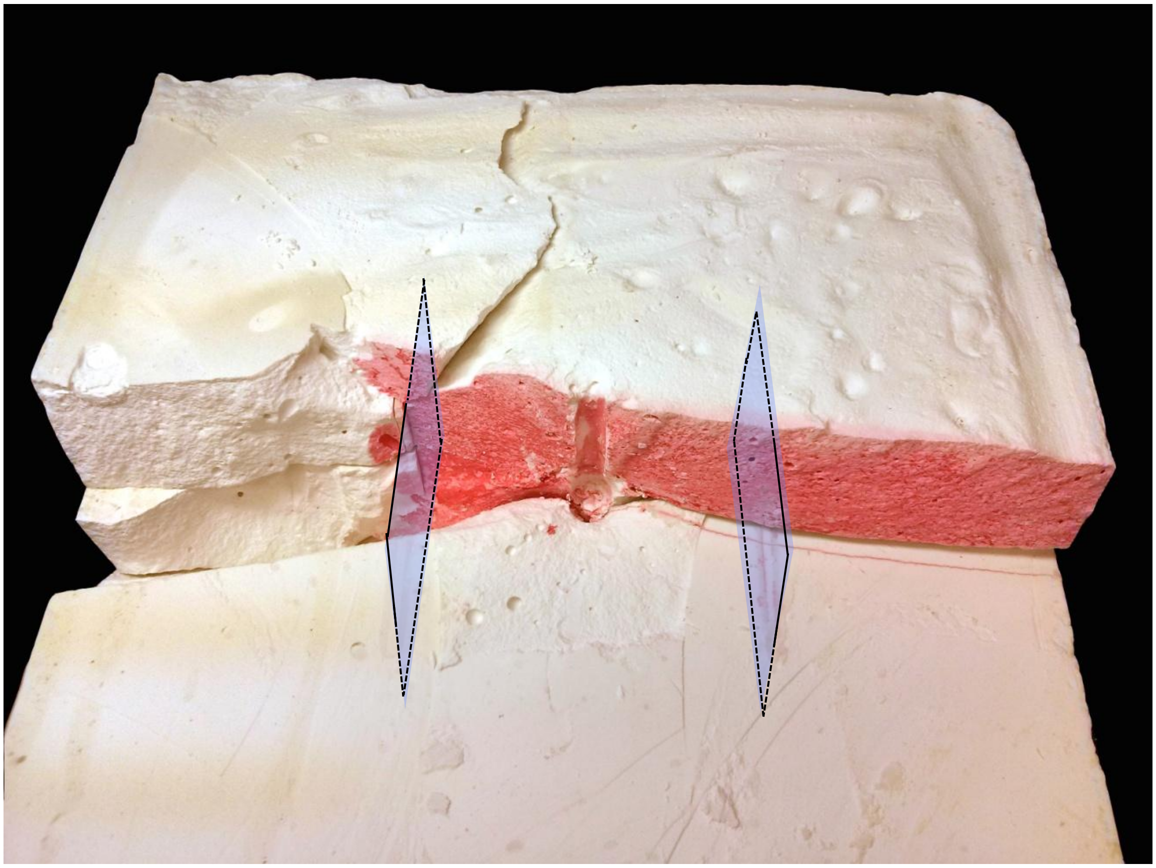

Figure 4.8: Side view photo of the block sample in test 2 shows hydraulic fracture (in red dye) crossing the embedded discontinuity (marked in blue shade) on the right side and crossing with an upwards height bypass on the left side

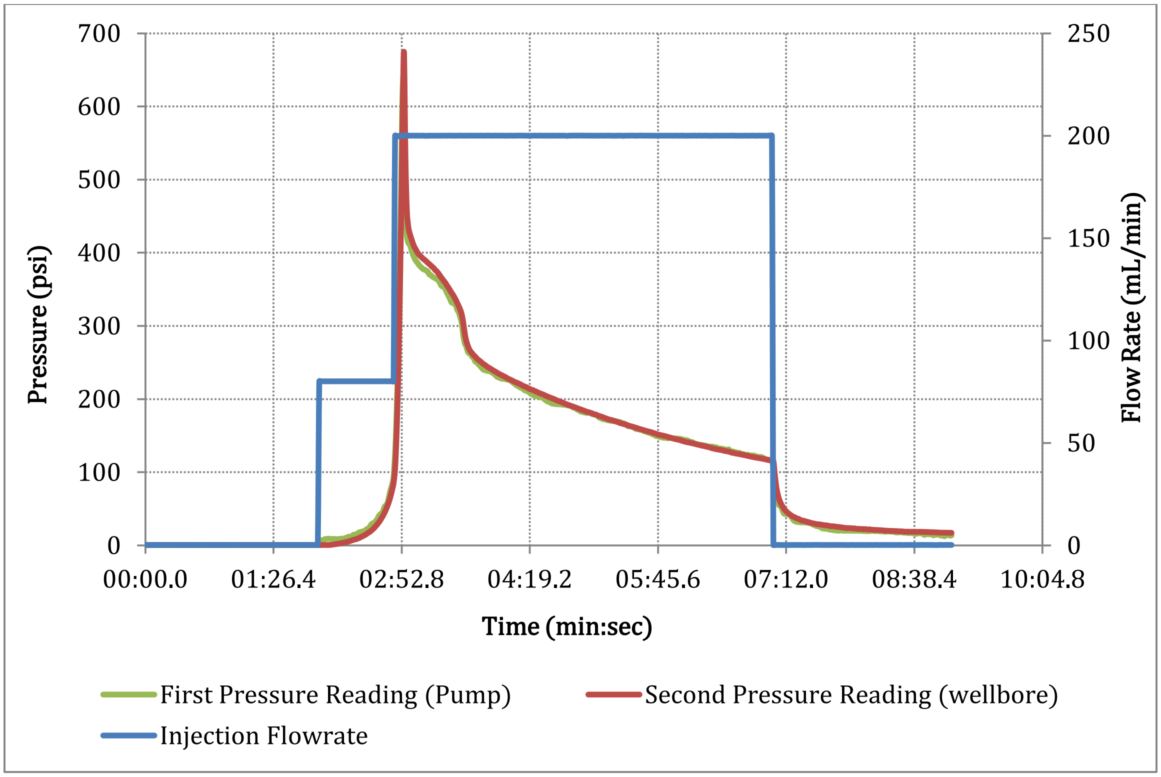

Figure 4.9: Injection pressure and flow rate profiles for hydraulic fracturing test 2

4.1.3 Test 3

Test 3 was similar to test 2 but with different synthetic-rock material. Test 3 used regularly-sized, orthogonal pre-existing inclusions of the same type as the host layer, which was hydrostone. This test primarily assesses the effect of the PEF cementation on HF-PEF intersection outcomes. Test 3 resulted in HF crossing the pre-existing inclusions (Figures 4.10-4.15).

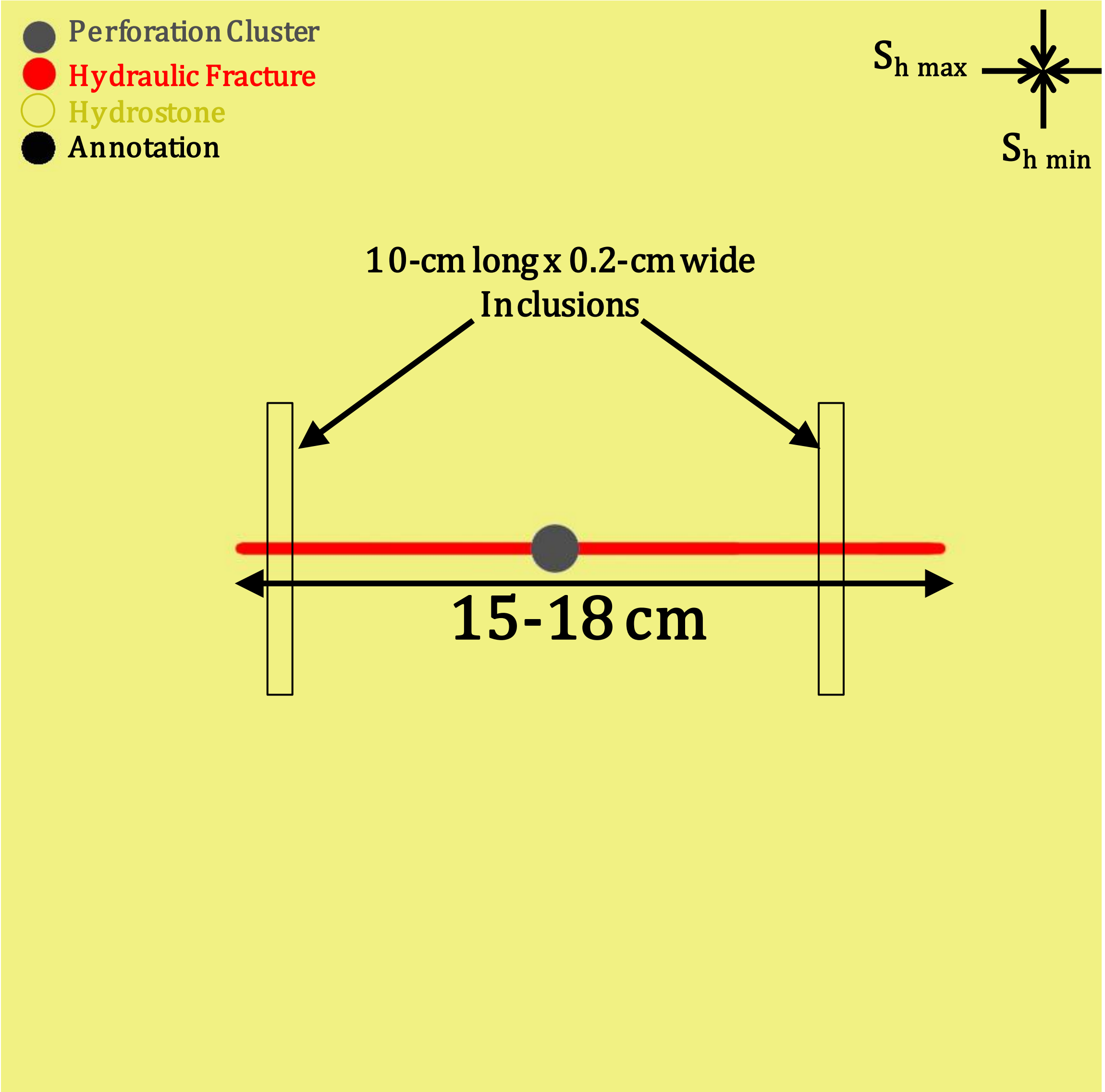

Figure 4.10: Top view illustration of the middle section of the block sample in test 3

Figure 4.11: Top view photo of the middle section of the block sample in test 3 shows hydraulic fracture (in red dye) planar crossing of embedded inclusions (in yellow shade)

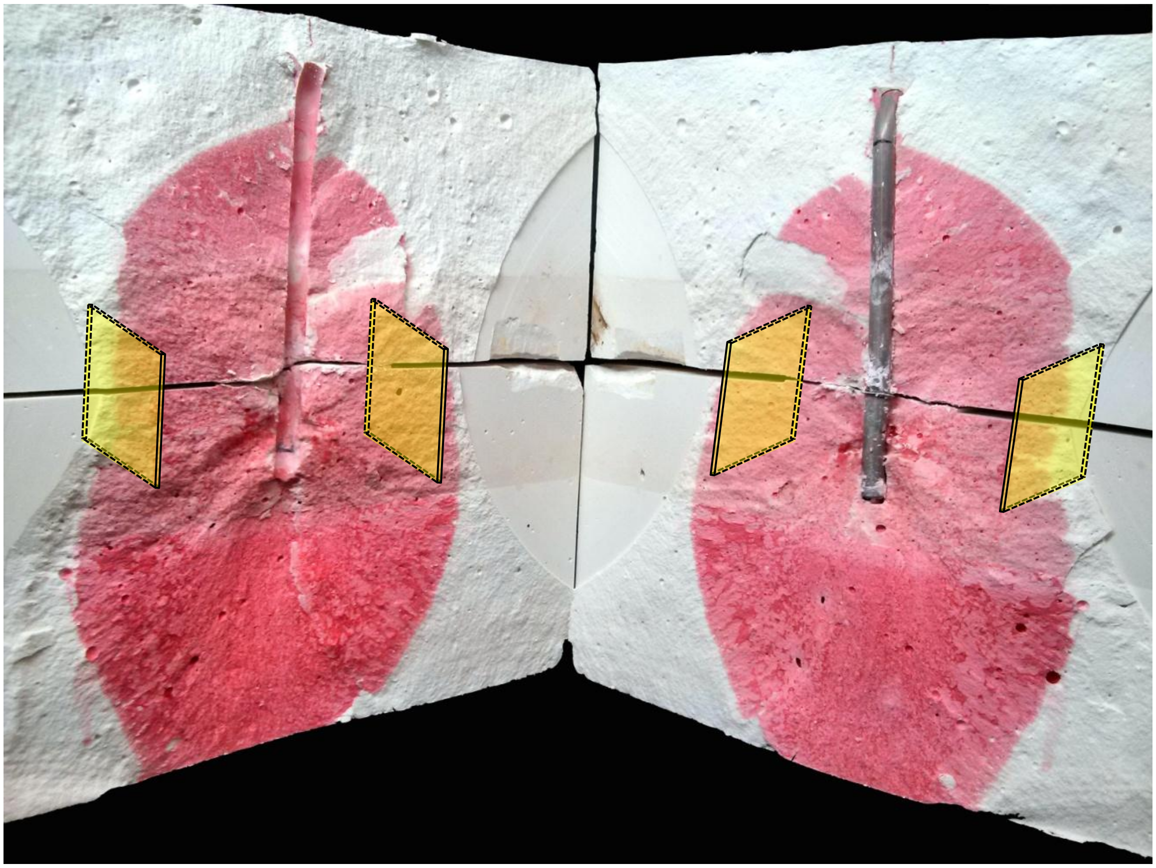

Figure 4.12: Cross-sectional view photo of the block sample in test 3 shows hydraulic fracture (in red dye) planar crossing of embedded discontinuities (marked in yellow shade) and bedding planes

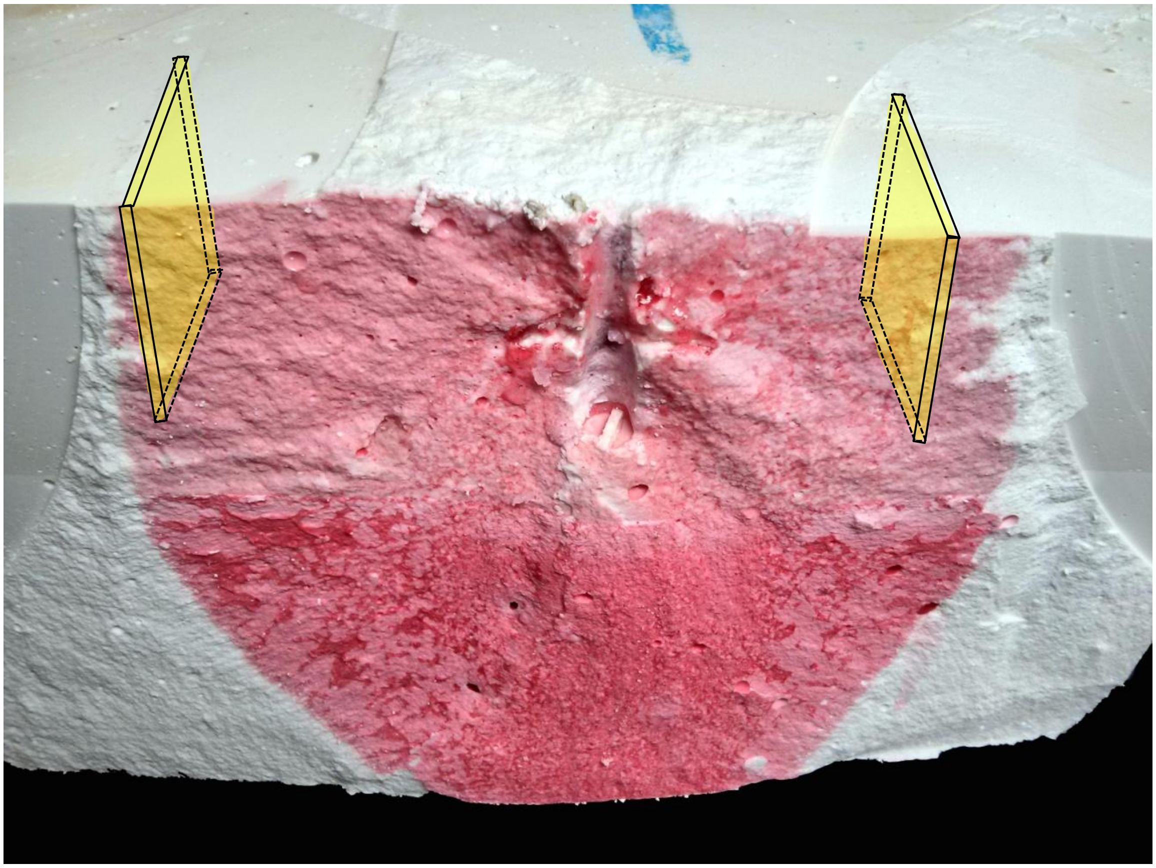

Figure 4.13: Close-up side view photo of the sample in test 3 shows hydraulic fracture (in red dye) crossing embedded discontinuities (marked in yellow shade) on both right and left sides as well as crossing bedding plane through height growth downwards

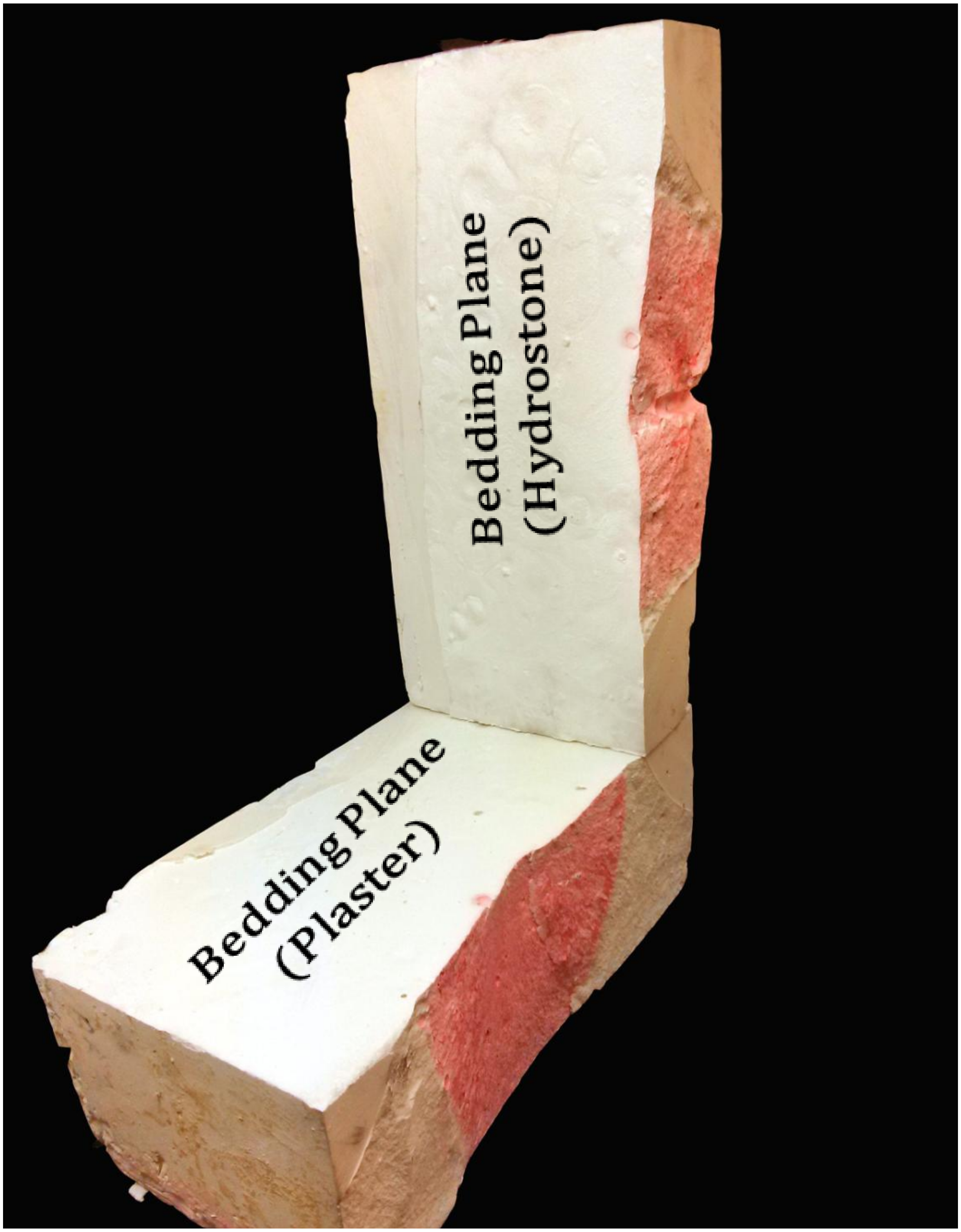

Figure 4.14: Side view photo of the block sample in test 3 shows hydraulic fracture (in red dye) planar crossing of a bedding plane without fluid leakage along the bedding-plane interface

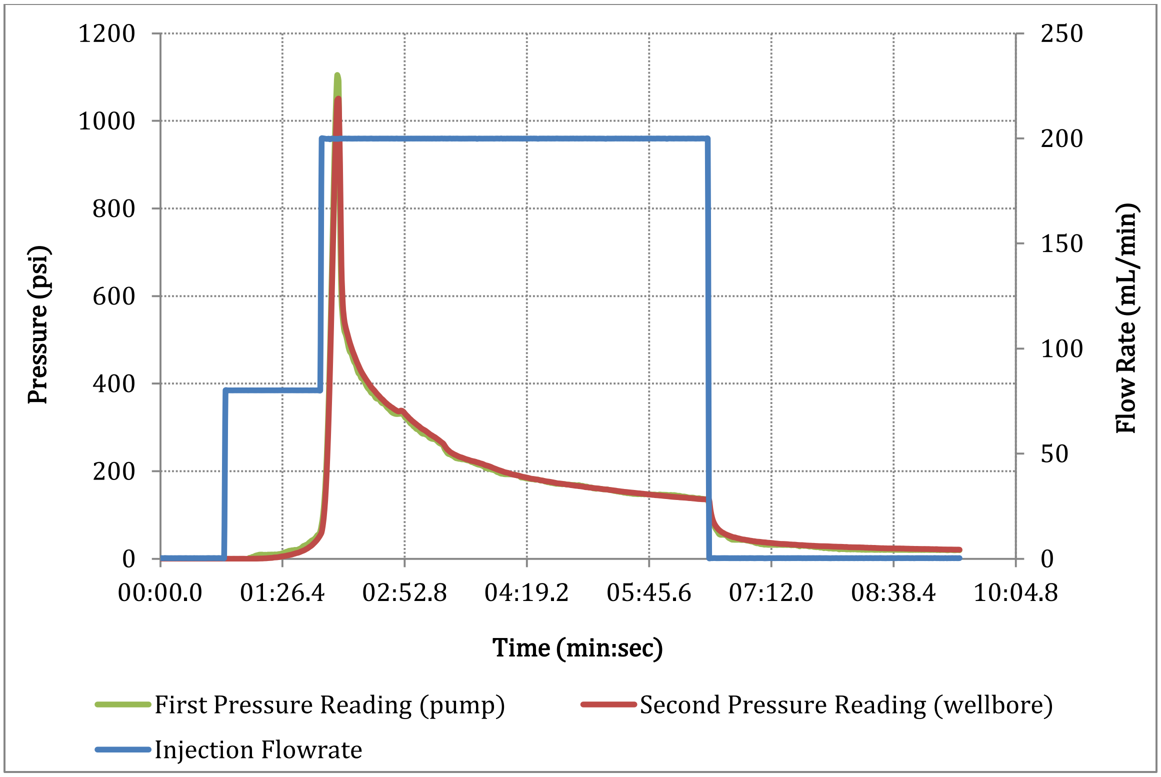

Figure 4.15: Injection pressure and flow rate profiles for hydraulic fracturing test 3

4.1.4 Test 4

The sample in this test was similar to test 2 but using thicker pre-existing inclusions. Test 4 used exaggeratedly wide, orthogonal pre-existing inclusions of the same type as the host layer, which was plaster. This test primarily examines the effect of PEF aperture on HF-PEF intersection outcomes. Test 4 resulted in HF crossing the pre-existing inclusions with some deflections and non-planar behavior (Figures 4.16-4.20).

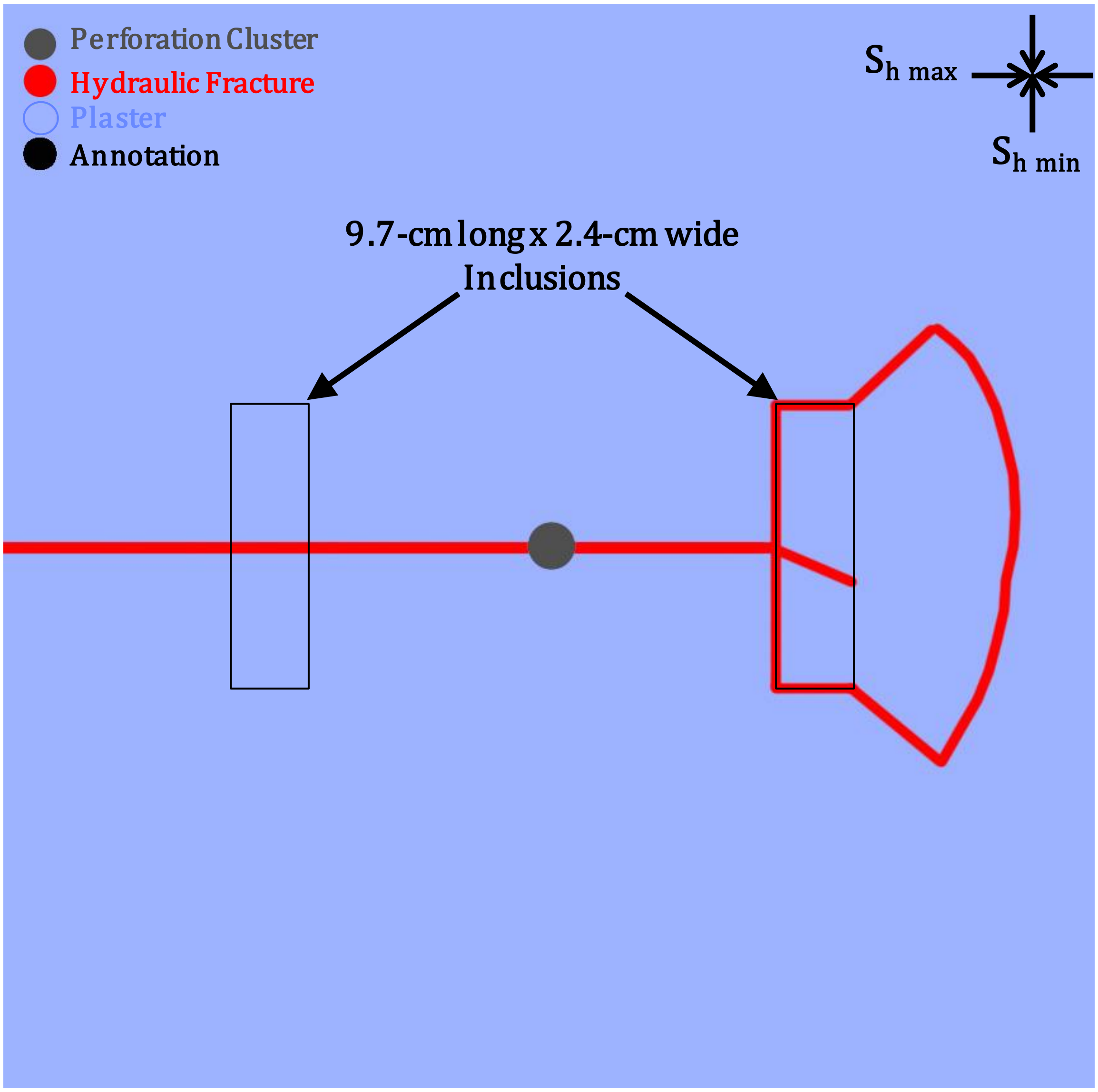

Figure 4.16: Top view illustration of the middle section of the block sample in test 4

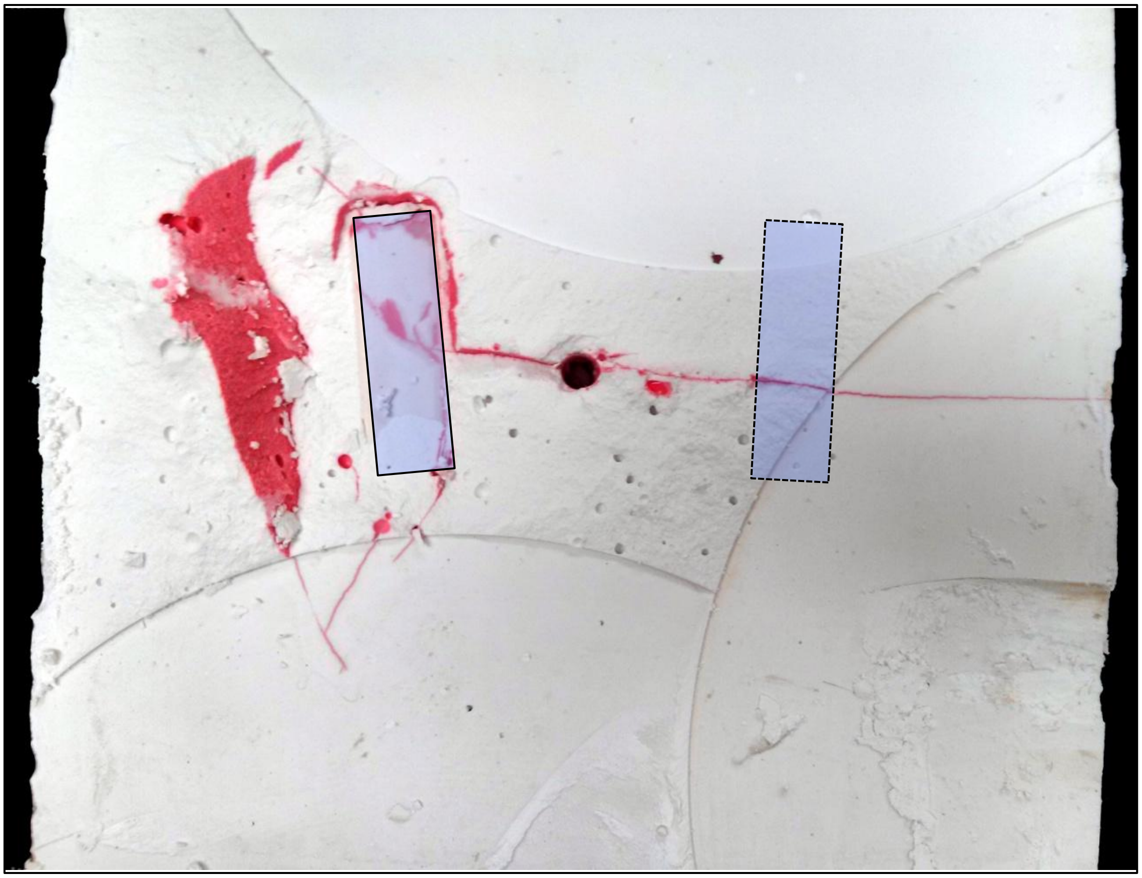

Figure 4.17: Top view photo of the middle section of the block sample in test 4 shows hydraulic fracture (in red dye) crossing and deflecting from embedded discontinuities (marked in blue shade)

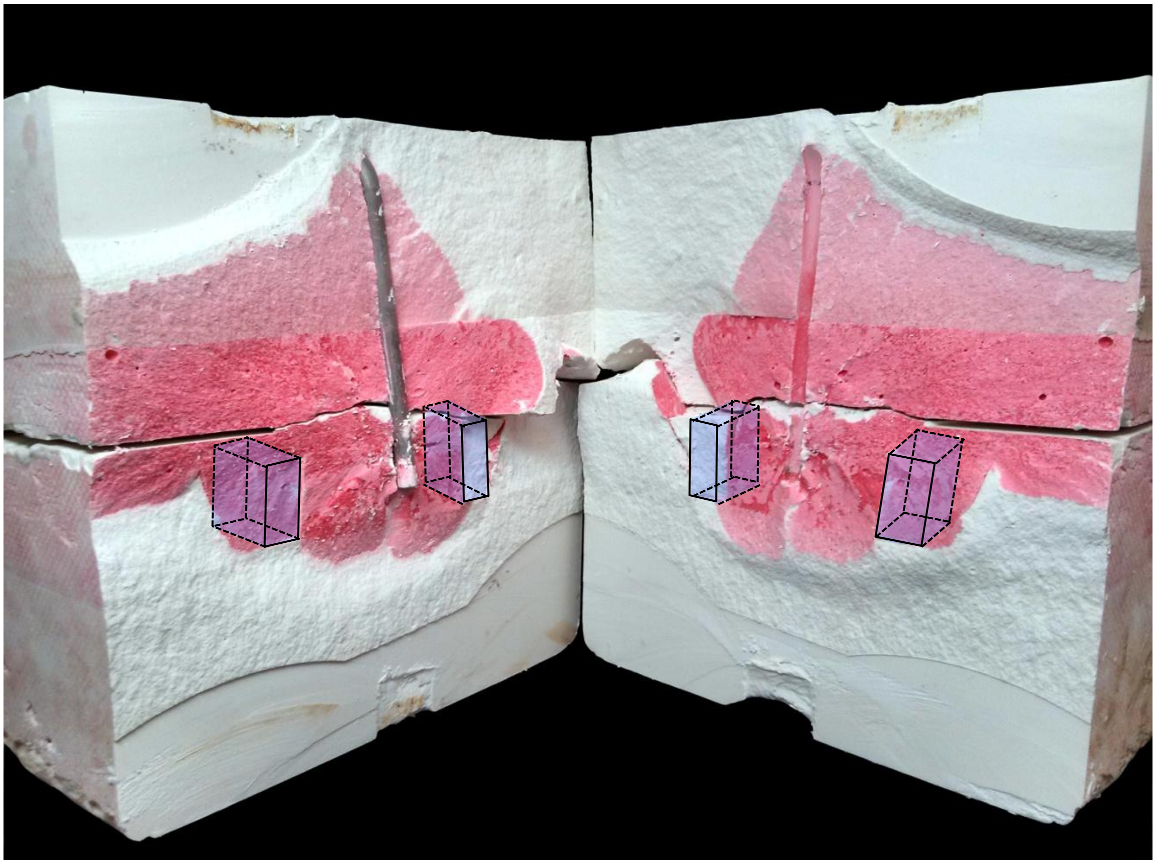

Figure 4.18: Cross-sectional view photo of the block sample in test 4 shows hydraulic fracture (in red dye) planar crossing of an embedded discontinuity (marked in blue shade) from one side, leaking along the interface and deflecting off of the other embedded discontinuity on the other side, and planar crossing of bedding planes

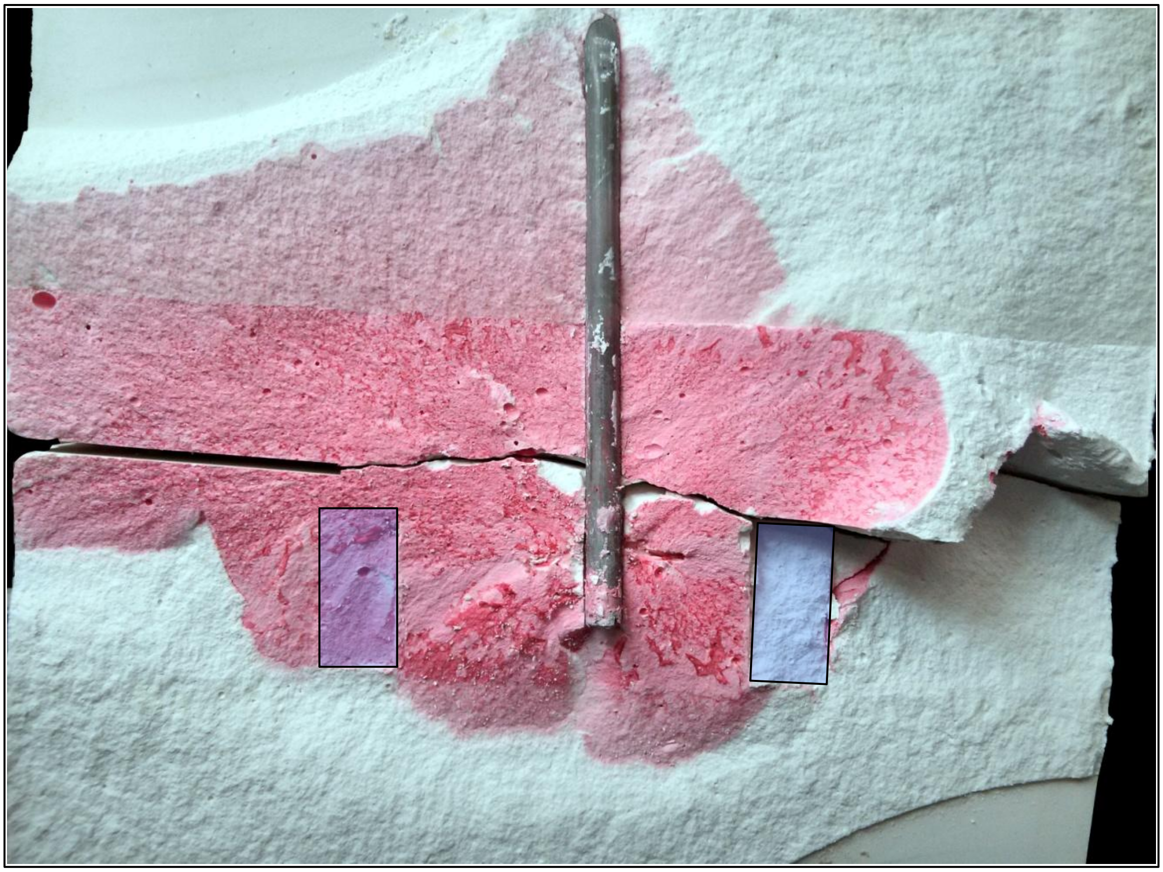

Figure 4.19: Cross-sectional view photo of the block sample in test 4 shows hydraulic fracture (in red dye) crossing and deflecting from embedded discontinuities (marked in blue shade)

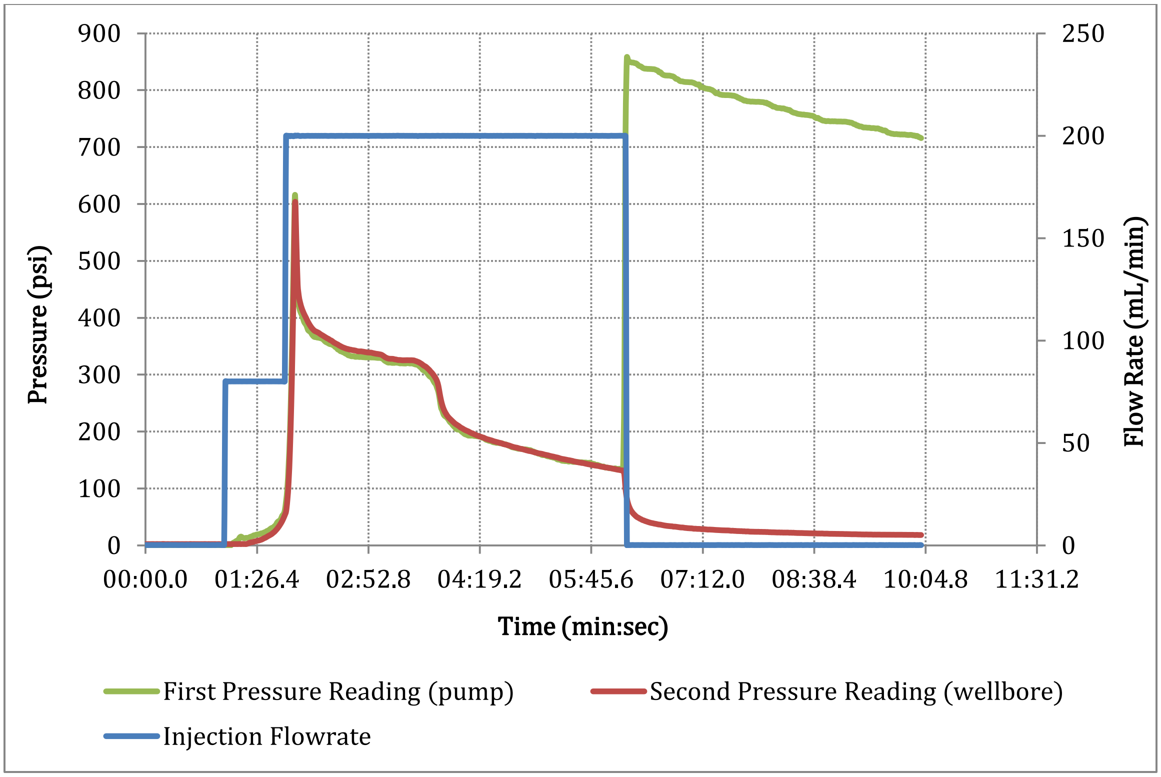

Figure 4.20: Injection pressure and flow rate profiles of hydraulic fracturing test 4

4.1.5 Test 5

Test 5 was identical to test 3 except for the use of thicker pre-existing inclusions. Test 5 used exaggeratedly wide, orthogonal pre-existing inclusions of the same type as the host layer, which was hydrostone. This test primarily examines the effect of PEF aperture on HF-PEF intersection outcomes. Test 5 resulted in HF crossing the pre-existing inclusions with some leakage along portions of the pre-existing inclusions (Figures 4.21-4.26).

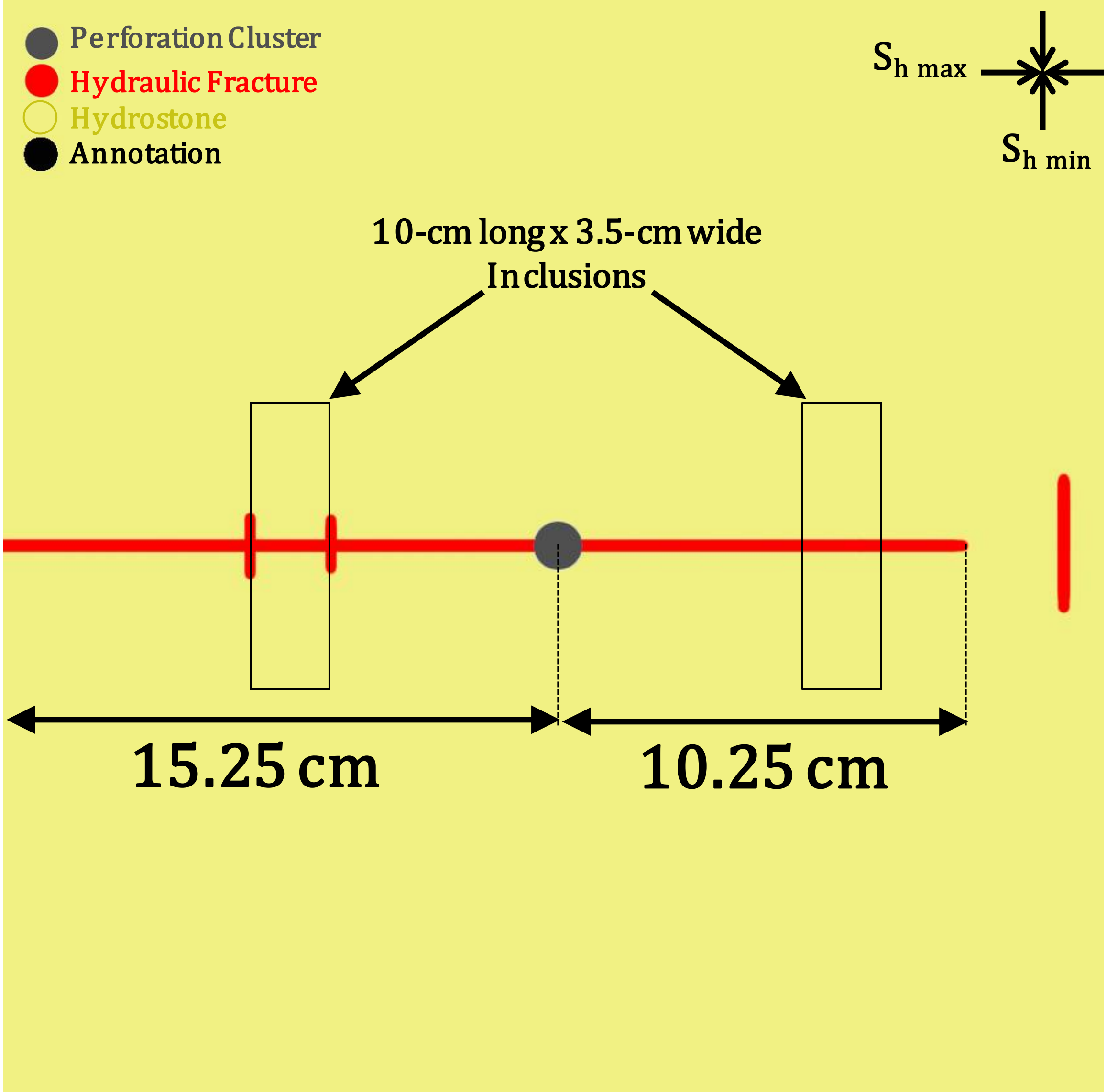

Figure 4.21: Top view illustration of the middle section of the block sample in test 5

Figure 4.22: Top view photo of the middle section of the block sample in test 5 shows hydraulic fracture (in red dye) planar crossing embedded discontinuity (marked in yellow shade)

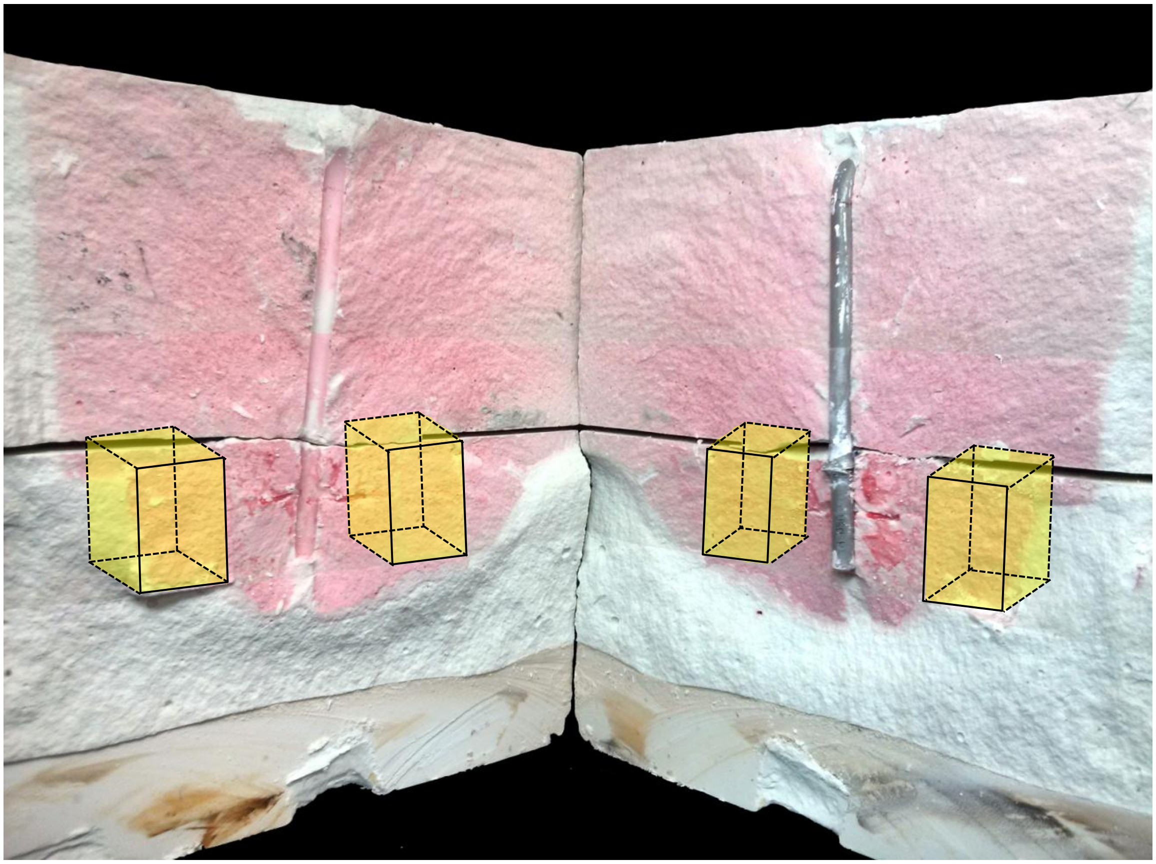

Figure 4.23: Cross-sectional view photo of the block sample in test 5 shows hydraulic fracture (in red dye) planar crossing embedded discontinuities (marked in yellow shade) and bedding planes

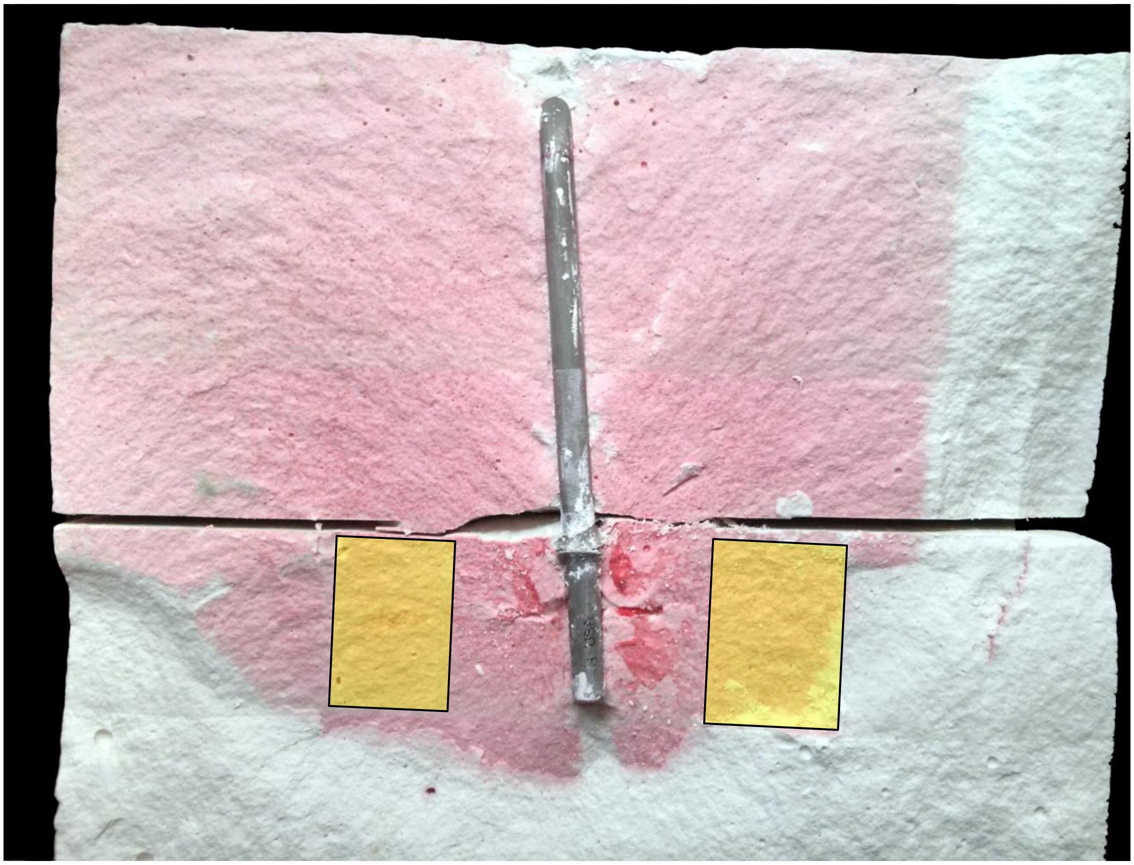

Figure 4.24: Cross-sectional view photo of the block sample in test 5 shows hydraulic fracture (in red dye) planar crossing embedded discontinuities (marked in yellow shade) and bedding planes

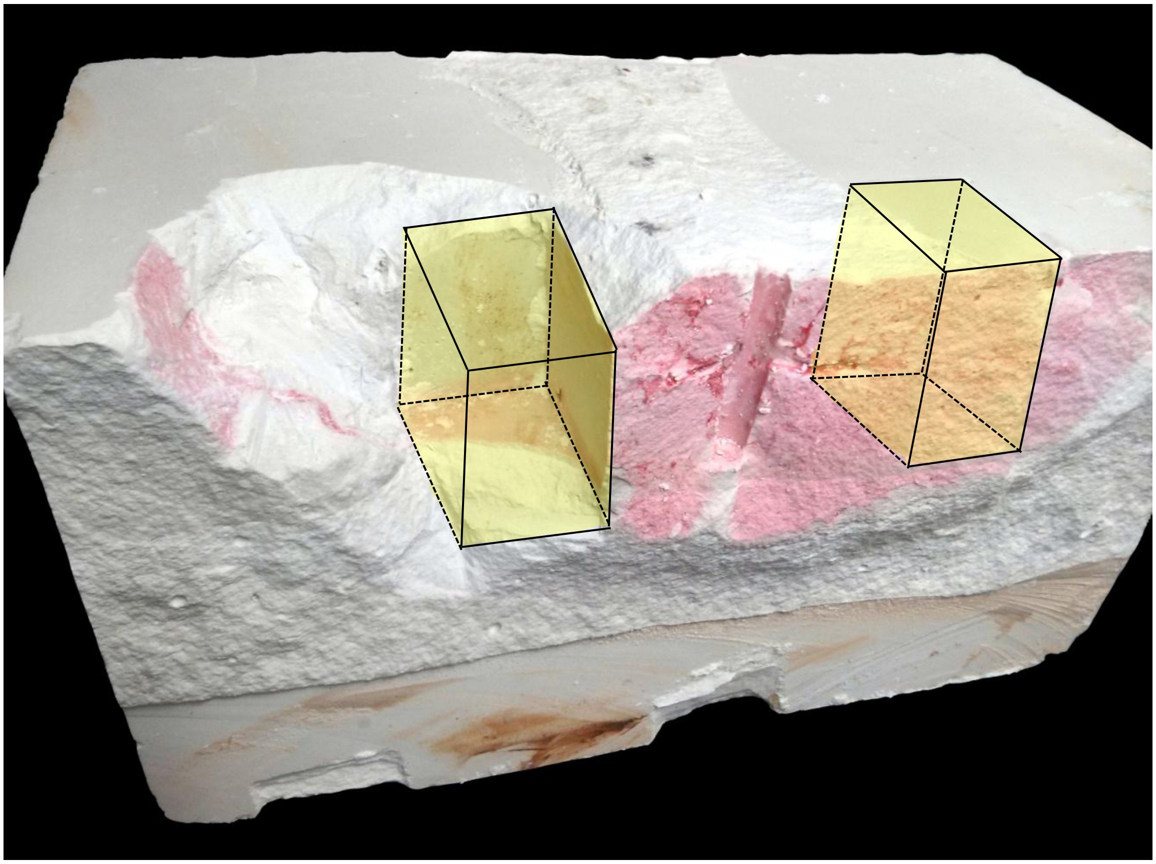

Figure 4.25: Side view photo of the block sample in test 5 shows hydraulic fracture (in red dye) crossing an embedded discontinuity (marked in yellow shade) on the right side and fracturing fluid leaking along the bottom interface of another embedded discontinuity on the left side

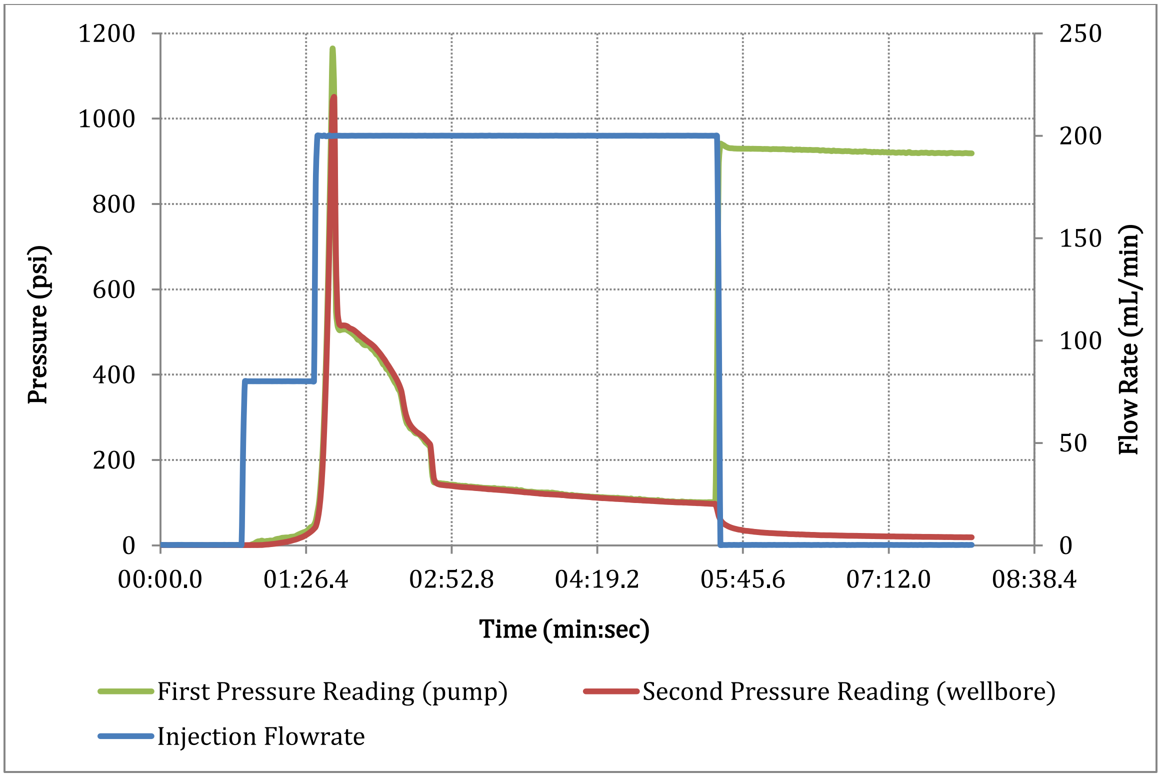

Figure 4.26: Injection pressure and flow rate profiles of hydraulic fracturing test 5 (the jump in pressure towards the end of the test was due to reaching stroke limits of the pump before it was shut off)

4.1.6 Test 6

Similar to tests 2 and 3, this test used regularly-sized, orthogonal pre-existing forms of discontinuity but without using cement-fill. In other words, test 6 used non-cemented, pressurized pre-existing inclusions to test for HF-PEF intersection outcomes. Test 6 resulted in HF deflection and branching out (Figures 4.27-4.32).

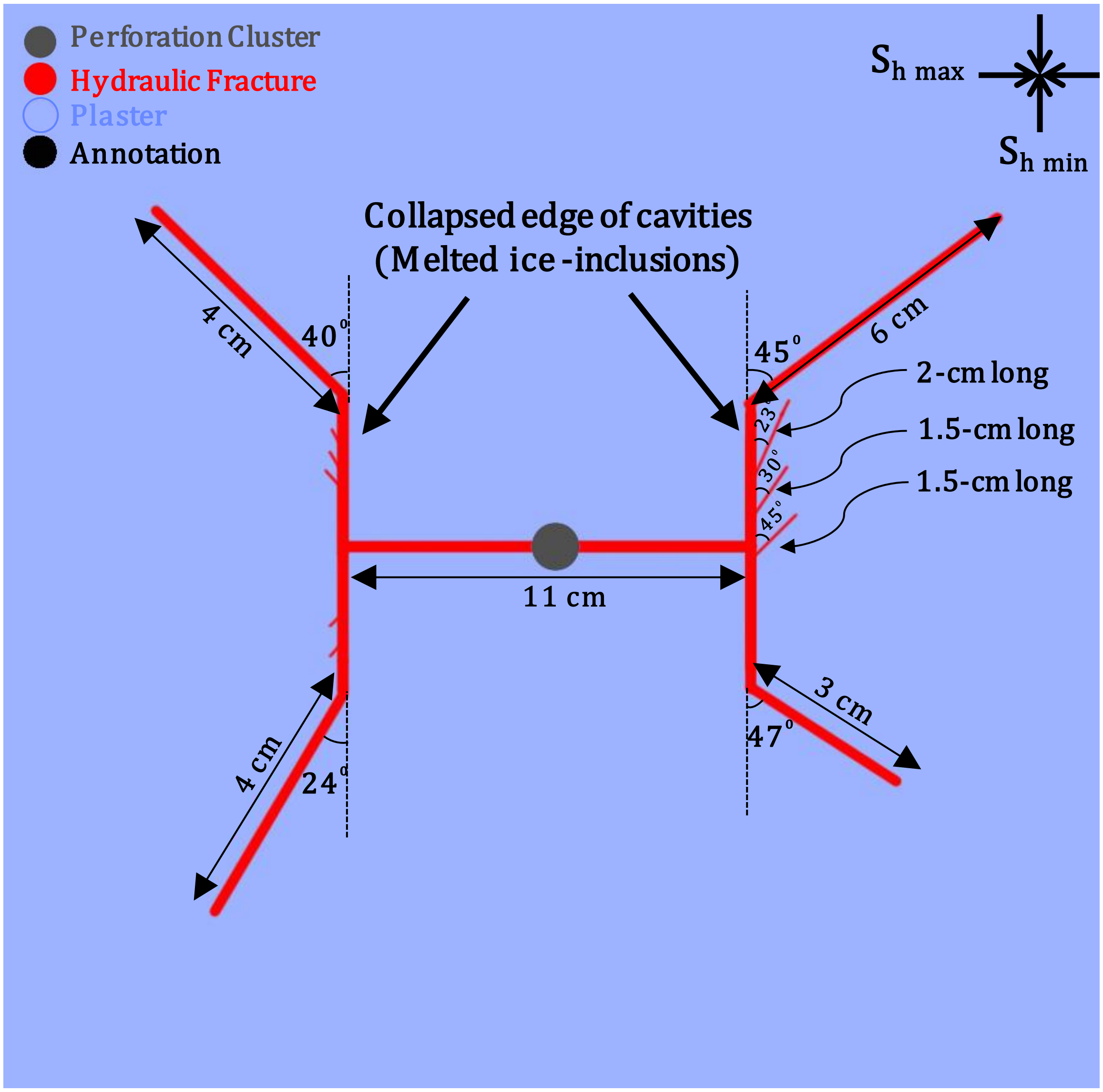

Figure 4.27: Top view illustration of the middle section of the block sample in test 6

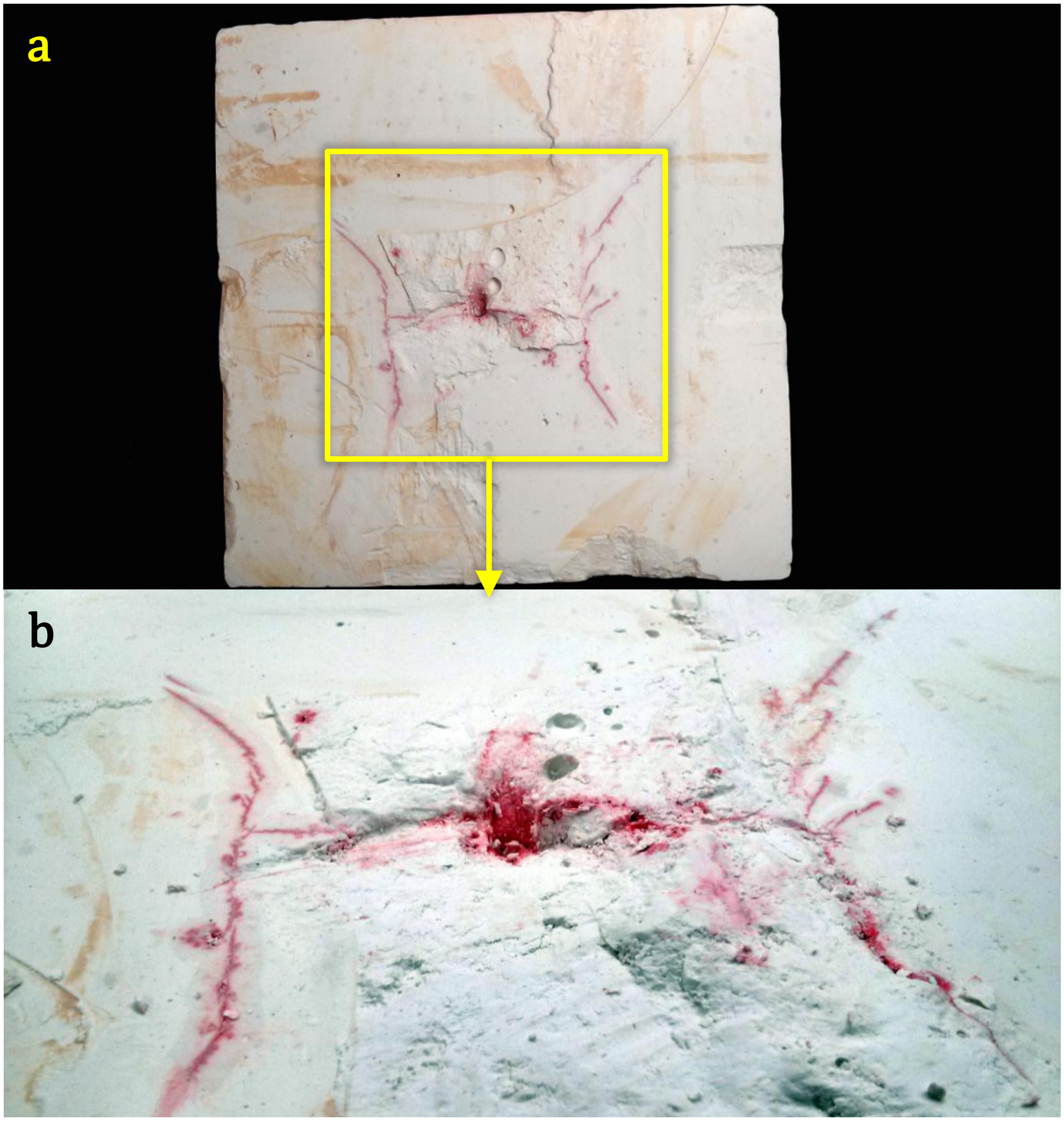

Figure 4.28: a) Top view photo of the middle section of the block sample in test 6 shows hydraulic fracture (in red dye) intersecting collapsed orthogonal cavities and deflecting along and off of them, b) close-up view photo of the middle section of the block sample in test 6 shows hydraulic fracture (in red dye) intersecting collapsed orthogonal cavities, reorienting along them, and resulting into multi-stranded, deflected fractures

Figure 4.29: Side view photo of the block sample in test 6 shows hydraulic fracture intersecting collapsed orthogonal cavities, reorienting along them, and deflecting off of them.

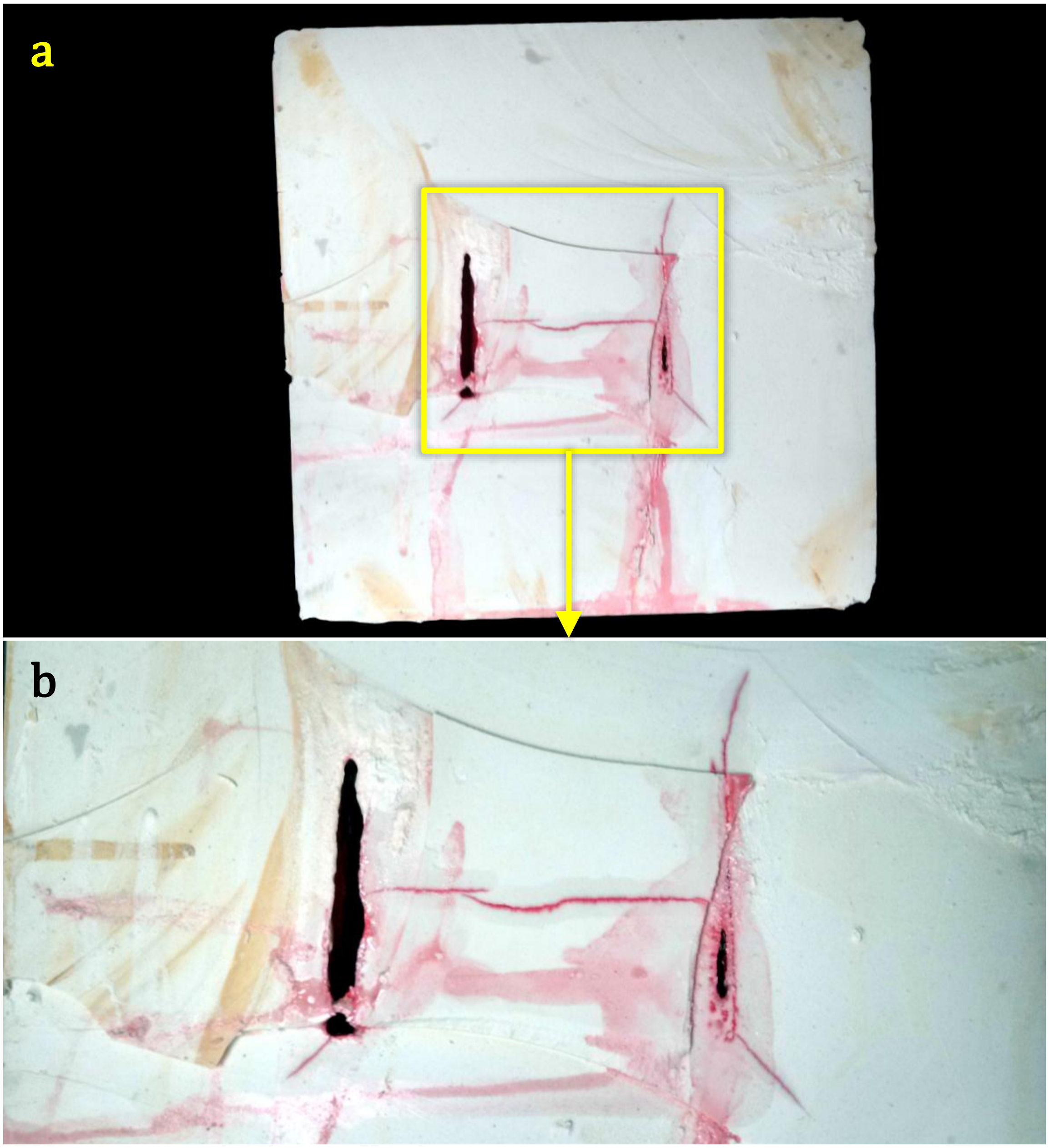

Figure 4.30: a) Bottom view photo of the lower bedding plane section of the block sample in test 6 shows hydraulic fracture (in red dye) intersecting embedded orthogonal cavities (note fracturing fluid traces along the bedding plane indicating fluid leakage along the interface of the layer boundaries), b) close-up bottom view photo of the lower bedding plane section of the block sample in test 6 shows hydraulic fracture (in red dye) intersecting orthogonal cavities, arresting at the intersection points, and propagating into deflected paths from the side edges of the cavities

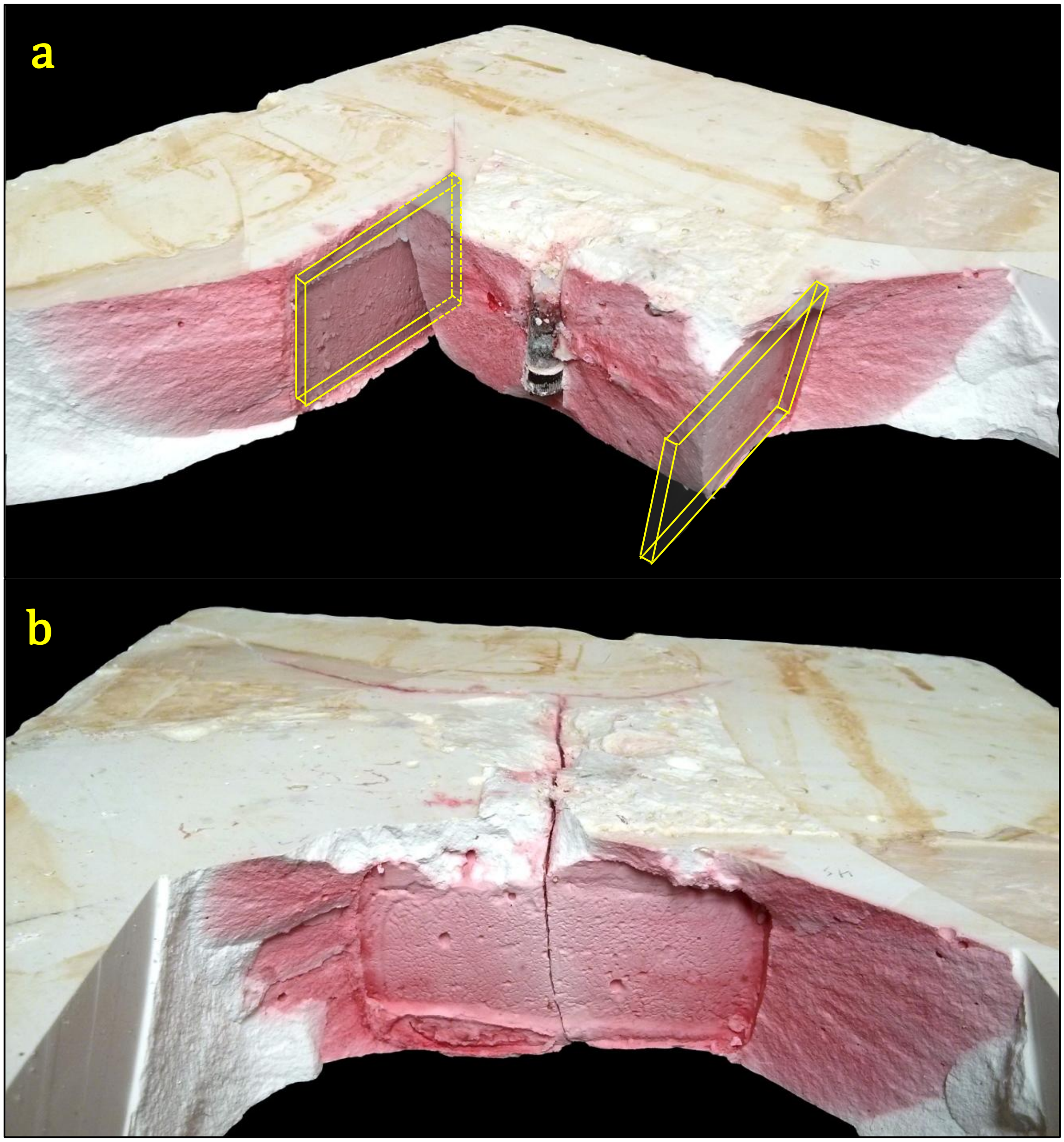

Figure 4.31: a-b) Side view photos of block sample in test 6 shows hydraulic fracture (in red dye) intersecting embedded orthogonal cavities and deflecting from their side edges

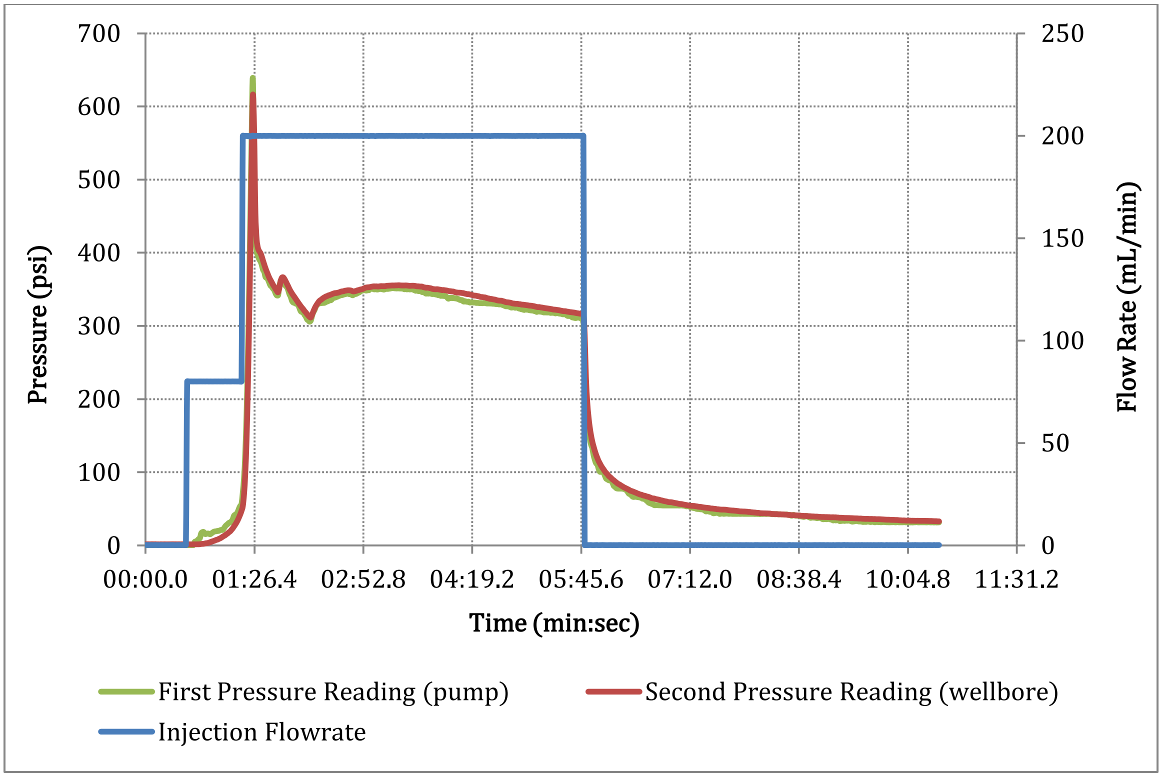

Figure 4.32: Injection pressure and flow rate profiles of the hydraulic fracturing test 6

4.1.7 Test 7

Like tests 2 and 3, test 7 also used regularly-sized, orthogonal pre-existing inclusions but had contrasting synthetic-rock material for the pre-existing inclusion and the host layer. That is, hydrostone inclusion in plaster host layer. This test primarily tests for the effect of PEF cementation on HF-PEF intersection outcomes. Test 7 resulted in HF deflection and branching out propagation (Figures 4.33-4.36).

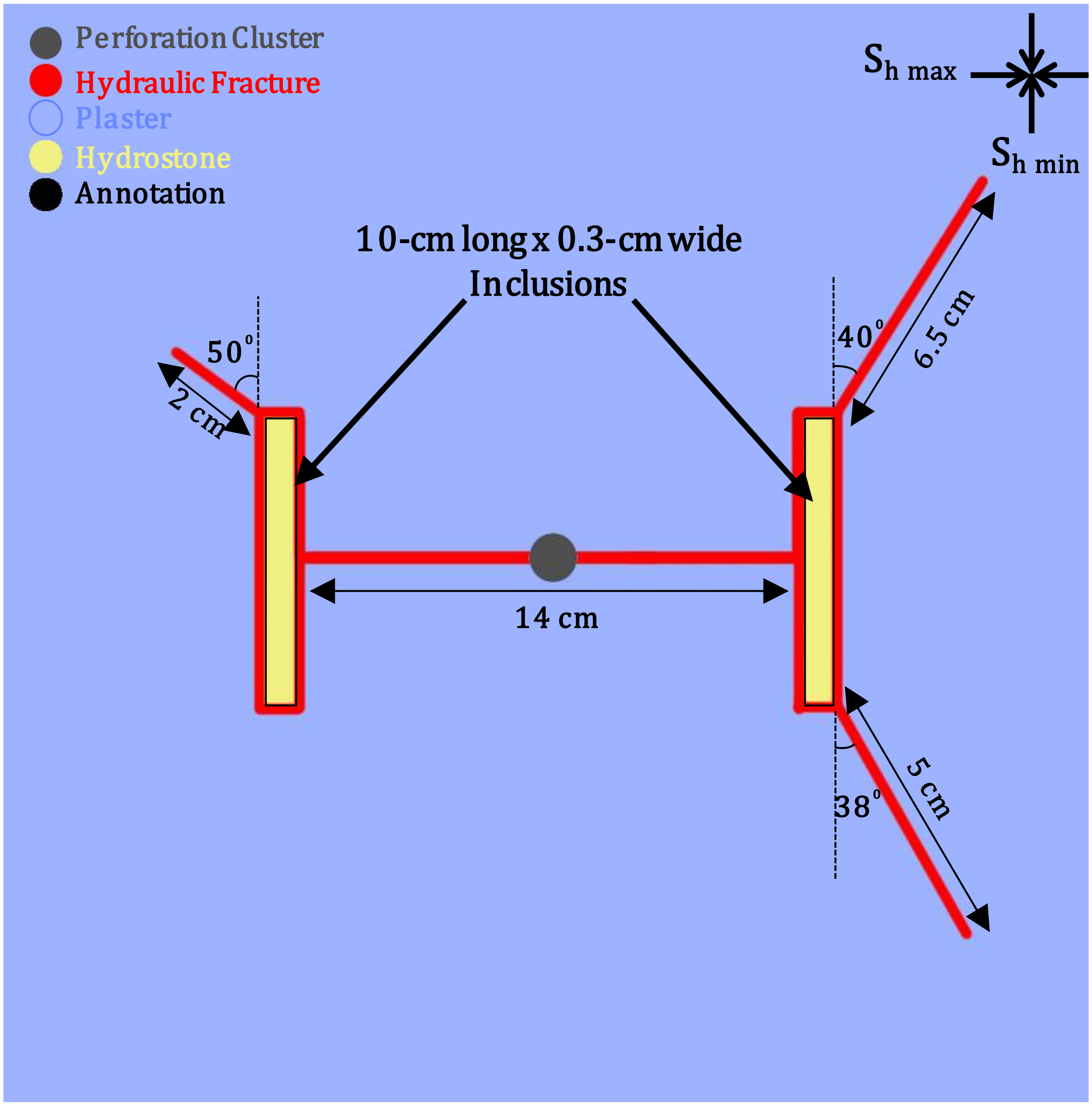

Figure 4.33: Top view illustration of the middle section of the block sample in test 7

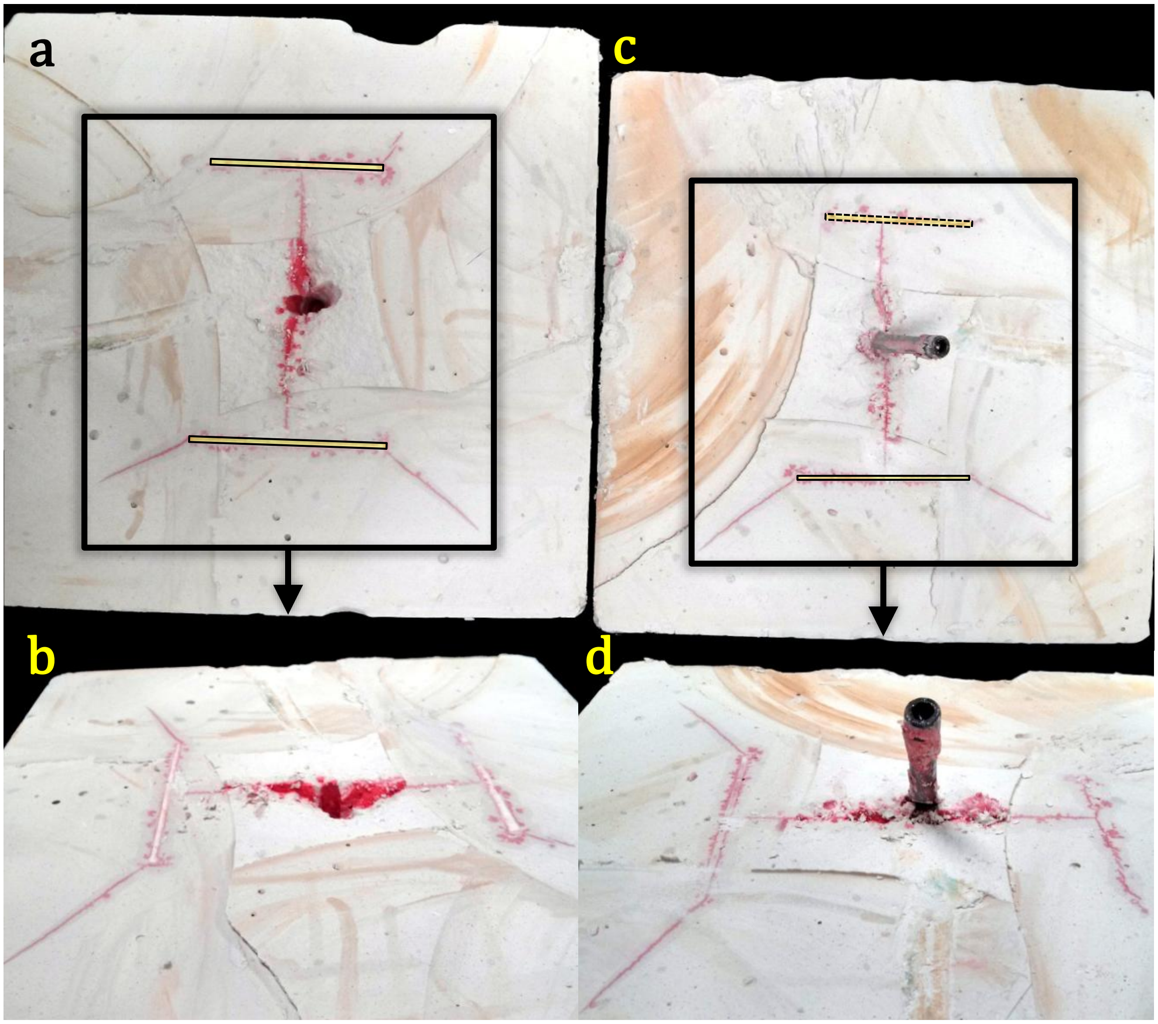

Figure 4.34: a-b) Top view photos and c-d) bottom view photos of the middle section of the block sample in test 7 shows hydraulic fracture (in red dye) intersecting embedded discontinuities (marked in yellow shade), leaking along their interfaces, and deflecting off of their side edges

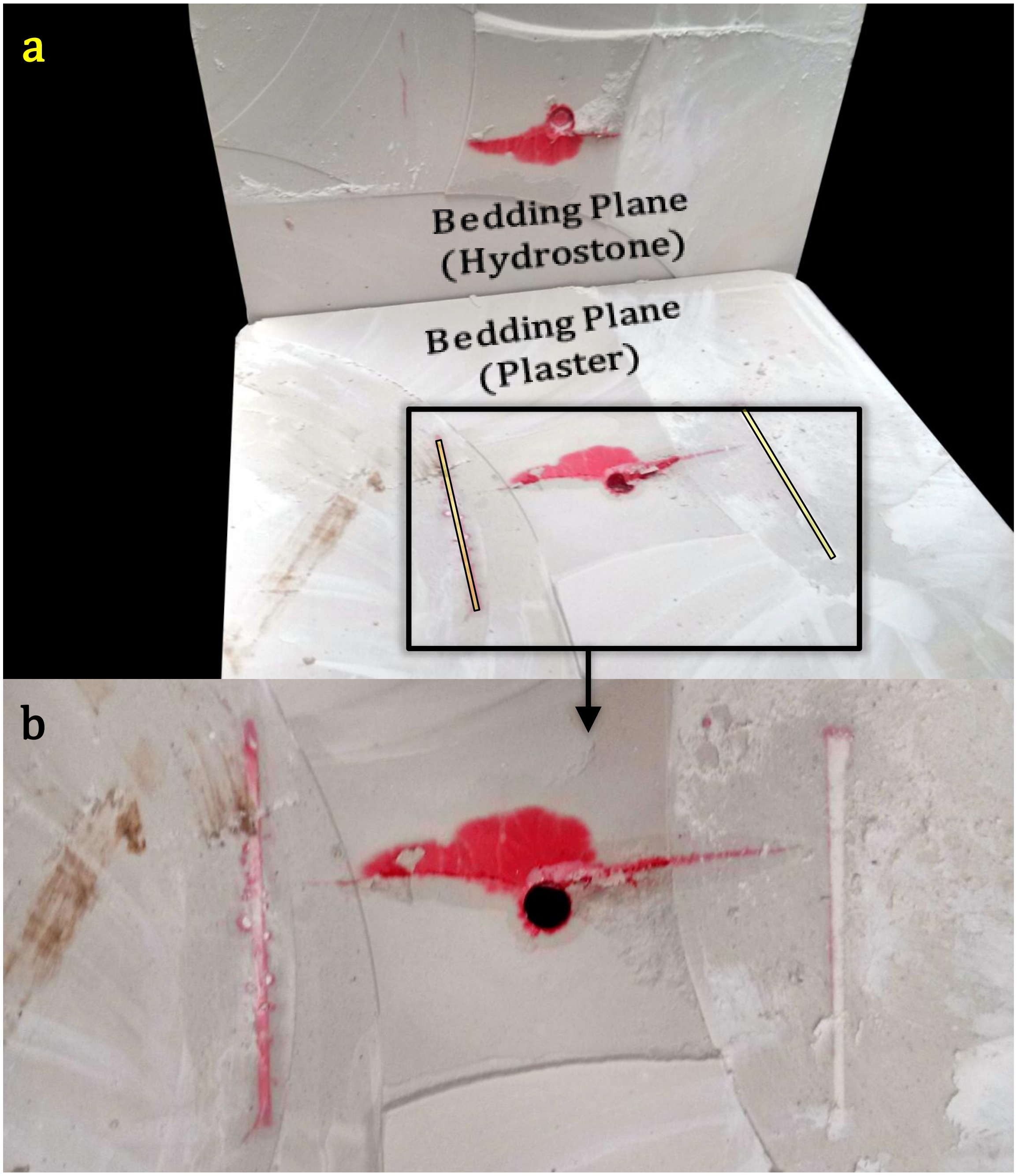

Figure 4.35: a) Side view photo of the lower bedding plane of the block sample in test 7 shows hydraulic fracture (in red dye) height arrest at the bedding plane interface with marks of fluid leakage along the interface (embedded discontinuities are marked in yellow shade), b) bottom view photo of the lower bedding plane shows hydraulic fracture (in red dye) intersecting embedded discontinuities and leaking along their interfaces

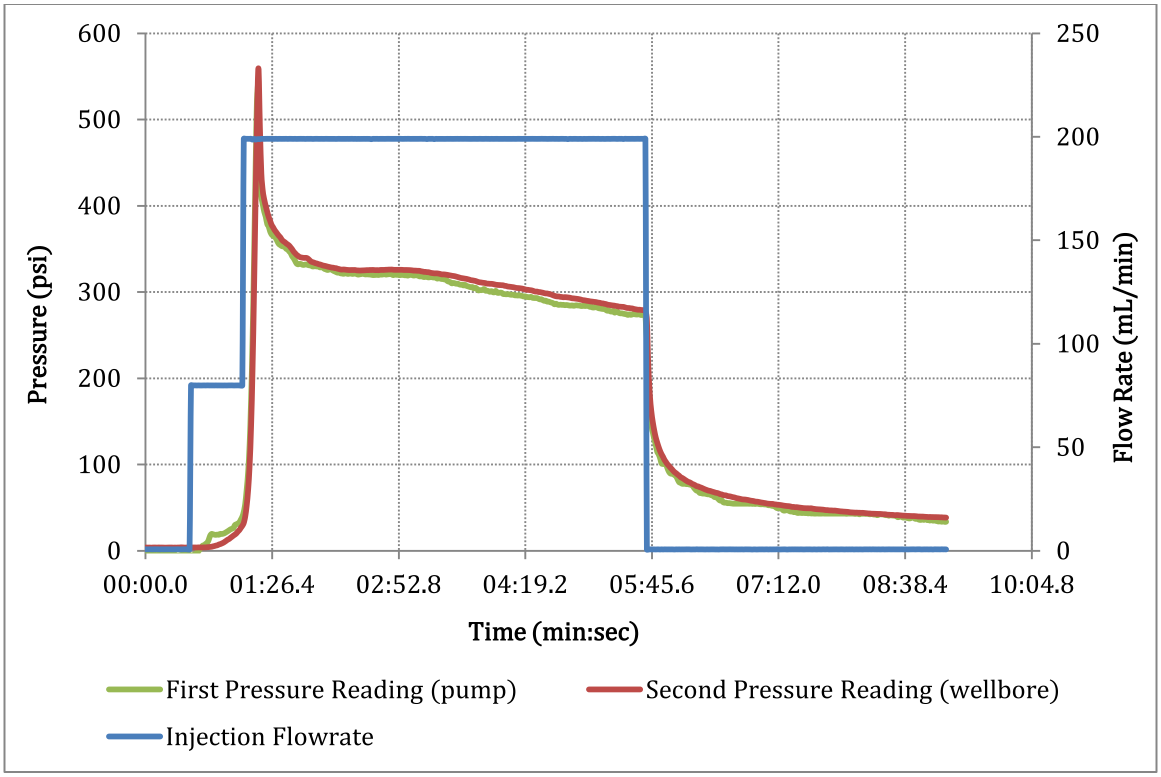

Figure 4.36: Injection pressure and flow rate profiles of the hydraulic fracturing test 7

4.1.8 Test 8

Test 8 is similar to tests 2 and 4 but using exaggeratedly tall pre-existing inclusion. This test used tall, orthogonal pre-existing inclusion of the same type as the host-layer, which was plaster. The primary objective of this test was to test the effect of PEF relative height on HF-PEF intersection outcomes. The test resulted in HF deflection and branching-out propagation (Figure 4.37-4.41).

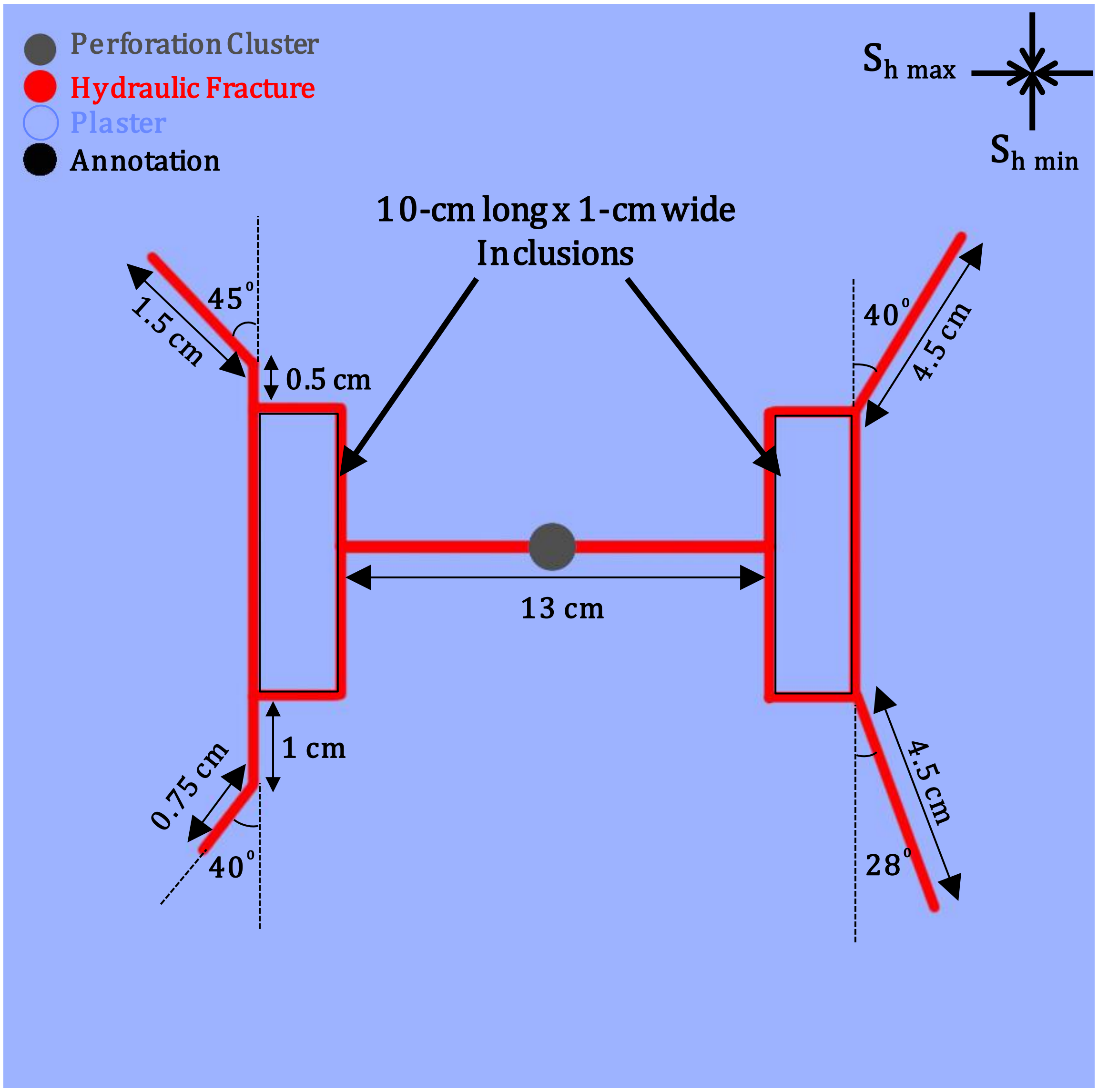

Figure 4.37: Top view illustration of the middle section of the block sample in test 8

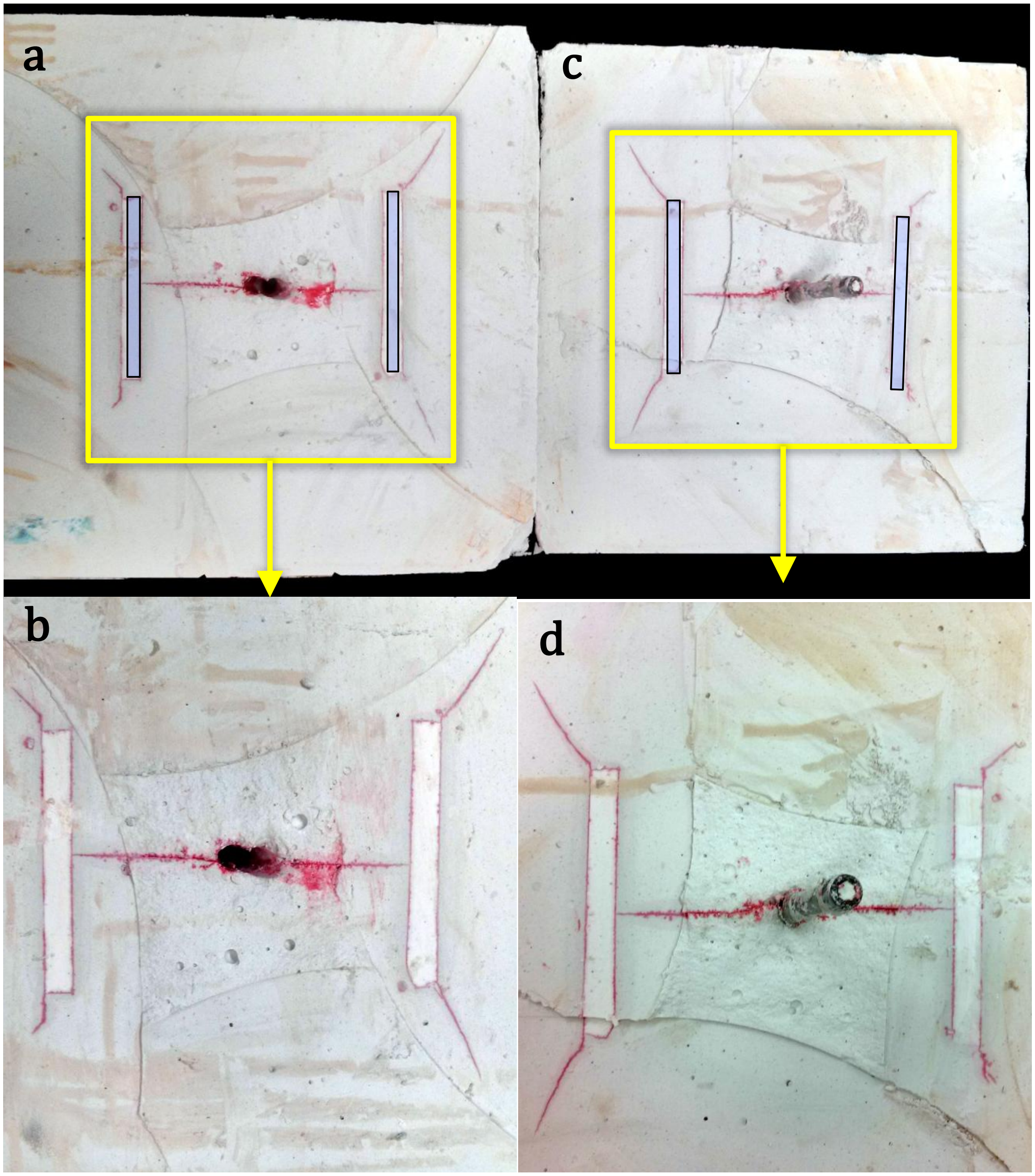

Figure 4.38: a-b) Top view photos and c-d) bottom view photos of the middle section of the block sample in test 8 shows hydraulic fracture (in red dye) intersecting embedded discontinuities (marked in blue shade), leaking along their interfaces, and deflecting off of their side edges

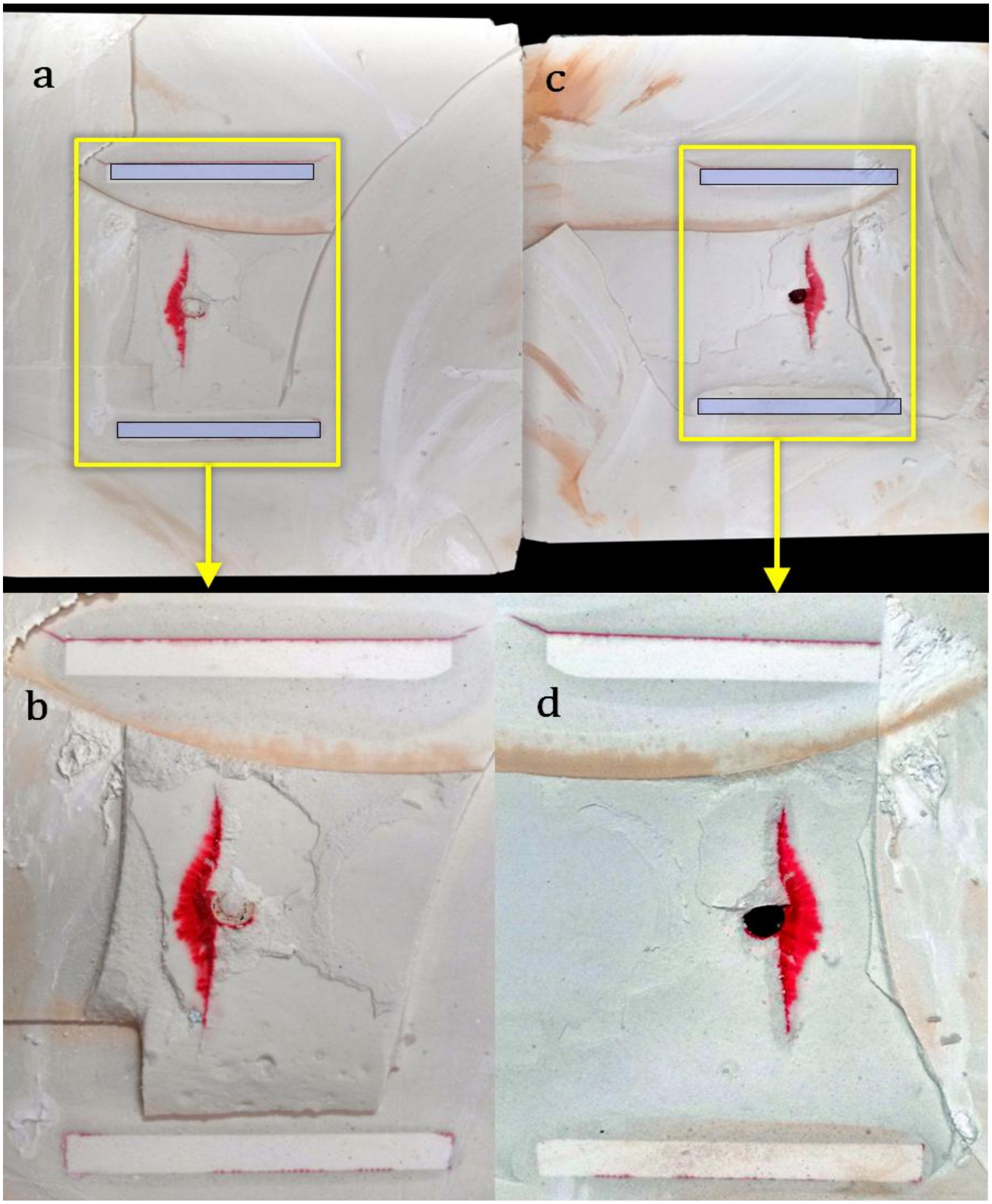

Figure 4.39: a-b) Top view and c-d) bottom view photos of the lower bedding plane of the block sample in test 8 shows hydraulic fracture (in red dye) height arrest at the bedding plane interface with marks of fluid leakage along the interface (embedded discontinuities are marked in blue)

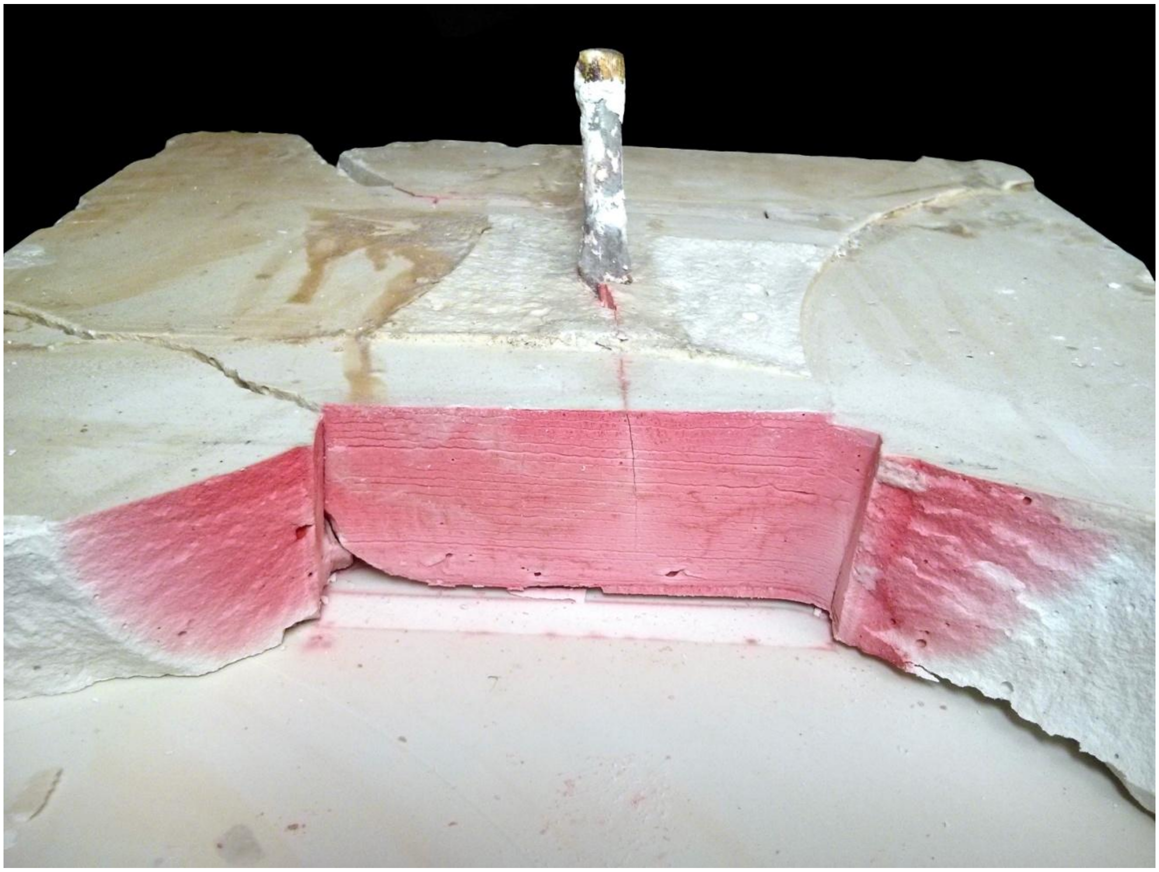

Figure 4.40: Side view photo of block sample in test 8 shows hydraulic fracture (in red dye) intersecting an embedded discontinuity, reorienting along its interfaces, and deflecting off of its side edges (note that the embedded discontinuity is removed in this photo to allow better visibility)

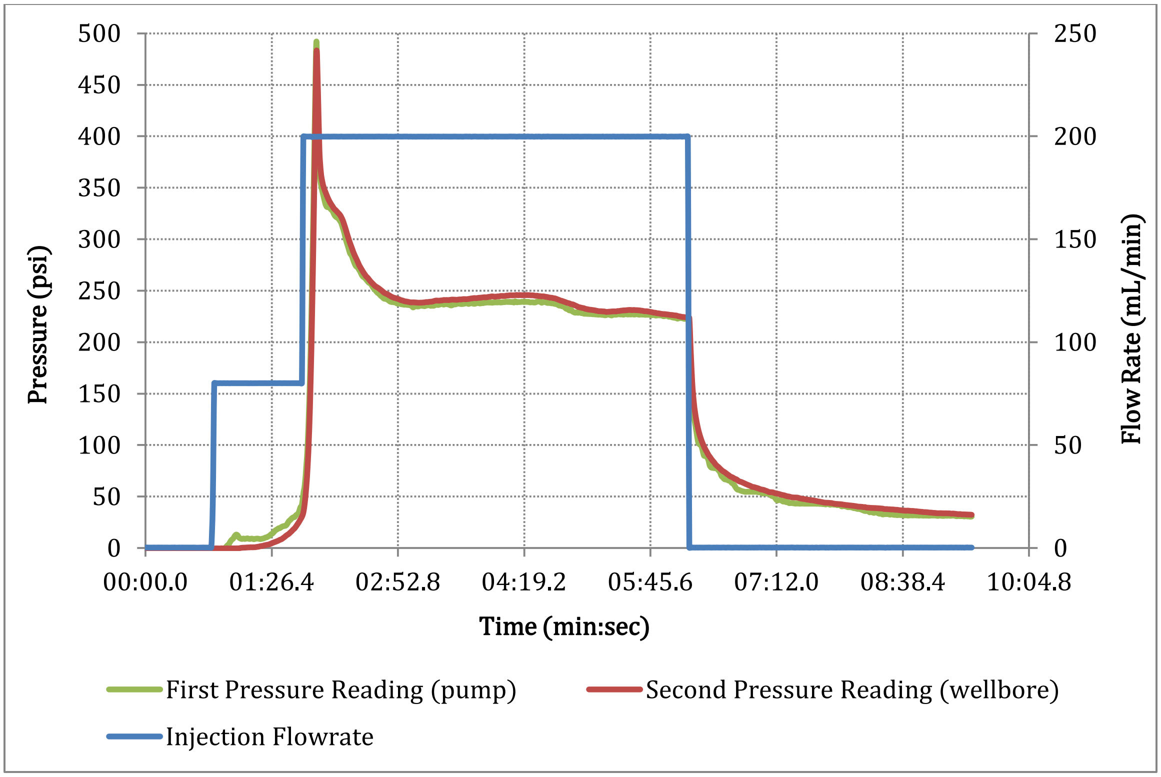

Figure 4.41: Injection pressure and flow rate profiles of the hydraulic fracturing test 8

4.1.9 Test 9

Test 9 used three fracturing sources to test for simultaneous multiple hydraulic fractures. The test resulted in only one HF with non-planar propagation behaviors. Figures 4.42-4.45 summarize test 9 laboratory results.

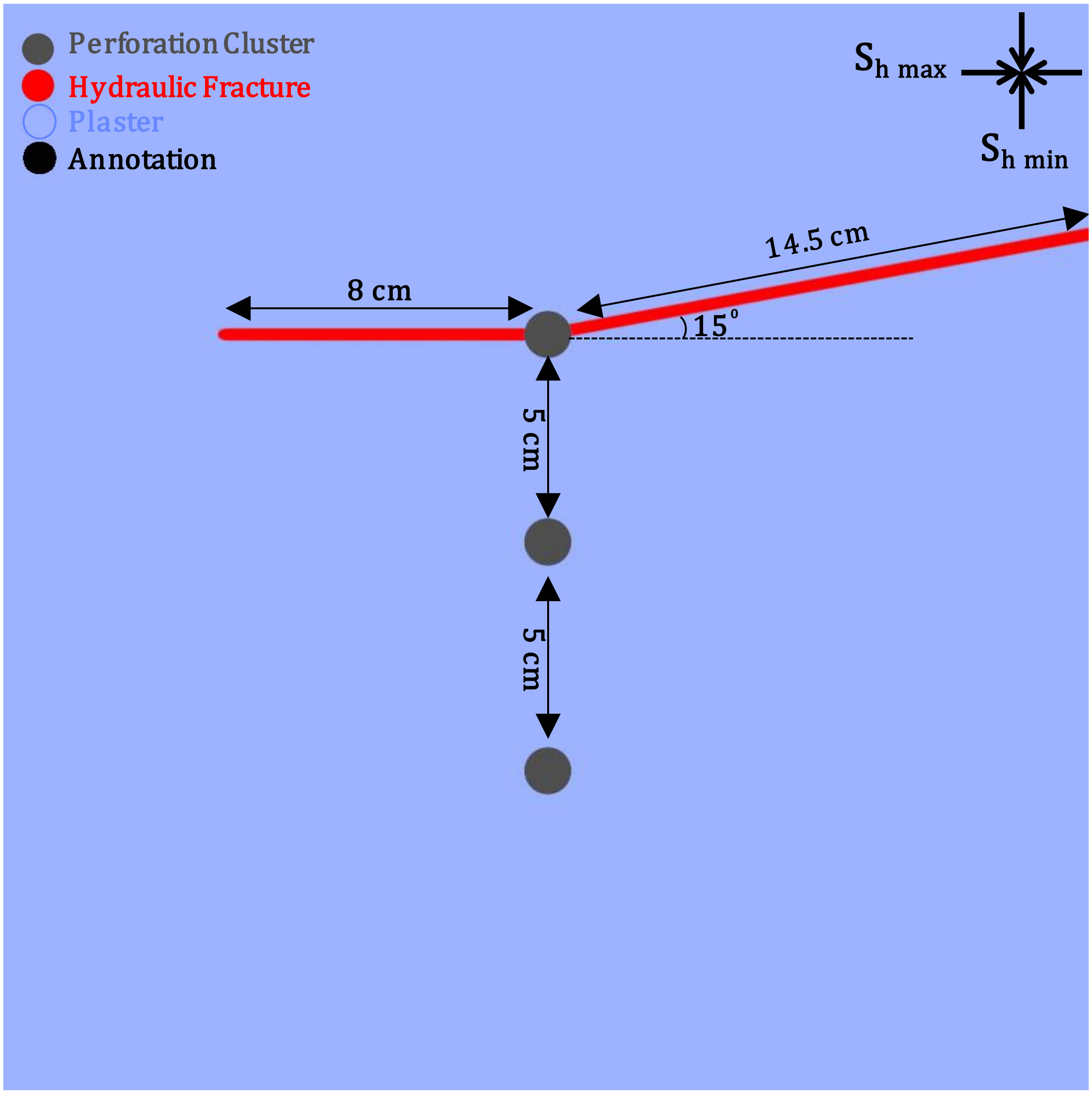

Figure 4.42: Top view illustration of the middle section of the block sample in test 9 (note that injection flow direction was from top to bottom)

Figure 4.43: Top view photo of the middle section of the block sample in test 9 shows three perforation clusters (black holes) with a hydraulic fracture (in red dye) propagating from the first perforation cluster on the right with minor outwards curvature (note that injection flow direction was from right to left)

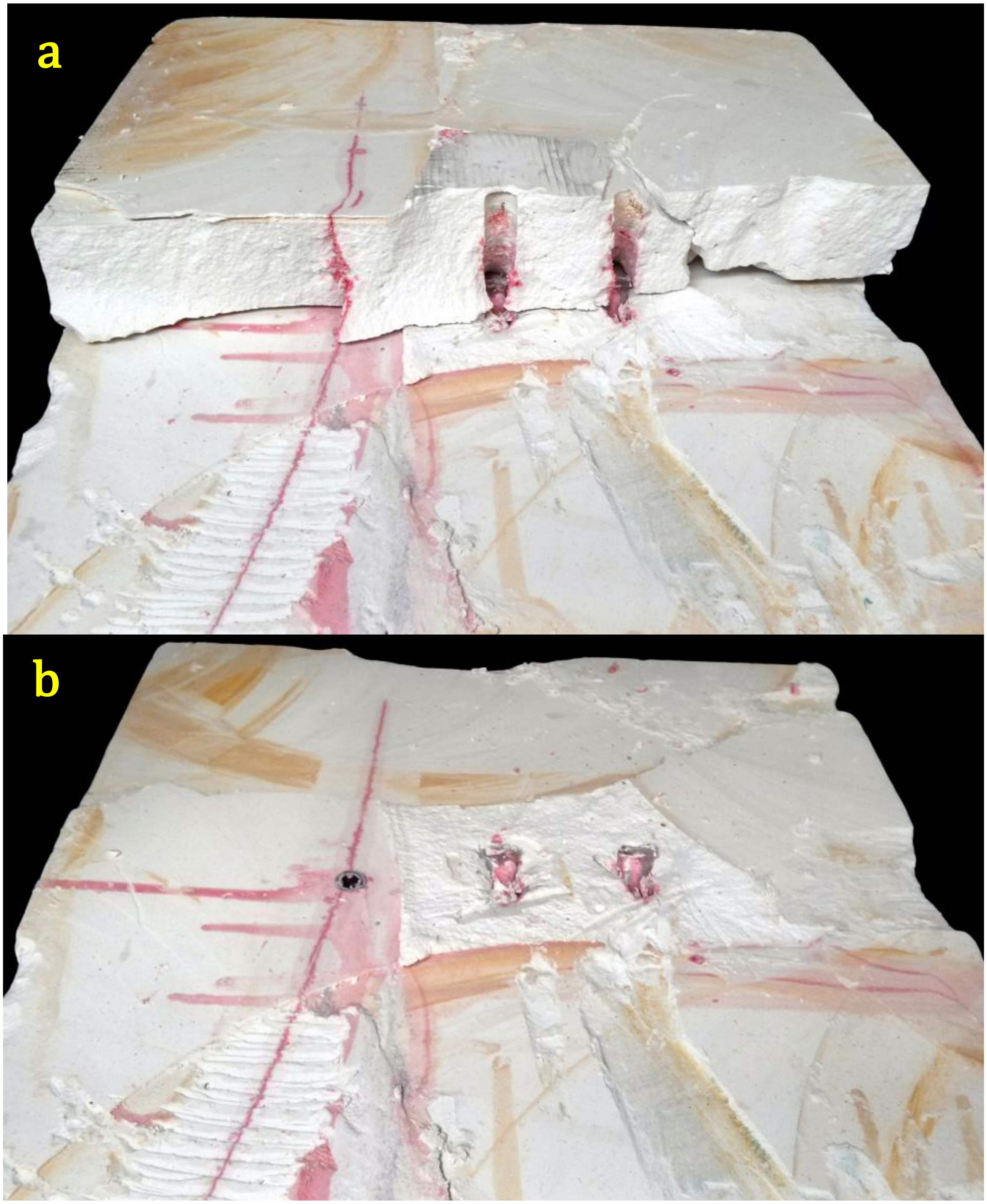

Figure 4.44: a) Side view and b) bottom view photos of the middle section of the block sample in test 9 shows three perforation clusters with a hydraulic fracture (in red dye) propagating from the first perforation cluster on the left with minor outwards curvature (note that injection flow was from left to right)

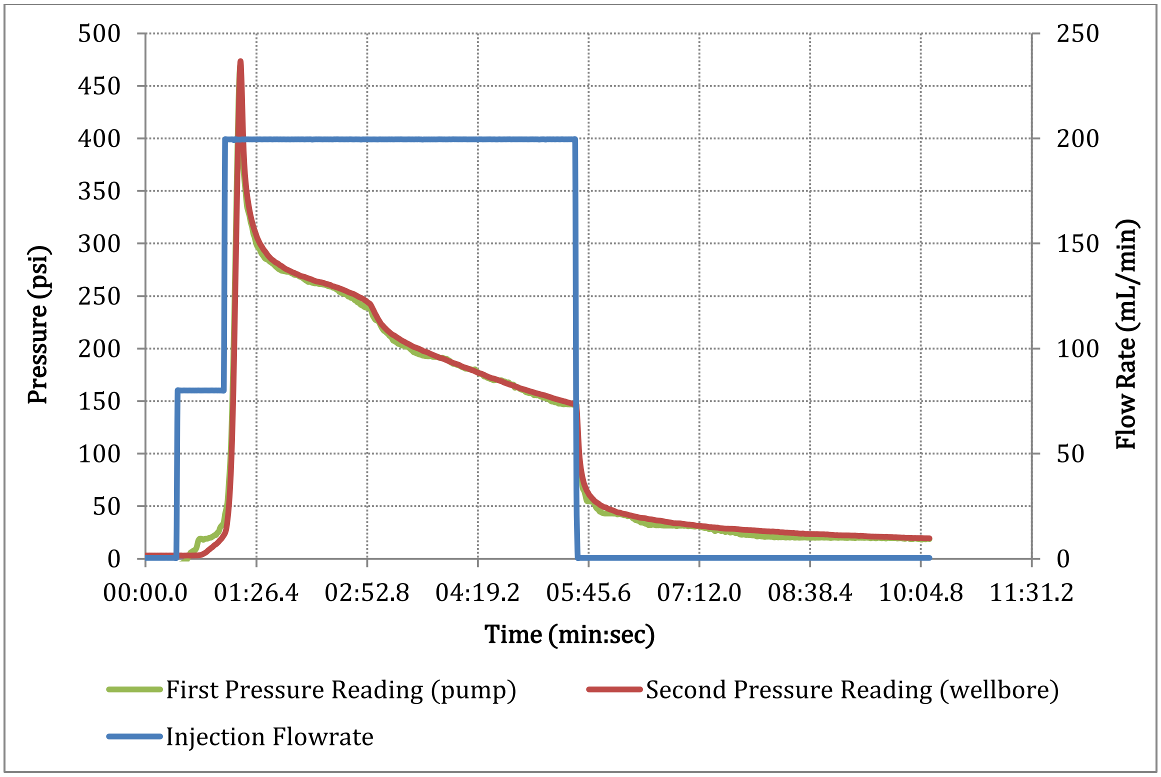

Figure 4.45: Injection pressure and flow rate profiles of the hydraulic fracturing test 9

4.1.10 Test 10

Test 10 adopted a similar set up as test 9 but with some adjustments to the sizes of the fracturing sources. The three fracturing sources used in test 9 were adjusted in this test by increasing their respective sizes into the injection direction. Similar to test 9, test 10 also tested for simultaneous multiple hydraulic fractures. Test 10 resulted in two fractures of different sizes and propagation orientations (Figures 4.46-4.49).

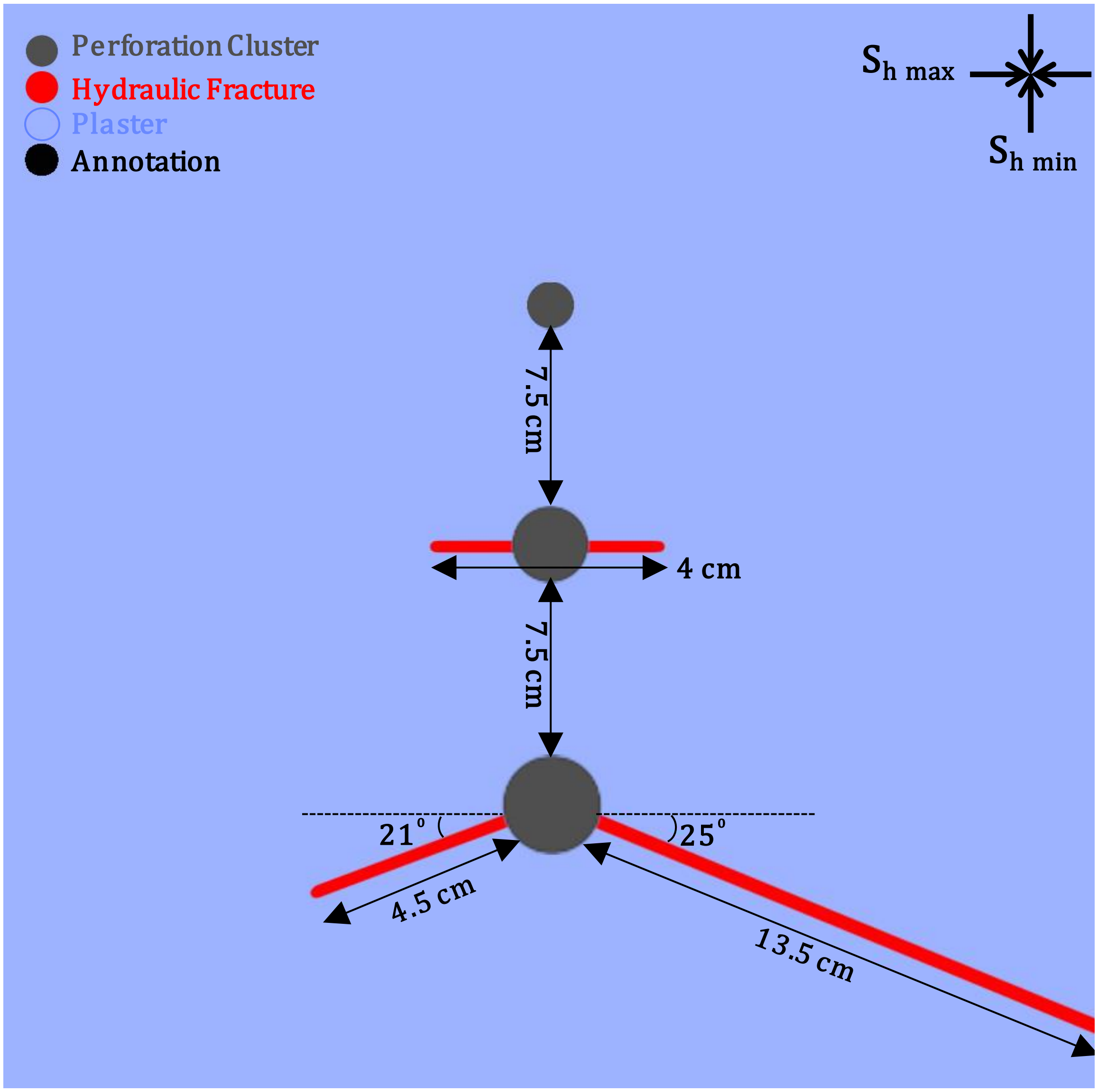

Figure 4.46: Top view illustration of the middle section of the block sample in test 10 (note that injection flow direction was from top to bottom and the first perforation cluster from the top was plugged due to experimental difficulties)

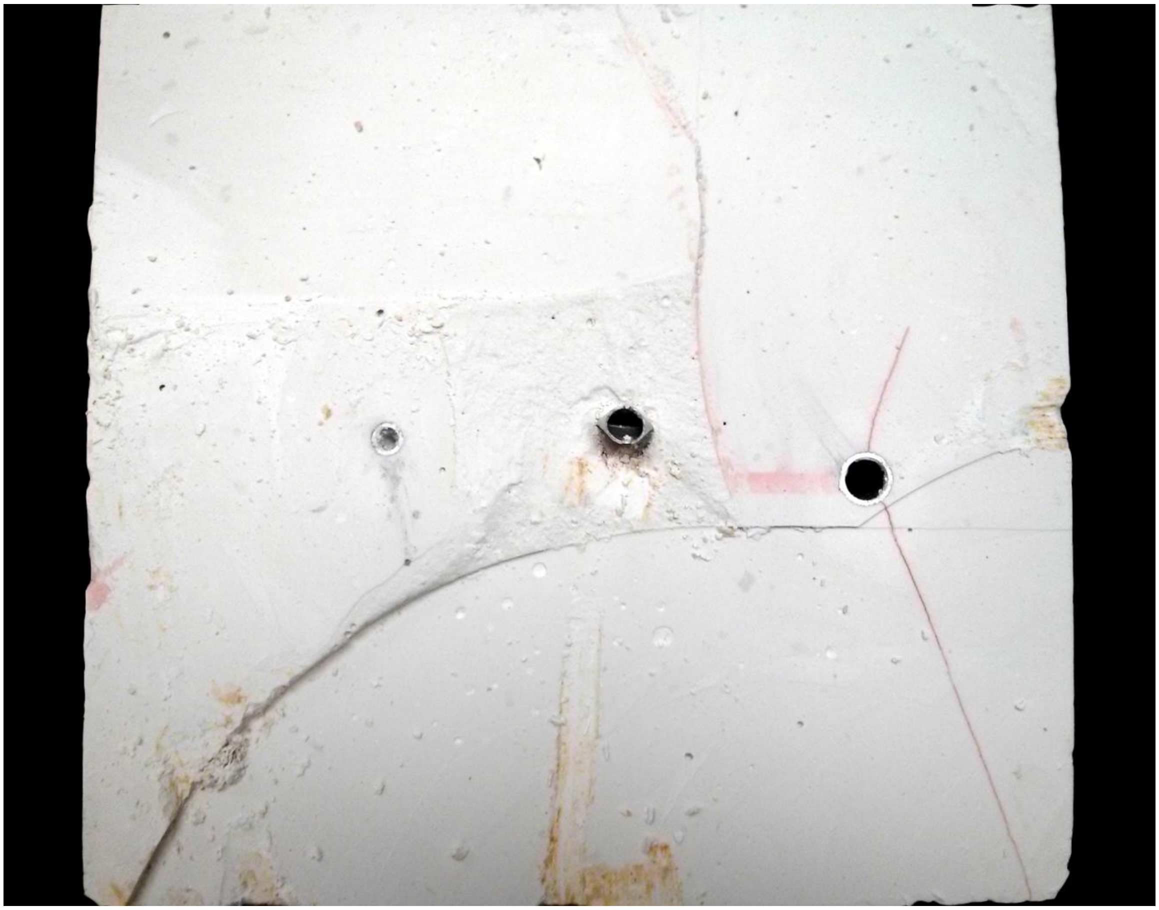

Figure 4.47: Bottom view photo of the middle section of the block sample in test 10 shows three perforation clusters (black holes) with a small hydraulic fracture propagating from the middle cluster (invisible in this photo) and another hydraulic fracture (in red dye) propagating from the third cluster on the far right with outwards curvature (note that injection flow was from left to right and the first cluster on the far left was plugged due to experimental difficulties)

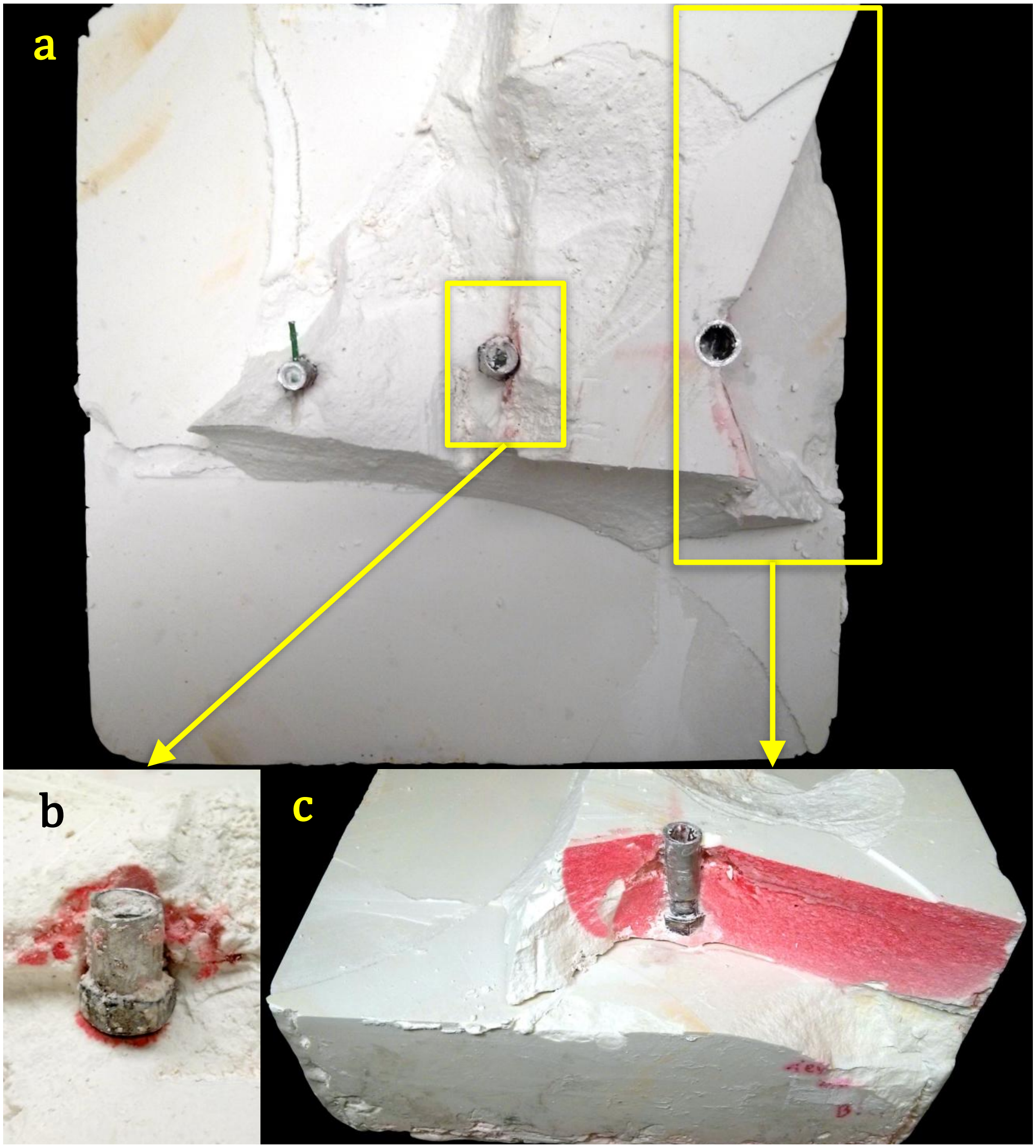

Figure 4.48: a) Top view photo of the middle section of the block sample in test 10 shows three perforation clusters with a small hydraulic fracture (in red dye) propagating from the middle cluster and another one propagating from the third cluster on the far right (note that the injection flow was from left to right and the first cluster on the far left was plugged due to experimental difficulties), b) cross sectional view photo shows the small fracture from the middle cluster, and c) side view photo shows the hydraulic fracture from the third cluster on the far right curving outwards

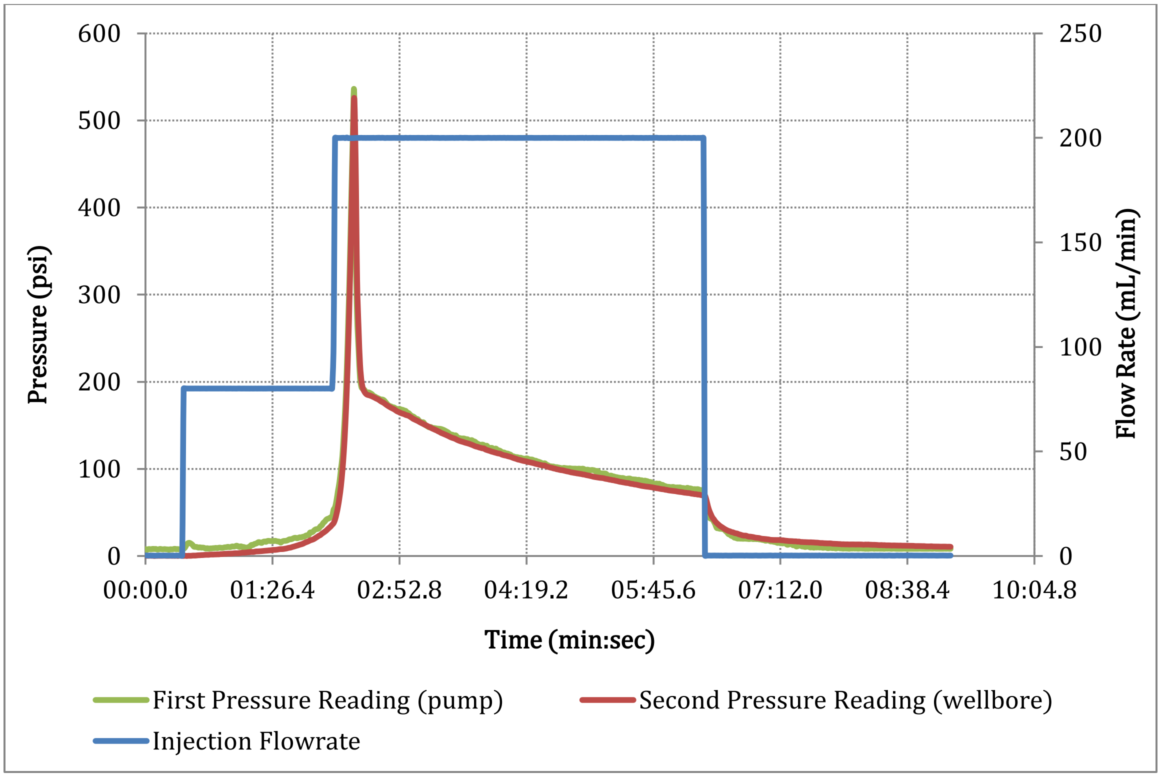

Figure 4.49: Injection pressure and flow rate profiles of the hydraulic fracturing test 10

4.1.11 Test 11

The set ups of tests 9 and 10 were further adjusted to impose limited-entry-like effect on the fracturing injection. Test 11 used smaller-sized fracturing sources with cross-linked gel fracturing fluids to test for simultaneous multiple hydraulic fractures. Test 11 resulted in three hydraulic fractures of different sizes and orientations (Figures 4.50-4.52).

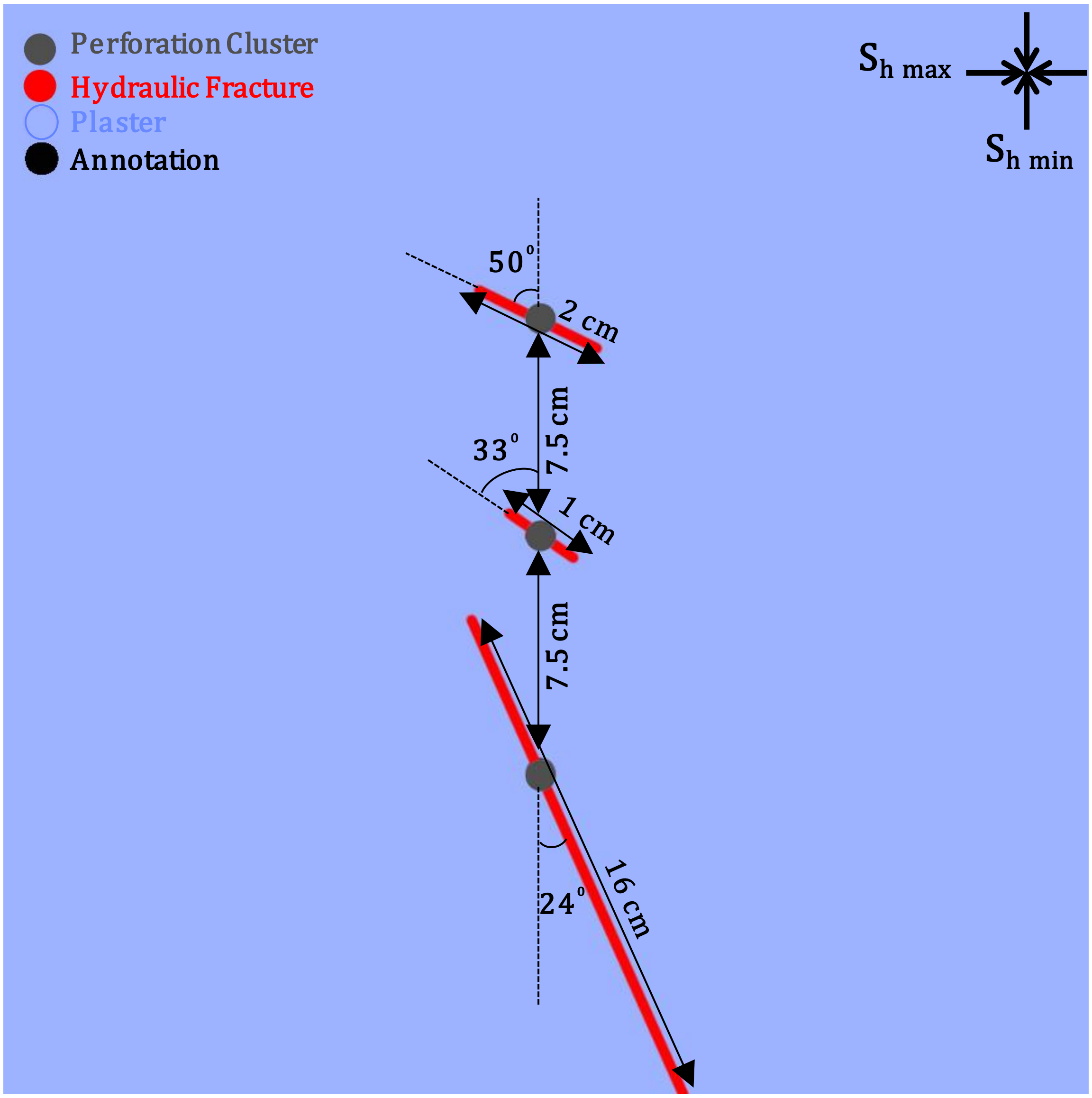

Figure 4.50: Top view illustration of the middle section of the block sample in test 11 (note that the injection flow direction was from top to bottom)

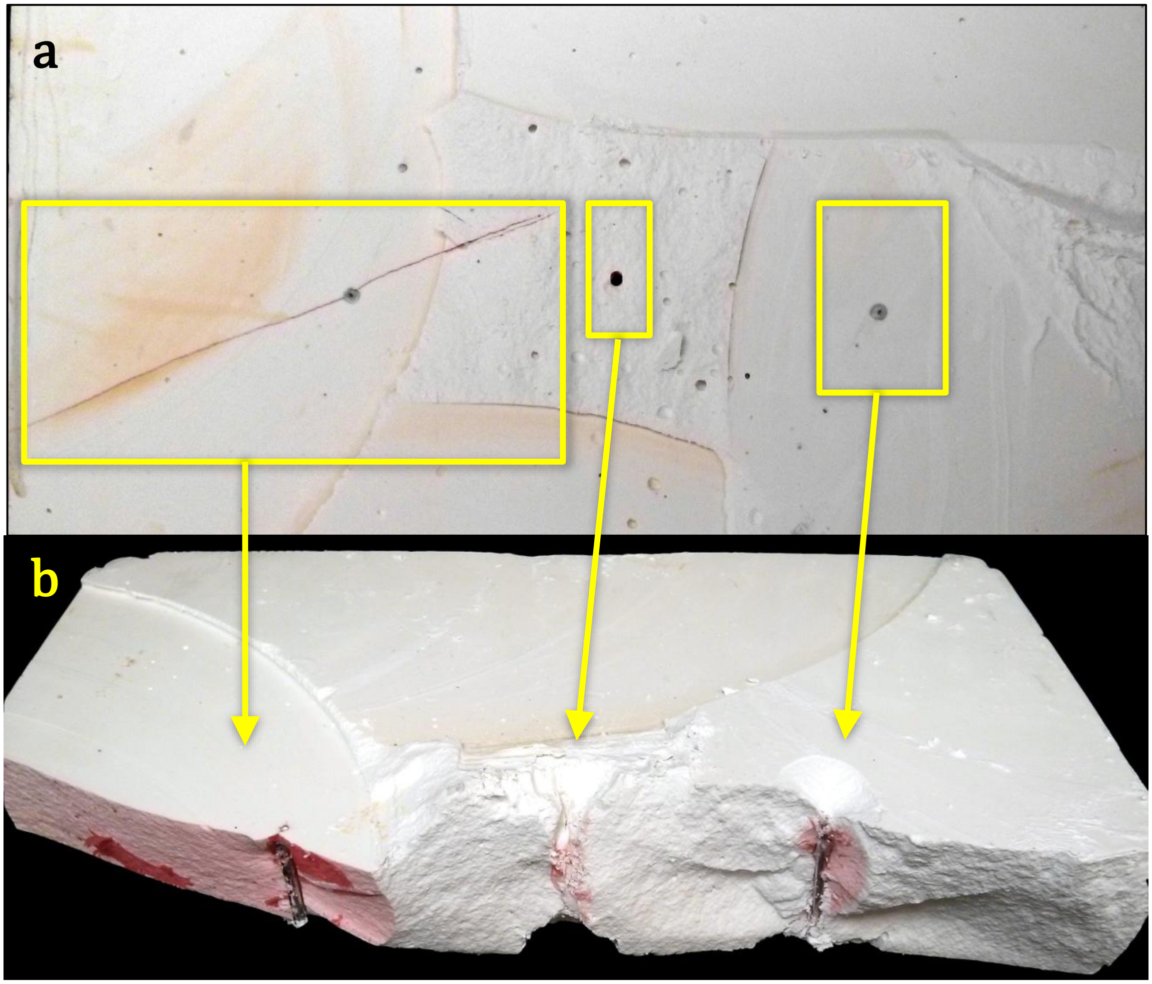

Figure 4.51: a) Top view and b) side view photos of the middle section of the block sample in test 11 shows three perforation clusters with highly angled hydraulic fractures (in red dye) of different sizes (note that the injection flow direction was from right to left)

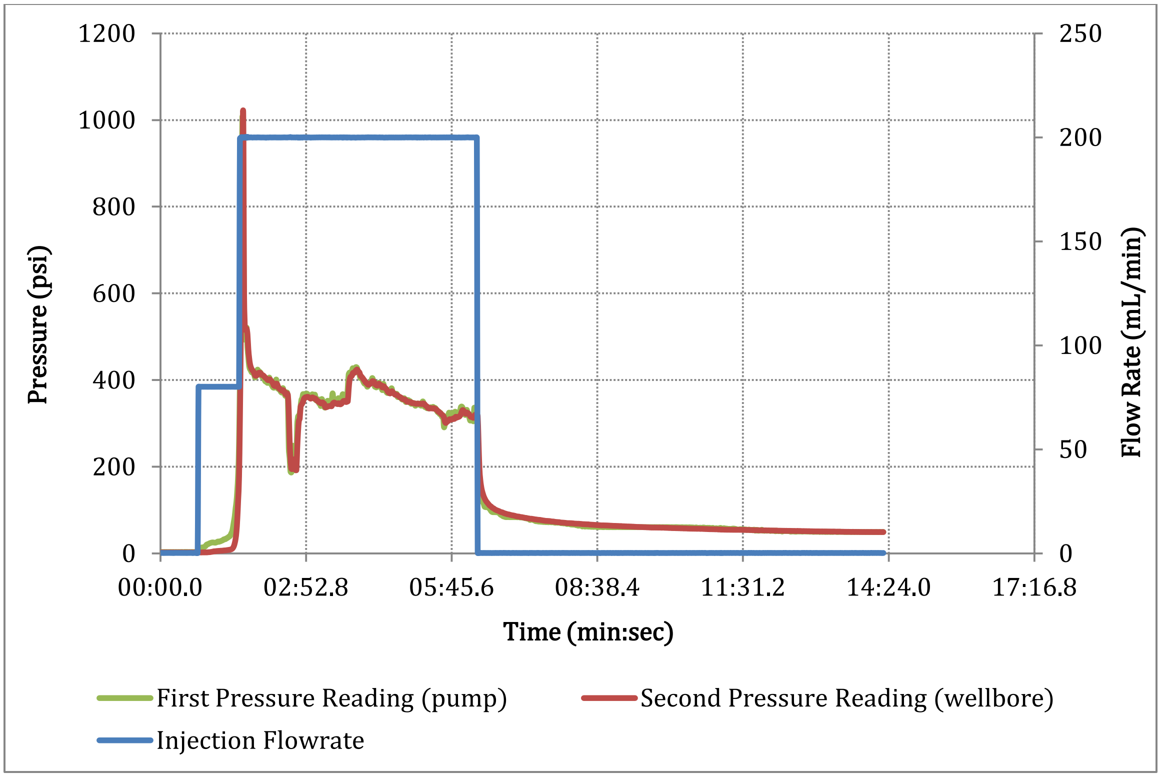

Figure 4.52: Injection pressure and flow rate profiles of the hydraulic fracturing test 11

4.2 EXPERIMENTAL MEASUREMENT DATA

The measurement data summarized in this section are average approximations of experimental values obtained either during this work or from previously published works including Bahorich 2012, Hosseini 2012, and Wang 2013. The presented data characterize relevant properties of various experimental components. Tables 4.3 through 4.7 present data describing fully-cured hydrostone cement, fully-cured plaster cement, bonded interfaces, gel-based fracturing fluids, and wellbore piping components respectively.

Table 4.3: Average property measurements characterizing a fully-cured hydrostone cement

Type	Property	Value	Unit
Petrophysical	Porosity	45.7	%
	Permeability	8.3	mD
	Bulk Density	1.8	g/mL
Mechanical	Young's Modulus (E)	218,750	psi
	Unconfined Compressive Strength (UCS)	3,666	psi
	Tensile Strength (T)	700.0	psi
	Fracture Toughness (K_{IC})	0.28	MPa*m$^{0.5}$

Table 4.4: Average property measurements characterizing a fully-cured plaster cement

Type	**Property**	**Value**	**Unit**
Petrophysical	Porosity	66.2	%
	Permeability	40.3	mD
	Bulk Density	1.4	g/mL
Mechanical	Young's Modulus (E)	200,000	p si
	Unconfined Compressive Strength (UCS)	1,000	psi
	Tensile Strength (T)	297.0	psi
	Fracture Toughness (K_{IC})	0.12	$MPa*m^{0.5}$

Table 4.5: Semi-circular bending test results for bonded interfaces

Sample #	**Layer-Inclusion Bond Type**	**K_{IC} (MPa*m$^{0.5}$)**
1	Plaster-Plaster	0.116
2	Hydrostone-Hydrostone	0.175
3	Plaster-Hydrostone	0.117
4	Hydrostone-Plaster	0.160
5	Plaster-Hydrostone (Bedding Plane)	0.184

Table 4.6: Average property measurements characterizing gel-based fracturing fluids

Type	**Property**	**Value**	**Unit**
Linear-Gel	Viscosity constant (K_v)	170.6	cP * second$^{(n-1)}$
	Fluid-behavior power component (n)	0.9	—
	Apparent Fluid Density	0.7	g/mL
Cross-Linked Gel	Viscosity constant (K_v)	61,775.0	cP * second$^{(n-1)}$
	Fluid-behavior power component (n)	0.519	—
	Apparent Fluid Density	1.1	g/mL

Table 4.7: Average pipe roughness values of the wellbore components

Wellbore Component Material	**Roughness**	**Unit**
Aluminum	0.0014	mm
Brass	0.0014	mm
Stainless Steel	0.0400	mm

Chapter 5: Discussion of Results

This chapter provides data analyses and discussions of the results obtained and outlined previously. The first section of this chapter discusses the results pertaining to hydraulic fracture interaction with pre-existing fractures and the second section discusses the results of the interaction between simultaneous multiple hydraulic fractures.

5.1 HYDRAULIC FRACTURE INTERACTION WITH PRE-EXISTING FRACTURES

This section studies how hydraulic fractures geomechanically interact with pre-existing fractures by attempting to analyze the various segments of the fracturing pressure profiles and some aspects of the fracture propagation patterns primarily based on the results of laboratory fracturing tests 2 through 8. It is worthy to note that these tests represent hydraulic fracturing systems with the same values of in-situ stresses (i.e. 100, 75, 25 psi), fracturing fluid properties (i.e. guar-based linear gel), fracturing injection rate (i.e. 200 mL/minute), and HF-PEF intersection angle (i.e. 90^0 degrees). Therefore, the following discussions deal with examining the roles of some parameters pertaining to the properties and geometry of the pre-existing fractures (i.e. cementation, aperture, and relative height) on the outcome of the HF-PEF intersection (i.e. crossing vs. deflection).

5.1.1 Pressure Analyses

5.1.1.1 Fracture Initiation

Fracture initiation pressure was most dependent on the mechanical properties and the stress state of the host rock near the wellbore. The seven laboratory tests, which had the same system parameters except PEF's cementation and geometry, exhibited reasonable consistency in fracture initiation pressures per host rock type; hydraulic fractures initiated at around 1050 psi in hydrostone and 600 psi in plaster. These experimental results exhibit a fairly comparable trend to the theoretical predictions.

Equation 5.1 expresses the theoretical prediction of the formation break down at the wellbore wall (Zoback 2007). Thus, using the experimental horizontal stress values of 25 psi and 75 psi while assuming 0 psi pore pressure, the breakdown pressure is predicted to be dictated by the tensile strength of the layer, which is reported at ~700 psi for hydrostone and ~297 psi for plaster. The difference in magnitudes between the experimental and theoretical results is probably attributed to the uncertainties in the actual values of the local stresses around the wellbore and the pore pressure. Nevertheless, the presence or the conditions of the pre-existing fractures away from the near-wellbore region did not have any effect on the values or trends of the fracture initiation pressure.

$$P_b = 3\,S_{h\,min} - S_{h\,max} - P_p + T_0 \tag{5.1}$$

5.1.1.2 Fracture Extension

After fracture initiation and prior to halting injection, fracturing pressure responses are indicative of HF-PEF interaction mechanisms and of HF height growth mechanics. Examining the results from tests 2 through 8, there are three types of pressure responses that can be identified in the fracture extension region: gradual declines, gradual increases, and abrupt increases (bumps). Tests 2, 3, 4, and 5 exhibited a general trend of gradual pressure declines whereas tests 6, 7, and 8 showed a mixture of increasing and declining pressure trends. Particularly, test 6 exhibited an abrupt pressure increase creating a distinctive pressure bump.

It was found that in the cases where the HF-PEF intersection mode was crossing, the fracture extension pressure was generally declining. In other words, when the HF propagation was dominantly planar and had no sudden diversions from the maximum principal stress direction, the fracturing pressure remained bump-free. Figure 5.1 shows fracture extension pressures of tests 2, 3, 4, and 5 where the HFs crossed the PEFs. It must be noted that these tests had the limitation of HF breaking out of the block samples which caused some pressure drops due to fracturing fluid leaking outside the samples. Although there was no live monitoring of the crack tip during the tests, laboratory observations and analyses during and after the injection, some of which were reported in Table 4.2, were fairly convincing to attribute these pressure drops to HF breaking out of the block samples.

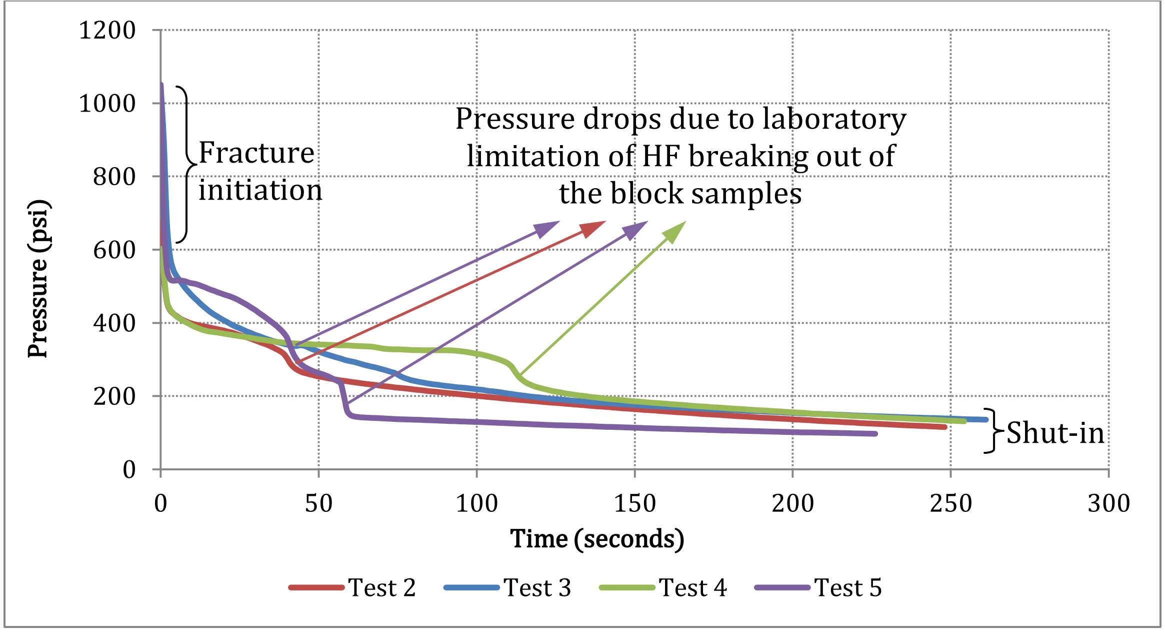

Figure 5.1: Hydraulic fracture extension pressures of tests with crossing HF-PEF intersection mode generally exhibit gradual declines (sharp drops exhibited in the pressure profiles are attributed to the laboratory test limitation of HF breaking out of the block samples allowing the fracturing fluid to leak, test 5 concave-down shape is not clearly understood but may be related to the HF concurrent, nearly-equal growth rate in height and length as indicated by its dimensions)

In the cases where the HF-PEF intersection mode was deflection, the fracture extension pressure exhibited a mixture of increasing and declining behaviors. In other words, laboratory evidences suggest that when the HFs suddenly deflected away from the direction of the maximum principal stress, higher injection pressures were required to drive their propagations. Figure 5.2 shows fracture extension pressures of tests 6, 7, and 8 where HFs deflected into the direction of the orthogonal PEFs and branched out off of the PEFs' side edges. Although only test 6 had a very distinctive pressure bump, which corresponds to the initial deflection of one of its HF wings at the intersection point with one of the pressurized non-cemented PEFs, all three tests exhibited general increasing pressure trends past HF-PEF intersections followed by some declines. Therefore, it could be concluded that when the HF propagation suddenly changes from the direction of the minimum horizontal stress into the direction of the maximum horizontal stress, i.e. HF deflects into the direction of orthogonal PEFs, an increase in the fracturing pressure may be observed due to the increase in the magnitude of the stresses acting perpendicularly on the HF walls. When the HF propagation starts to turn back towards the direction of the minimum horizontal stress, i.e. HF kinks off the side edges of orthogonal PEFs, the pressure increasing trend stops and begins to decrease.

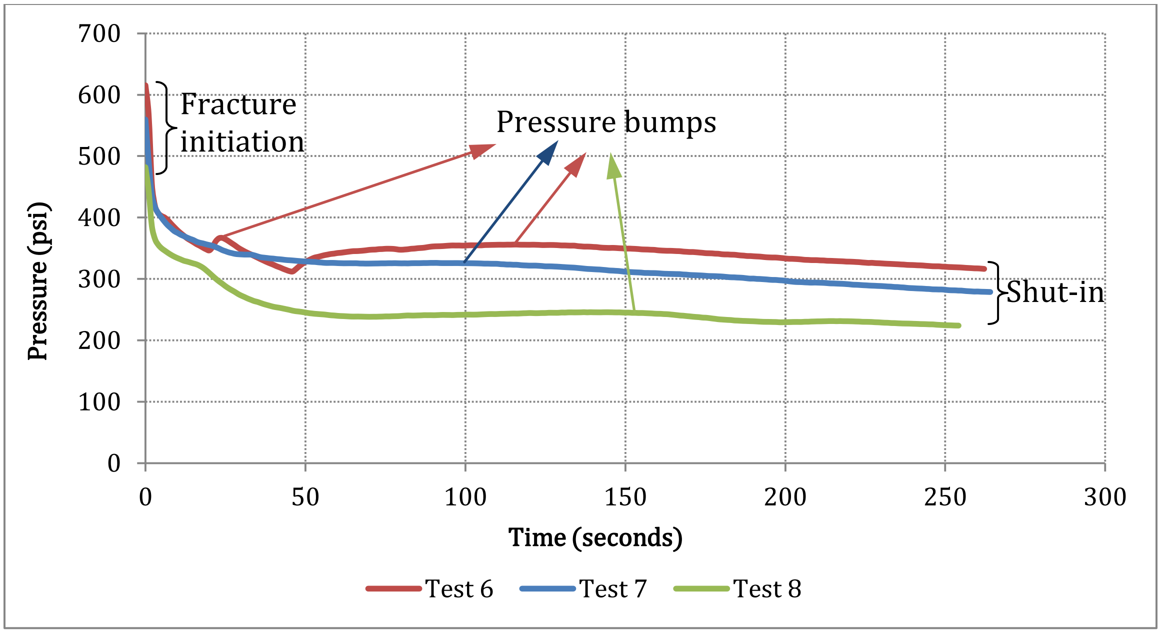

Figure 5.2: Hydraulic fracture extension pressures of tests with deflection HF-PEF intersection mode exhibit bumping behaviors (i.e. a sudden or gradual increase followed by a decline)

Taking a closer look at test 6, which displays the most apparent pressure bumps, a numerical simulation model was used to further analyze its pressure behaviors. The numerical approach of the model used is detailed in Wu and Olson (2014), and the results are displayed in Figures 5.3 and 5.4. The analysis clearly shows that the increase in pressure occurs as a result of the HF deflection along the direction of the PEFs, which in this case are parallel to the minimum horizontal stress direction. Although the simulation and laboratory pressure results in Figure 5.4 show a fair match of the overall trend, the perfect symmetry assumed in the numerical model is not realistic. Hence, the pressure responses of section 2 of the laboratory data in the plot are interpreted by possibly having one wing of the HF intersected and deflected into the PEF on one side, causing the first pressure bump, before the second HF wing had reached the PEF on the other side.

Therefore, once the second HF wing intersected and deflected into the PEF, another pressure bumping trend was observed.

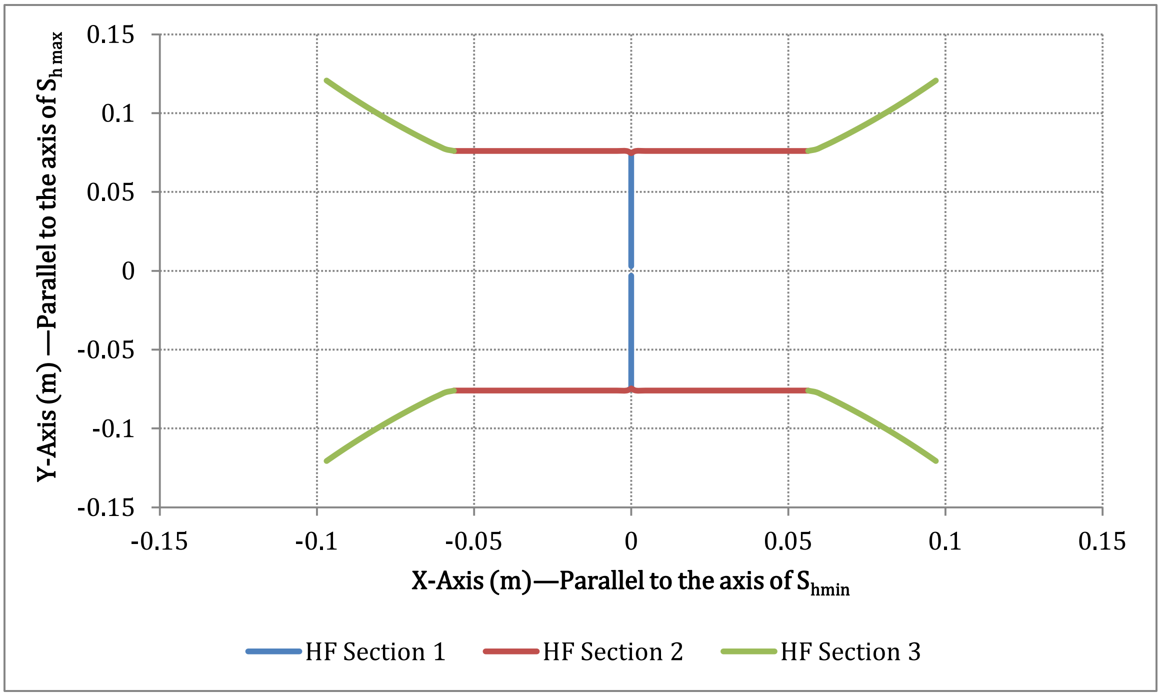

Figure 5.3: HF propagation simulation results for test 6 reasonably depicts the laboratory-obtained overall pattern and geometry presented in Figures 4.27 through 4.31

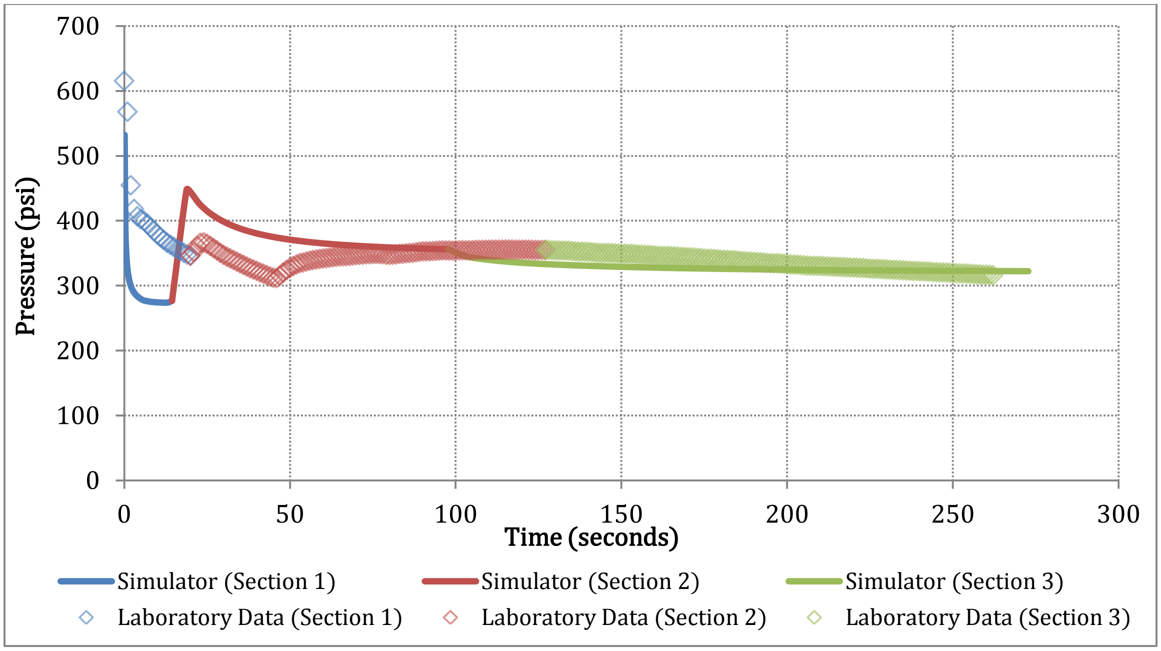

Figure 5.4: Fracture-extension pressure comparison between numerical simulation and laboratory results for test 6 (the first two bumping trends exhibited in the laboratory data are interpreted by the asymmetric propagation of HF wings, which may have intersected the corresponding PEFs at a different time)

5.1.1.3 Fracture Closure

Analysis of the fracturing shut-in pressure after the injection is halted provides insights about fracture closure. Pressure transient analysis (method 1) and the G-function (method 2) were used to estimate the closure pressures of tests 2 through 5 (crossing) and 6 through 8 (deflection). Equations 5.2 through 5.5 list the main G-function formulations used in method 2 (Nolte 1979 and Castillo 1987). Since the crossing tests had the limitation of HFs breaking out of the block samples, assessing the impact that it might have had on closure pressures was required. Therefore, two calibration tests with better HF containment inside the block sample with non-branching HF propagation behaviors were used for verification. Table 5.1 lists the pressure-closure results of all tests.

$$t_D = \frac{t - t_{ISIP}}{t_{ISIP}} \tag{5.2}$$

$$g(t_D) = \left(\frac{4}{3}\right)\left((1 + t_D)^{\frac{3}{2}} - t_D{}^{\frac{3}{2}} - 1\right) \qquad (5.3)$$

$$G(t_D, t_D^*) = \left(\frac{4}{\pi}\right)\left[g(t_D) - g(t_D^*)\right] \qquad (5.4)$$

$$\grave{p} = \frac{\partial P}{\partial G} \qquad (5.5)$$

Table 5.1: Fracture closure average estimations for fracturing tests with pre-existing fractures

HF-PEF Intersection Mode	Test #	ISIP (psi)	Closure Pressure Method 1 (psi)	Closure Pressure Method 2 (psi)	$S_{h\ min}$ (psi)	$S_{h\ max}$ (psi)	S_v (psi)
Crossing Calibration	A	131	50	31	25	75	100
	B	73	43	24	25	75	100
Crossing	2	96	54	20	25	75	100
	3	95	59	25	25	75	100
	4	82	49	22	25	75	100
	5	54	38	22	25	75	100
Deflection	6	197	112	45	25	75	100
	7	181	112	49	25	75	100
	8	161	96	42	25	75	100

Although each estimation method, i.e. transient pressure vs. the G-function, has a different set of results, the general trends for closure pressure estimates are consistent in both methods. It is clear that the range of closure pressure values in tests 2, 3, 4, and 5 is roughly half the range in tests 6, 7, and 8. Therefore, given the parameters of all seven tests, there may only be two major factors causing this difference in closure pressure ranges: The laboratory issues of HF containment inside the block samples of some tests and the type of the HF-PEF intersection outcomes.

Since all four tests that show low closure pressure values had the issue of HF breaking out the block samples, it is required to verify whether this limitation had much impact on the closure pressure estimations. Thus, the results from tests 2, 3, 4, and 5 were compared with two calibration tests A and B that did not have HF containment problems and had similar HF propagation outcomes, i.e. non-branching, as tabulated in Table 5.1.

This comparison shows that the HF block containment issues may have partially reduced the closure pressure results; it suggests that the pseudo reduction in closure pressure might have not exceeded 25%. In other words, if closure pressure results for tests 2, 3, 4, and 5 were to be corrected for the pseudo reduction caused by the HF containment problems, a maximum of 25% increase would be added to the results, which does not significantly change their low pressure range.

On the other hand, the type of the HF-PEF intersection outcomes is another factor that might have actually caused this difference in closure pressure values. All four tests with the low closure pressure range had fairly planar, non-branching HF propagations perpendicular to the direction of the minimum horizontal stress. Thus, a low closure pressure range around the value of the minimum remote stresses, i.e. 25 psi, is reasonable. However, the other three tests with the high closure pressure range had a deflected, branching-out HF propagation patterns with three main fracture sections of distinctive orientations: the first HF section was in the direction of the maximum horizontal stress, the second HF section deflected orthogonally into the direction of the PEFs, and the third HF section kinked partially back towards the direction of the maximum horizontal stress at the side edges of the PEFs. Hence, it could be concluded from the laboratory results that complex propagation, i.e. branching-out, yields relatively higher average values of closure pressures than fractures with simpler propagation, i.e. planar, due to the higher stresses acting on the walls of the various HF sections as illustrated in Figure 5.5.

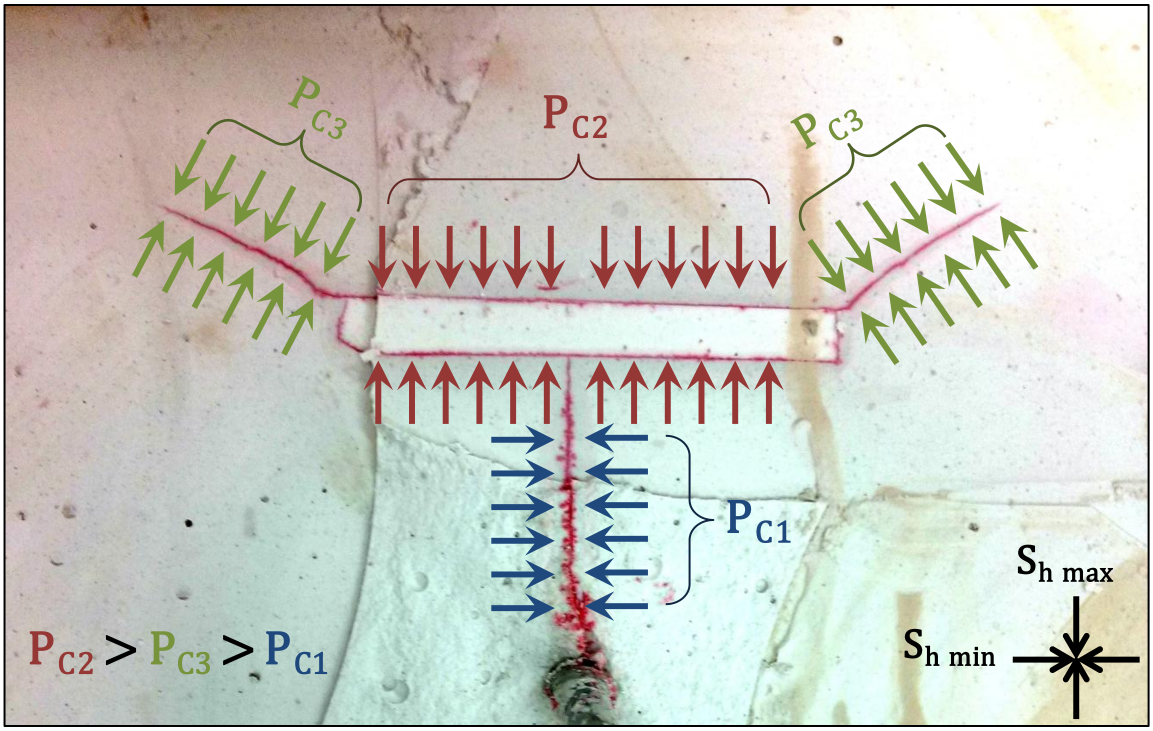

Figure 5.5: Top view photo of the middle section of the block sample in test 8 shows deflected, branching-out hydraulic fracture propagation (in red dye) resulting from its intersection with a pre-existing inclusion, which yielded three fracture segments each of which has a distinctive orientation and consequently is subjected to closure stresses of different magnitudes: First segment is perpendicular to the direction of the minimum horizontal stress, the second segment is perpendicular to the direction of the maximum horizontal stress, and the third segment is angled away from either horizontal stresses

Further analysis on the shut-in pressure data from the deflection tests with the complex, branching out HF propagation patterns may offer more detailed interpretations of the higher average values of fracture closure pressure presented previously. For example, taking a closer look at the shut-in pressure data of test 8, multiple fracture closure signatures can be identified. The G-function's pressure derivative versus shut-in time plot shown in Figure 5.6 illustrates three possible flat regions, which indicate fracture closures, at 100, 55, and 25 psi (the corresponding bottomhole pressures are 66, 55, and 43 psi respectively). Each value of those closure pressures is possibly associated with a particular segment of the hydraulic fracture based on their orientation with respective to remote and local in-situ stresses. The HF section perpendicular to the minimum horizontal stress has the lowest closure pressure since the remote stress acting on its walls, i.e. $S_{h\ min}$, is only 25 psi whereas the deflected HF section perpendicular to the maximum horizontal stress has the highest closure pressure since the remote stress acting on its walls, i.e. $S_{h\ max}$, is 75 psi.

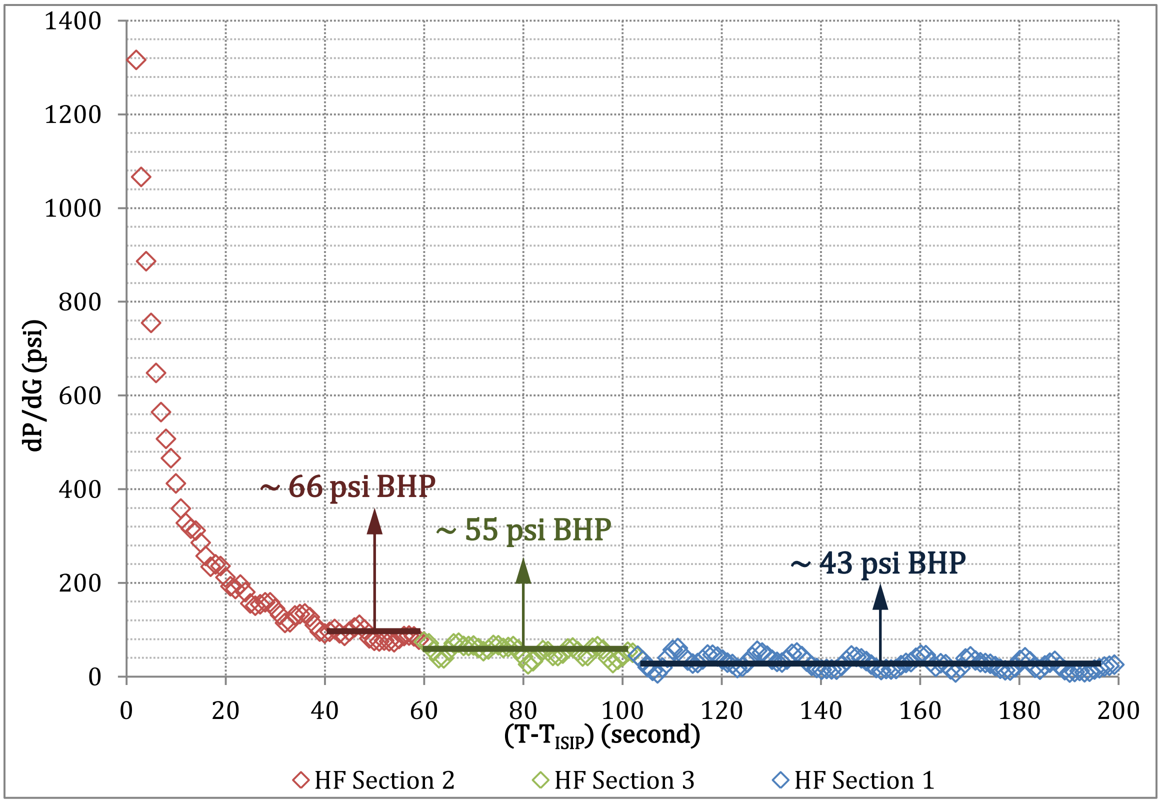

Figure 5.6: The G-function's pressure derivative versus shut-in time plot for test 8 shows three possible closure pressures each of which may correspond to a specific segment of the deflected, branching out hydraulic fracture

5.1.2 Hydraulic Fracture Propagation Analyses

5.1.2.1 Symmetry and Planarity

Despite the laboratory's well-controlled environment, perfect symmetry was not observed in any of the fracturing tests. This experimental evidence indicates that even minor sources of system heterogeneity may alter symmetric propagation of HF wings. Similarly, complete planarity was uncommon. Almost all the laboratory fracturing tests with pre-existing fractures had some HF segments that exhibited non-planar behaviors. These laboratory observations of asymmetry and non-planarity are in agreement with the hydraulic fracture complexity that is commonly recorded in field applications in naturally fractured formations (Weng et al. 2011 and Kresse et al. 2013).

5.1.2.2 Crossing vs. Non-Crossing

This section discusses the roles of PEF cementation, aperture, and relative height in HF crossing intersected PEFs. The term "crossing" is being used to indicate HF propagation through the PEF completely; HF propagates from the host rock past the PEF interface into the PEF cement-fill and propagates again from the cement-fill past the PEF interface into the other side of the host rock.

Effect of Pre-Existing Fracture Cementation

The presence or absence of mineral cementation inside PEFs exerts a strong control on the outcome of HF-PEF interactions. Using different cement-fill types relative to the host rock material alters properties such as cohesion (S_0) and internal friction coefficient (μ_0), which govern HF-PEF intersection mode. The scope of the fracturing tests with respect to the type of the PEFs' cement-fill can be categorized into: Strongly bonded, weakly bonded, and cement-free (Table 5.2). In order to experimentally and quantifiably assess the strength of the bond between the host rock and the PEF cement-fill, which is analogous to the effects of the cohesion and internal friction, semi-circular bending (SCB) tests were used to test for apparent fracture toughness along the bonded interfaces of the different material under zero confinement. Higher fracture toughness values indicate stronger bonds, which are harder to crack. Hence, bonds' apparent fracture toughnesses can be normalized using the average fracture toughness in the layer to create an index measuring resistance to fracture for bonded interfaces as expressed in Equation 5.6. This bond-to-layer fracture toughness ratio or index gives indications of the ability of the interface bond to resist fracture relative to the material on each side of the interface; higher ratios indicate stronger bonds that are more resistant to fracture (Table 5.3).

$$\frac{Bond\ Apparent\ K_{IC}}{Layer\ Average\ K_{IC}} = \frac{Bond\ Apparent\ K_{IC}}{\left(\frac{Host\ Layer\ K_{IC} +\ Cement\ Fill\ K_{IC}}{2}\right)} \tag{5.6}$$

Table 5.2: Laboratory fracturing tests categorized by PEF's cement-fill type

Cement-Fill Type	**Test #**	**Host Rock Material**	**PEF Cement-Fill Material**	**HF-PEF Intersection Mode**
Strongly Bonded	2	Plaster	Plaster	Crossing
	3	Hydrostone	Hydrostone	Crossing
	4	Plaster	Plaster	Crossing
	5	Hydrostone	Hydrostone	Crossing
Weakly Bonded	7	Plaster	Hydrostone	Deflection
Cement Free	6	Plaster	Pressurized-fluid	Deflection

Table 5.3: Results of PEF-cement-fill-to-host-layer bond strength assessment using SCB tests

Layer-Inclusion Bond Type	**Bond Apparent K_{IC} (MPa*m$^{0.5}$)**	**Bond-to-Layer K_{IC} Ratio**	**Analogous to Test #**	**HF-PEF Intersection Mode**
Plaster-Plaster	0.116	0.97	2 & 4	Crossing
Plaster-Hydrostone (bedding Plane)	0.184	0.92	3 & 4	Crossing
Hydrostone-Hydrostone	0.175	0.63	3 & 5	Crossing
Plaster-Hydrostone	0.117	0.59	7	Deflection

It is clear from the results that strongly-bonded PEF interfaces have fracture toughness ratios above 0.63. This range of relatively high fracture toughness values indicates that the PEF interfaces are fairly as resistant to fracture as the material on either side of them, i.e. the material of the host layer and the PEF cement-fill. Therefore, HF was able to cross the PEF interfaces in all the strongly-bonded tests tabulated previously because those bonded interfaces were able to remain intact and transmit the HF across them. Inversely, weakly-bonded and cement-free PEF interfaces have fracture toughness ratios equal to or below 0.59, which indicate low resistance to fracture. Thus, those interfaces were not able to remain intact upon HF-PEF intersection, which created an easier path for the HF to deflect into. Figure 5.7 compares the HF-PEF intersection outcomes of two block samples tested in the laboratory for the effect of the material type of the cement-fill relative to the host layer and clearly shows strongly-bonded interfaces (i.e. hydrostone-hydrostone) allowed hydraulic fracture crossing while weakly-bonded interfaces (i.e. plaster-hydrostone) resulted in HF deflection. Figure 5.8 shows the same comparison as the previous figure but without any annotations to allow for complete visibility.

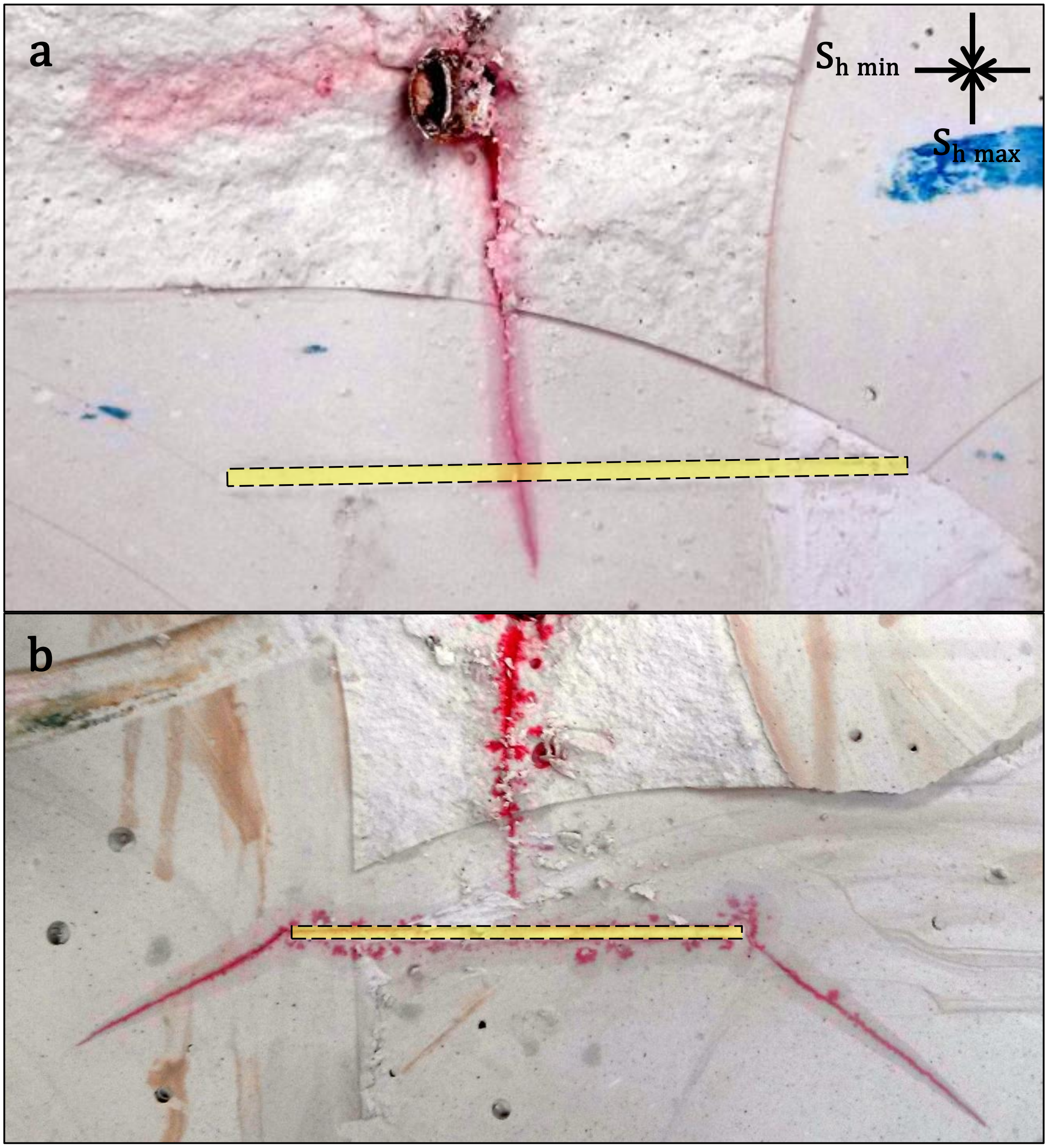

Figure 5.7: a) Top view photo of the middle section of the block sample in test 3 shows hydraulic fracture (in red dye) crossing a pre-existing inclusion (boxed in yellow shade indicating hydrostone) embedded in a layer of hydrostone and b) a similar view photo of the block sample in test 7 shows hydraulic fracture deflecting into and branching-out off a pre-existing inclusion (boxed in yellow shade indicating hydrostone) embedded in a layer of plaster

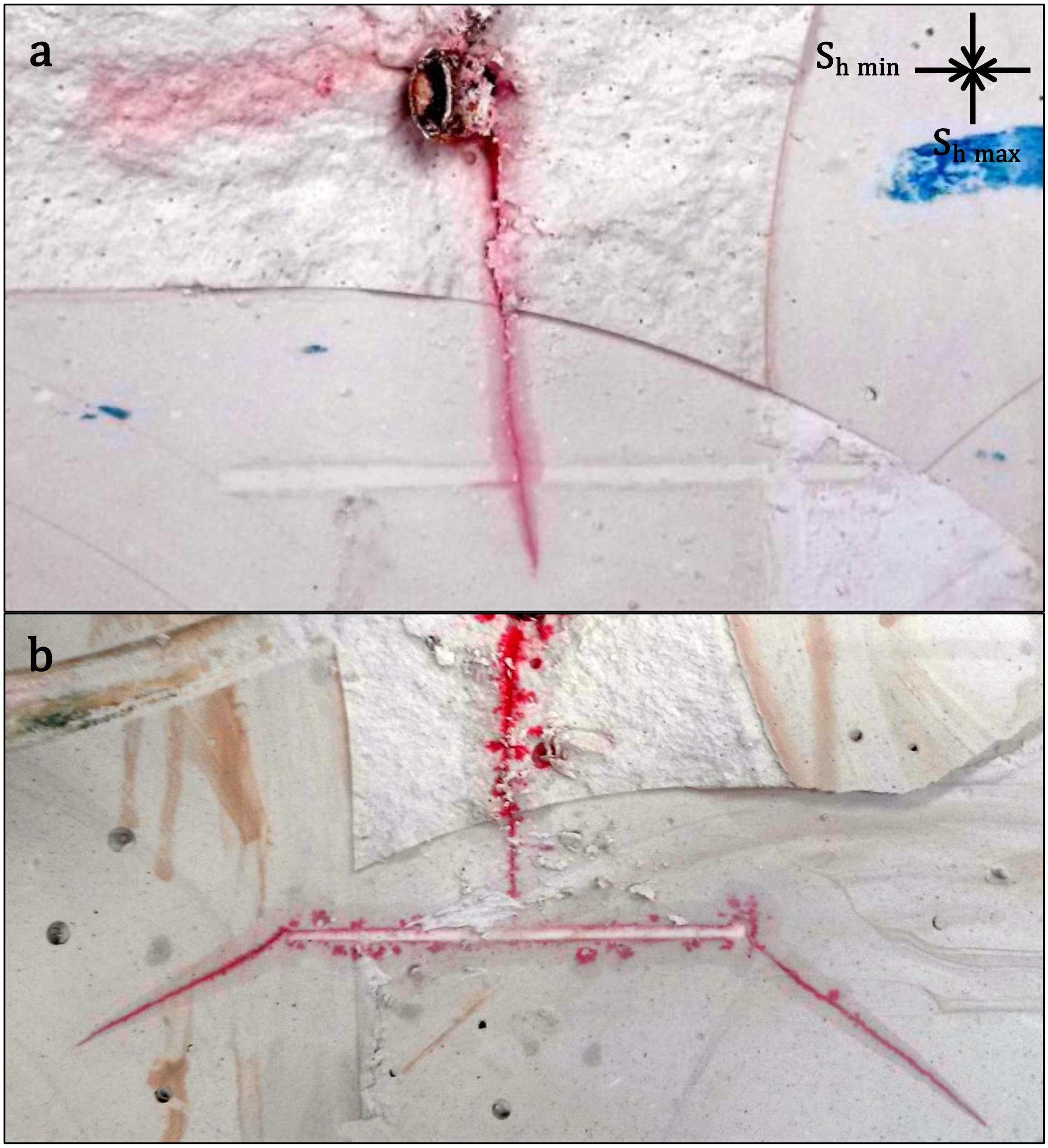

Figure 5.8: Same illustration as in the previous figure but without annotations to allow for complete visibility

Furthermore, since the tests discussed in this section primarily differ in the type of the PEF cement-fill only, it was attempted to identify the PEF's critical cohesion and internal friction coefficient values at or above which HF crosses the PEFs. Wu and Olson

(2014) fracturing numerical model was used to simulate the laboratory fracturing cases generically in order to obtain the threshold values of S_0 and μ_0 for crossing. Table 5.4 summarizes simulator input parameters. It was found that the minimum PEF cohesion value required for crossing was 800,000 Pascal in plaster host layers and 2,100,000 Pascal in hydrostone host layers with an internal friction coefficient of 0.6. Therefore, it could be interpreted from the laboratory data and the simulation results that the strongly-bonded cases fall at or above those numerical threshold values for crossing while weakly-bonded and cement free cases fall below them.

Table 5.4: Numerical simulation input for a generic laboratory fracturing test with pre-existing fractures

Parameter	**Symbol**	**Value**	**Unit**
Minimum Horizontal Stress	$S_{h\ min}$	25	psi
Maximum Horizontal Stress	$S_{h\ max}$	75	psi
Young’s Modulus	E	200,000 (plaster) 218,750 (hydrostone)	psi
Tensile Strength	T	297 (plaster) 700 (hydrostone)	psi
Poisson’s Ratio	ν	0.25	—
Leakoff Coefficient	C_L	0.000307	m/second$^{0.5}$
Height	H	0.1	m
Fluid Viscosity	μ	111	cP
Total Injection Flow rate	Q	200	milliliter/minute
Injection Time	t	262	second
HF-PEF Intersection Angle	—	90^0	degree

Effect of Pre-Existing Fracture Aperture

The effect of PEF aperture (width) on HF-PEF interaction outcomes was investigated, as some natural fractures experiments suggest that thicker fractures might be more likely to divert hydraulic fracture propagation. The laboratory testing results showed no clear impact of the width of the PEF inclusions on HF-PEF intersection mode as reported in Table 5.5. However, laboratory observations indicate a relationship between the width of the inclusion and the HF crossing behaviors and the stress-field conditions around the PEF inclusions. It seems that cleaner crossing patterns, i.e. simple planar crossing without deviations or jogging, were exhibited in the cases of inclusions with smaller widths. As the inclusion width increased, HF crossing tended to exhibit some non-planar deviatory behaviors. In particular, these behaviors seem to be impacted by the disturbance of the stress field observed around the exaggeratedly wide inclusions (Figures 5.9 and 5.10). The experimental results obtained from test 4 clearly shows non-planar HF propagation patterns past the intersection with the highly wide inclusion, which indicate that the stress field in that region might have been altered by the presence of the wide inclusion.

Table 5.5: Laboratory fracturing tests with pre-existing fractures of varying apertures

Cement-Fill Type	**Test #**	**PEF Width (mm)**	**HF-PEF Intersection Mode**
Strongly Bonded (Plaster-to-Plaster)	2	3	Crossing
	4	24	Crossing
Strongly Bonded (Hydrostone-to-Hydrostone)	3	2	Crossing
	5	35	Crossing

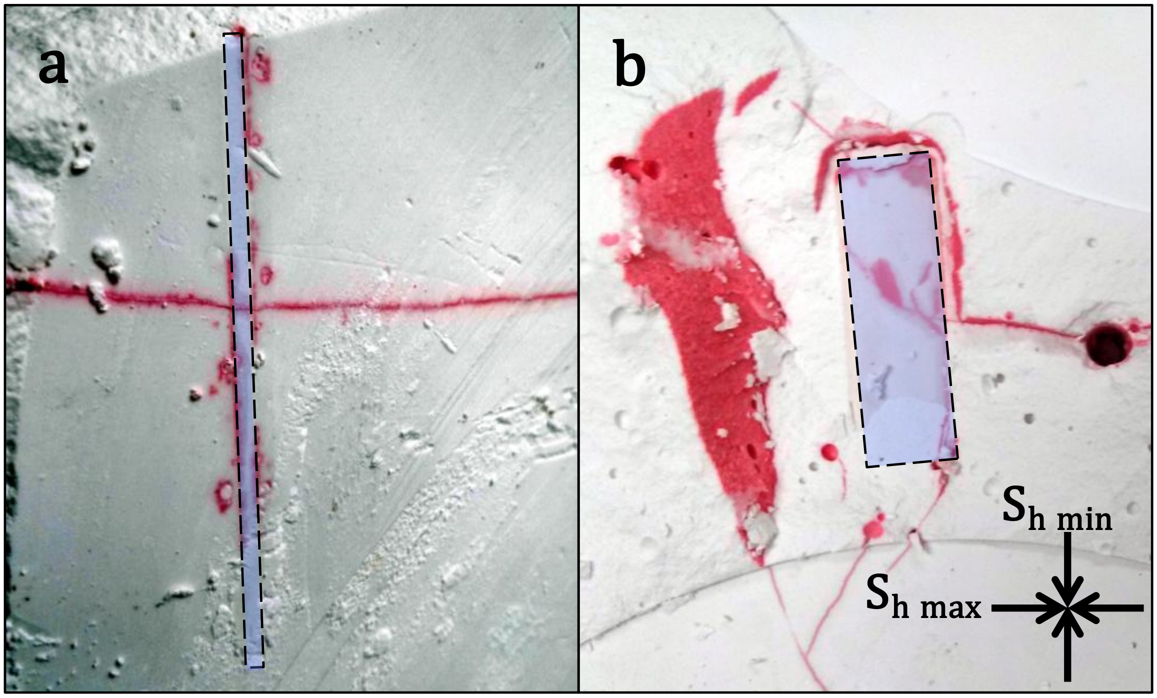

Figure 5.9: Top view photos of the middle sections of the block samples in a) test 2 and b) test 4 provide a comparison of hydraulic fracture (in red dye) crossing pre-existing inclusions (boxed in blue shade) of different widths which illustrates higher non-planarity with wider inclusions

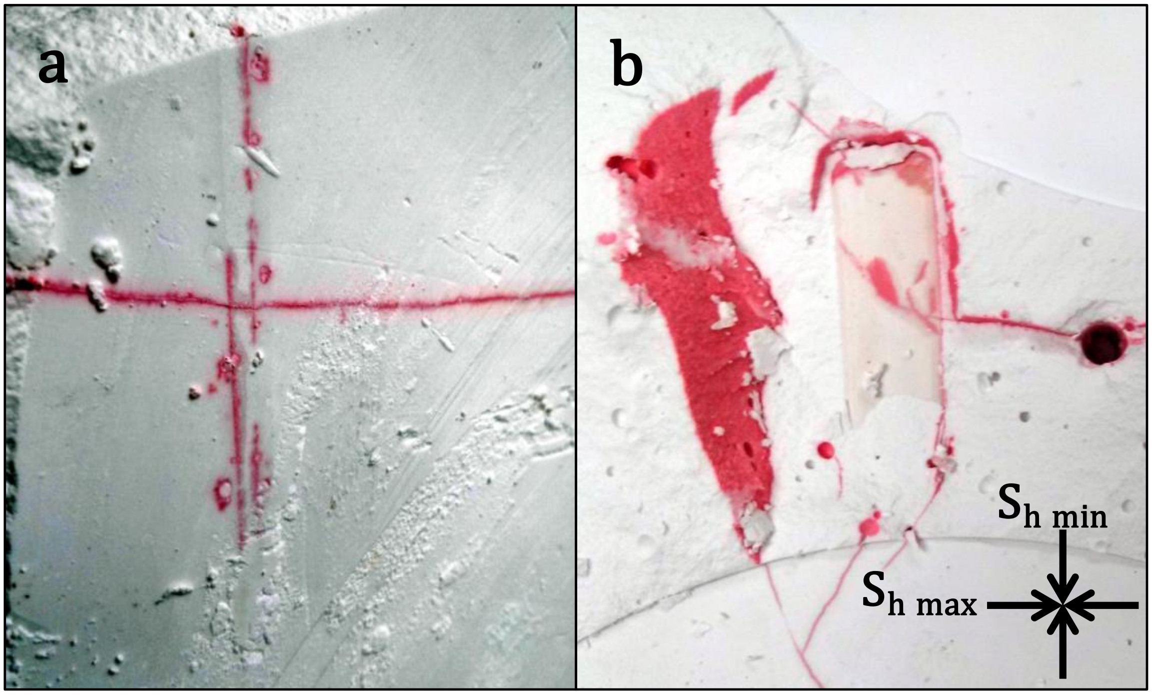

Figure 5.10: Similar illustration as in the previous figure but without annotations to allow complete visibility

Effect of HF Height Bypass

Experimental findings show that the occurrence of some HF height growth processes such as bypassing cemented PEFs impacts the outcomes of the HF-PEF intersection. For example, the results from three similar fracturing tests 2, 4, and 8 highlight the effect of the HF relative height at the intersection plane on the intersection outcome. Despite that all three tests had strongly-bonded PEF interfaces of the same type, i.e. plaster-to-plaster, their intersection modes differed based on the HF height relative to the height of the intersected PEF inclusions as shown in Table 5.6. It is clear from the results of the three tests that HF height growth along the intersection vertical axis increases the propensity for crossing. In particular, the fracturing cases where the HF-to-

PEF height ratios were higher than 2 exhibited crossing as in tests 2 and 4 whereas lower ratios below 0.5 exhibited deflections as in test 8.

Table 5.6: Laboratory fracturing tests with pre-existing fractures of varying heights

Test #	PEF Height (cm)	HF Height at Intersection (cm)	HF-to-PEF Height Ratio	HF-PEF Intersection Mode
2	4.8	10	2	Crossing
4	4.6	14	3	Crossing
8	23	11	0.5	Deflection

Examining the relationship between HF-PEF height bypass and HF actual crossing of cemented PEFs requires taking a closer look at the vertical axis of the HF-PEF intersection plane, i.e. along the height dimension. Applying the same concept of increased stress intensity loading ahead of the crack tip as the HF grows in propagation, the stress intensity loading at the cement-fill of the intersected PEFs increases similarly as the HF grows in height prior to crossing. As the HF height exceeds the height of the PEF, the HF begins to bypass the PEF, which further increases the stress intensity loading rate throughout the PEF cement-fill. Such increase in stress intensity loading is driven by the HF walls moving apart, i.e. HF grows in width. The HF wall movement drives the corresponding host-rock blocks behind each wall to move away from one another, which induces more stress intensity at nearby material around the crack tip (Fu et al. 2012). Once the critical stress intensity of the PEF cement-fill is reached, it cracks and the HF actually crosses through it. It is important to point out that the tensile strength of the PEF cement-fill relative to the host rock plays a role in whether HF actually breaks the cemented PEF. Bahorich (2012) observed in similar experiments little evidence of HF crossing cemented PEFs when the tensile strength of the intersected PEF cement-fill is much larger than the host rock (glass slides in plaster host rock); the intersection outcome resulted in HF height bypass and separation of the weakly bonded interfaces. The results from Bahorich (2012) suggest that the stress intensity loading induced on the cemented PEFs during HF height growth and bypass is likely to be ineffective in overcoming the critical stress intensity of the PEF cement-fill when the cement-fill is much stronger than the host rock. Figure 5.11 shows qualitative, two-dimensional illustrations of the relationship between HF-PEF height bypass and stress intensity loading along the PEF cement-fill and Figures 5.12 and 5.13 provide laboratory evidences of HF enabled crossing mainly due to HF height growth and bypass. However, further work is required to quantifiably evaluate the amount of the vertical intensity loading associated with HF-PEF height growth and bypass. Perhaps it is possible to update Renshaw and Pollard (1995) crossing criterion to account for the effect of HF-PEF relative heights and associated HF bypass mechanisms.

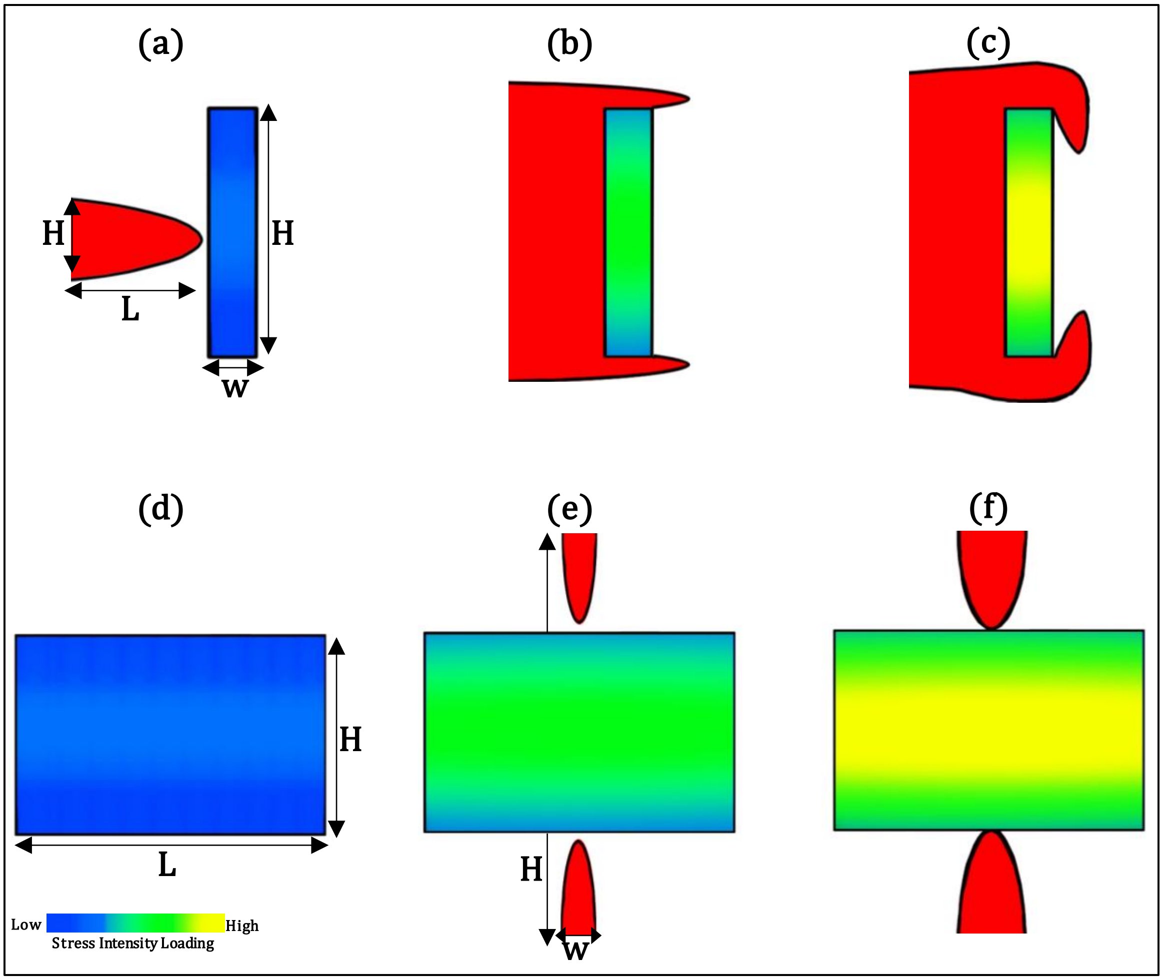

Figure 5.11: Two dimensional illustrations of the relationship between a hydraulic fracture (in red) approaching an orthogonal, cemented pre-existing fracture (triangle box) and the vertical intensity loading along the PEF cement-fill as the HF grows in height and bypasses the PEF—a) through c) show the PEF height-by-width plane while d) through f) show the PEF height-by-length plane

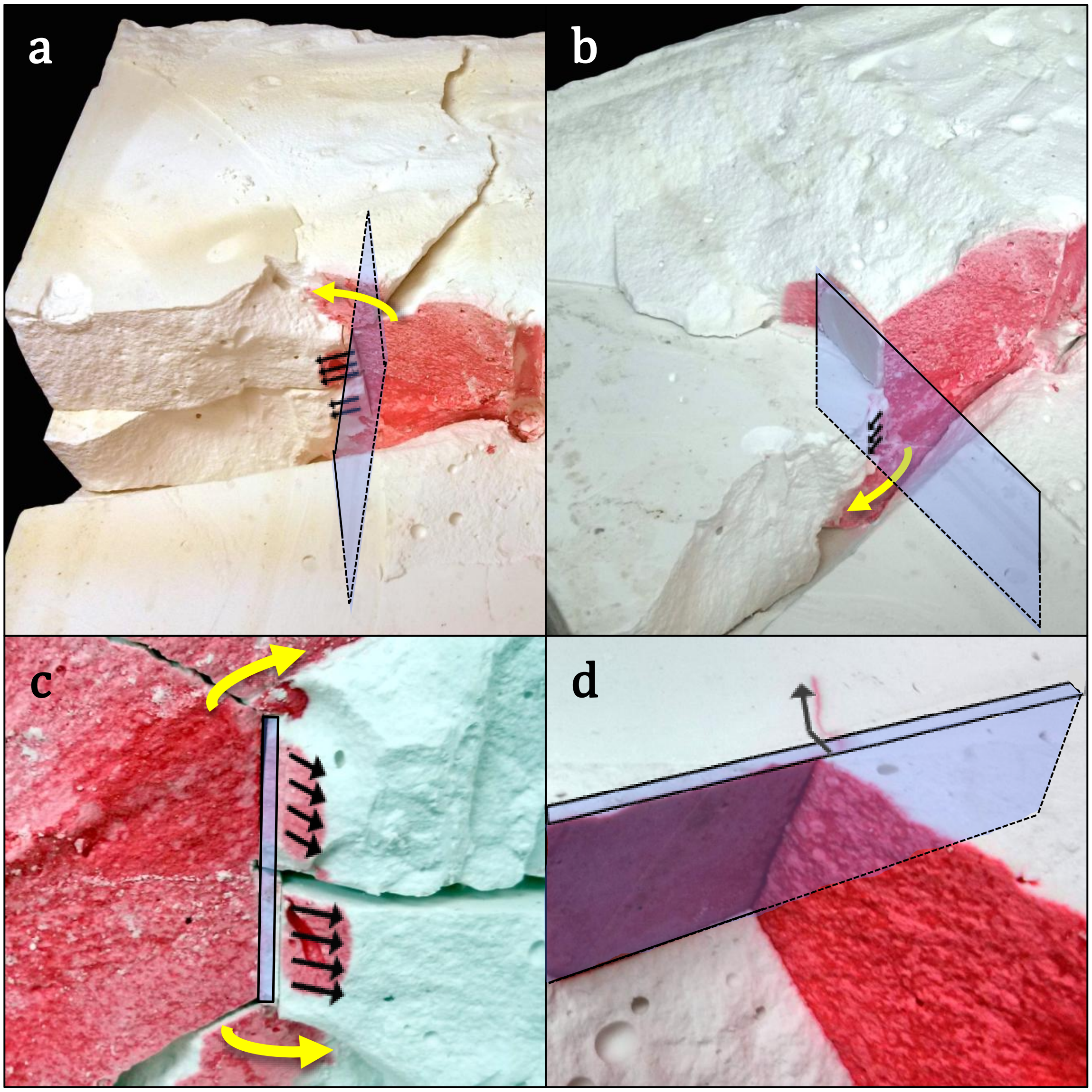

Figure 5.12: Four photos of various views of the block sample in test 2 showing hydraulic fracture (in red dye) intersecting a pre-existing inclusion (boxed in blue shade) illustrate the role of hydraulic fracture height growth and bypass (marked by yellow arrows) in enabling hydraulic fracture crossing the pre-existing discontinuity (marked by black arrows)

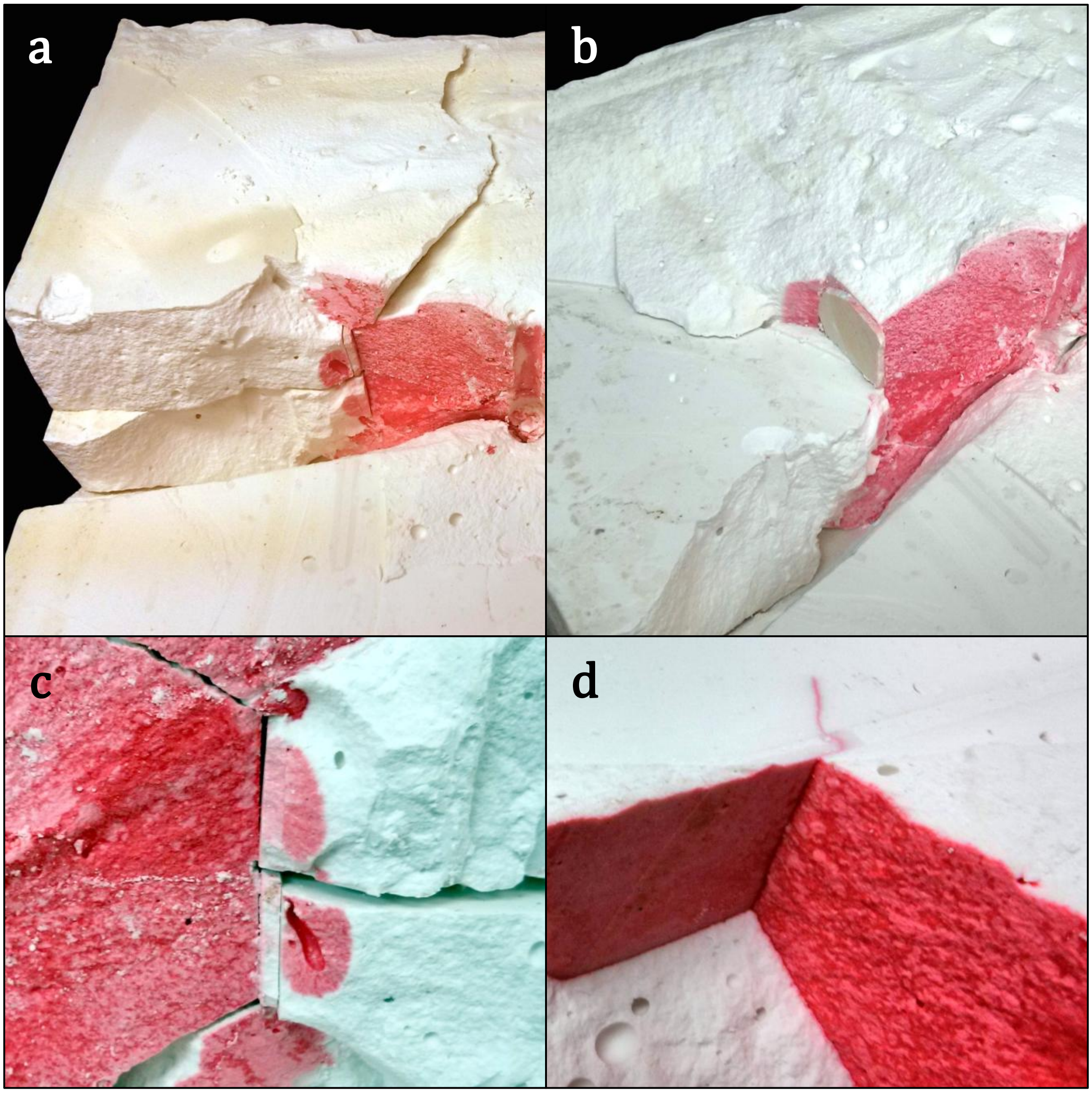

Figure 5.13: Similar illustration as in the previous figure but without annotations to allow complete visibility

5.1.2.3 Mixed Mode

Deflected HFs have exhibited some mixed-mode propagation behaviors. Signs of mixed-mode-I-II forces were identified in all the fracturing tests where complete or partial HF deflection occurred including tests 2, 4, 6, 7, and 8. Upon HF-PEF orthogonal intersection, HFs initially deflect along the PEFs and then branch out from the PEF side edges in mixed-mode-I-II fashions; deflected HFs propagating into the direction of the minimum horizontal stress along PEFs kink off at the side ends of the PEFs. These branch-out segments of HFs are the result of a mix of opening and sliding forces that act concurrently to propagate the HF in this fashion. It was found that the HF kink-off angles ranged from 22^0 to 50^0 with the majority of the cases exhibiting kink-off angles around 45^0 degrees.

Similarly, observations of mixed-mode-I-III propagation behaviors were clearly reported in test 6. Dilatant echelon cracks were observed in the deflected HF segments along the orthogonal PEF direction. These en-echelon cracks are the results of a mix of opening and tearing forces that concurrently drive HF propagation in this fashion. In order to quantifiably evaluate mode-III-to-mode-I stress intensity ratio, i.e. K_{III}/K_I, causing the en-echelon behaviors, Equations 5.7 and 5.8 are used (Pollard et al. 1982). Hence, analysis of test 6 data shows K_{III}/K_I values below 0.1 which indicates that the opening forces were roughly ten times higher than the tearing forces. Figure 5.14 shows mixed-mode propagation behaviors observed in the laboratory.

$$R = \frac{(2P + S_{h\,max} + S_{h\,min})}{(S_{h\,max} - S_{h\,min})} \tag{5.7}$$

$$\frac{K_{III}}{K_I} = \frac{(sin\,2\alpha)}{(R + cos\,2\alpha)} \tag{5.8}$$

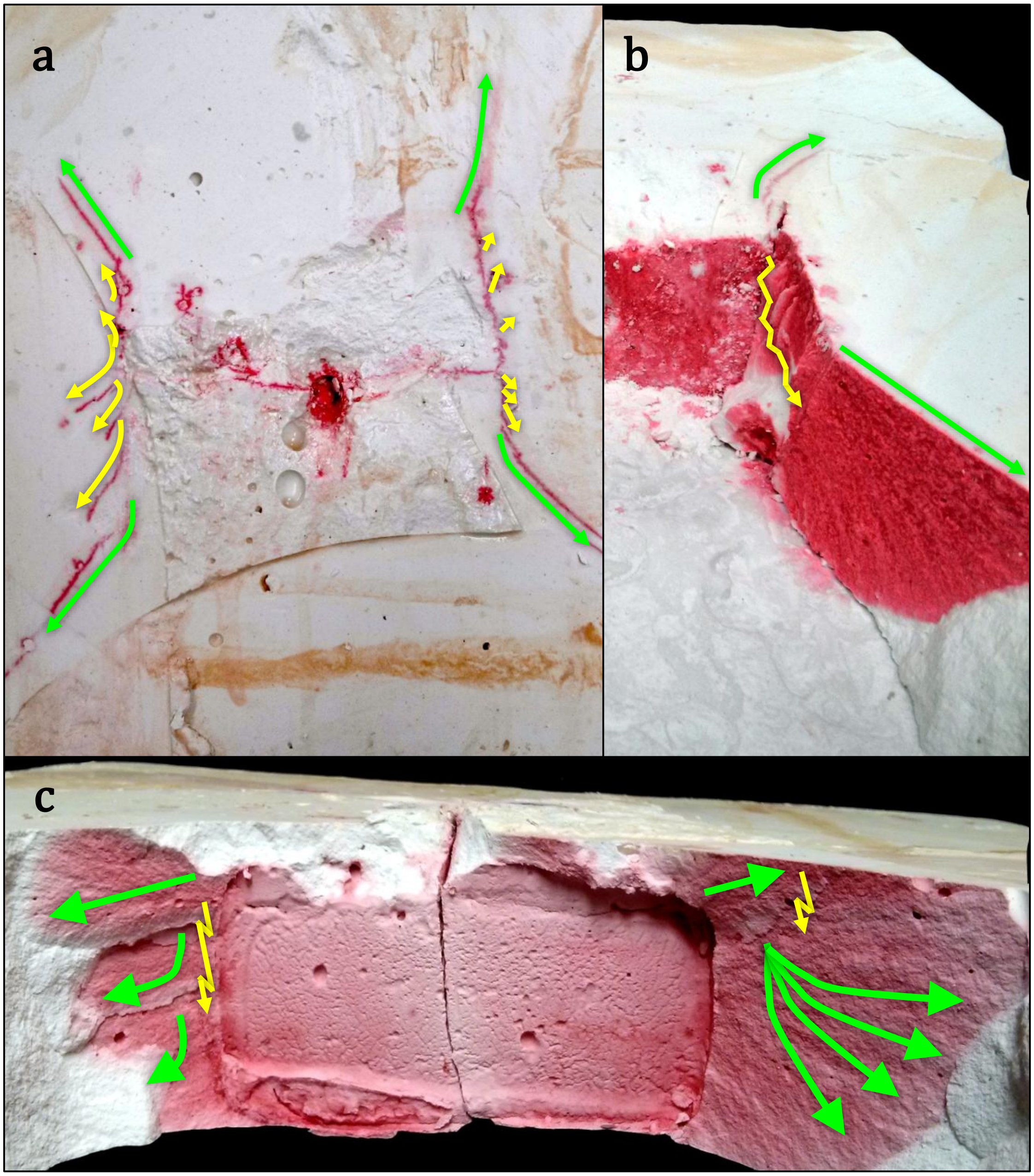

Figure 5.14: a) Top, b) side, and c) cross-sectional view photos of the middle section of the block sample in test 6 show hydraulic fracture (in red dye) intersecting a pre-existing discontinuity, deflecting along it while exhibiting mixed-mode-I-III en-echelon cracks (marked in yellow arrows), and branching out at the side edges of the pre-existing discontinuity in mixed-mode-I-II fashion (marked in green arrows)

5.2 INTERACTION BETWEEN SIMULTANEOUS MULTIPLE HYDRAULIC FRACTURES

Given the limited experimental successes in achieving simultaneous multi-fracture propagation, the discussion of the results is limited to qualitative analyses and broad remarks based on the outcomes of tests 9, 10, and 11. Although the set-up of the three tests was fairly comparable, they yielded a different number of simultaneous hydraulic fractures of different sizes; at least more than 75% of the fracturing fluid went into one fracture in all three tests. Despite the experimental limitations that might have contributed to the lack of proper simultaneous fracturing, a trend of results was observed. Therefore, the following sections attempt to assess those trends and identify some conclusions.

5.2.1 Formation Breakdown Pressure

Despite the volume of each hydraulic fracture, the number of the simultaneous hydraulic fractures initiated per test resulted in a trend of formation breakdown pressures. A higher breakdown pressure was observed when a larger number of simultaneous hydraulic fractures initiated as shown in Table 5.7.

Table 5.7: Plaster breakdown pressure results for the simultaneous multiple hydraulic fracturing tests

Test #	Number of HF	Breakdown Pressure (psi)* * corrected for wellbore pressure drop	Fracturing Fluid Type
9	1	473	Linear gel
10	2	526	Linear gel
11	3	~ 990	Cross-linked gel

The observed trend of increased breakdown pressure for larger number of simultaneous hydraulic fractures is in agreement with some of the findings reported in the petroleum engineering literature. Since hydraulic fracture initiation requires creating fracture width through pressurizing initial cracks and pushing the crack walls apart, it induces compressive stresses on the rock matrix behind each fracture wall, which dissipate after some distance. Hence, as more hydraulic fracturing sources are attempting to initiate fractures, more compressive stresses are being induced on the rock matrix in the areas neighboring to each fracturing source. Therefore, these induced compressive stresses require higher fracturing pressure in order to overcome them and create tensile failures, i.e. formation breakdowns.

5.2.2 Propagation Pattern

All three fracturing tests 9, 10, and 11 had three fracturing sources with comparable spacing between them. Although not all the fracturing sources initiated fractures, there were some propagation trends observed based on the number of the initiated hydraulic fractures. The underlining observations regarding the behaviors of the simultaneous multi-fracture propagation from those tests consist of two tendencies: Firstly, larger, i.e. dominant, fractures tend to initiate from outer fracturing sources while smaller fractures tend to form from the interior sources. Secondly, outer fractures tend to propagate in an outward-curving fashion while inner fractures are more aligned towards the direction of the maximum horizontal stress.

It was clearly observed that the dominant fracture always initiated from an outside fracturing source, i.e. located at an end-side of the fracturing stage. Since the interior fracturing sources, i.e. located at the middle of the stage, are subjected to relatively higher compressive stresses induced from neighboring fracturing sources, creating the fracture width required to drive the crack tip forwards in such regions of the rock is more difficult. Therefore, the propagation of the middle fractures is usually inhibited, which results in small-sized fractures. Hence, uneven distribution of injection fluids between the fracturing sources is further enhanced by the higher resistance to propagation induced on the middle fractures, which consequently allows larger fluid volume to go into outer fracturing sources creating larger fractures.

Moreover, it was found that outer fractures propagate with an outward curvature. The initial propagation angle away from the maximum horizontal stress increased as the number of the simultaneous hydraulic fractures increased as shown in Table 5.8. Thus, it could be inferred from the propagation deviation angles that larger interaction between the hydraulic fractures occurs when more fractures are simultaneously propagating, which is in agreement with most findings reported in the petroleum engineering literature.

Table 5.8: Simultaneous multi-fracture propagation angles for hydraulic fracturing tests 9, 10, and 11

Test #	**Number of HF**	**Outer HF Curvature Angle**	**Inner HF Curvature Angle**
9	1	15^0 Degrees	—
10	2	25^0 Degrees	0^0 Degree
11	3	66^0 Degrees	57^0 Degrees

5.3 DISCUSSION OF THE RESULTS IMPLICATIONS

The experimental results and analyses in this study have yielded a number of findings pertaining to hydraulic fracture interaction with pre-existing fractures and the interaction between multiple simultaneous hydraulic fractures, which are two subjects of high relevance to hydraulic fracturing applications in unconventional formations. Although utilizing laboratory-derived conclusions in actual field fracturing applications has some limitations, they provide very useful insights into the complex fracturing mechanisms that take place in such applications. Hence, the improved understanding resulted from such insights allows for making proper diagnoses and solutions to some of the challenges often reported in the field. In particular, the analysis of some challenges commonly faced in multistage fracturing treatments in naturally fractured reservoirs can be benefited by the findings of this study. Among those challenges, the issues of limited HF penetration into the reservoir, proppant premature screenout, partial fracturing fluid recovery in flowbacks, and improper fracturing stage designs may be better understood and handled.

Reservoir characterization knowledge is highly critical for fracturing applications in naturally fractured reservoirs. Particularly, information related to the natural fracture orientation, geometry, geomechanics, and geochemistry are very important to predict how they may influence the hydraulic fracturing treatments. Based on the objectives of the hydraulic fracturing treatment, addressing certain aspects related to the pre-existing fractures becomes necessary. For example, treatments targeting deep HF penetration into the reservoir should review crossing favorability of the HF-PEF intersections. Fracturing fluid selection could be reviewed based on the type of cementation inside the PEFs, i.e. strongly-bonded vs. weakly-bonded. Therefore, utilizing more viscous fracturing fluids at higher rates could yield favorable results for crossing as reported in other studies in the literature. Moreover, allowing HF height growth increases the propensity for crossing as highlighted by the experimental results presented previously. Inversely, when the treatment objectives favor areal extension in the reservoir, lower viscous fluids at lower rate becomes more suitable.

Additionally, proppant transportability is more susceptible to premature screenout in the cases where the HF-PEF intersections yield HF deflections. As highlighted from the laboratory results, HF deflections along the PEF causes sudden turns in the HF propagation whether at the intersection point or at the kink-off points at the PEF side edges. Thus, proppants are likely to bridge at those turns leaving segments of the HF unpropped and resulting in premature screenouts. Similarly, the full recovery of the injected fracturing fluids could be compromised in branching-out, deflected HFs. Since the propagation patterns of the deflected HFs as observed in the laboratory consists of multiple segments of different orientations, the different magnitudes of the corresponding closure pressures of those segments could cause volumes of the fracturing fluids to be left unrecovered. For instance, when the middle segments of the HF closes at a higher pressure than the end fracture segments, the fracturing fluids inside those end segments become trapped without proper paths into the wellbore during flowbacks. Therefore, partial volumes of the injected fluids remain unrecovered due to their entrapment inside farther segments of the HF.

Furthermore, the completion design of the fracturing stage in multistage fracturing wells such as wells with plug-and-perf completions is often suboptimal. It is commonly reported that a number of the stage perforation clusters is either under-producing or nonproducing, which question the effectiveness of the HF treatment. Laboratory results clearly show some destructive interaction between simultaneous multiple fractures resulting in complete or partial inhibition of the fracture propagation due to induced stresses. The stress interference between simultaneous fractures is sensitive to the spacing and the number of the fracturing sources per fracturing stage. Therefore, in many cases it may not be economical to include a large number of perforation clusters in the design of a fracturing stage especially when the spacing between the clusters is limited.

Overall, comprehensive review of the experimental results and data analyses presented in this study gives useful insights into some aspects of hydraulic fracturing unconventional formations. Such knowledge is very important for improving the understanding of some complex fracturing processes, enhancing the diagnoses of some reported challenges, and helping find some solutions to current problems.

Chapter 6: Conclusions

Hydraulic fracturing unconventional formations using current practices of multistage fracturing techniques is geomechanically dictated by two mechanisms: Hydraulic fracture (HF) interaction with pre-existing fractures (PEF) on one hand, and the interaction between simultaneous multiple hydraulic fractures on the other hand. Hence, studying relevant parameters that govern such interactions has been of an increasing interest to the petroleum upstream industry. It has been widely established that the propensity for HF crossing PEFs increases as the intersection angle is closer to 90^0 degrees. Similarly, it has been broadly accepted that closer spacing between simultaneous fracturing sources, i.e. perforation clusters, yield higher interaction between the propagating HFs. However, there remains a need for further discussions and evaluations of some mechanisms and behaviors that dominate such HF interactions. In particular, experimental data are desperately needed to provide, validate, or further support some findings related to such hydraulic fracturing topics. Therefore, this work uses a series of laboratory hydraulic fracturing tests on synthetic rocks to investigate hydraulic fracture propagation reactions and treatment pressure responses to intersected orthogonal pre-existing fractures and neighboring simultaneous fracturing sources. As a result, the following conclusions have been obtained:

1. HF intersection with orthogonal PEF may yield crossing, deflection, or a combination of both, mainly based on the PEF cementation type relevant to the host rock and the relative HF-PEF height ratio.
2. The hydraulic fracturing pressure responses may be indicative of the HF-PEF intersection outcomes.

3. Fracture-extension pressure behavior of sudden or gradual increases followed by declines has been identified as a signature to the branch-out deflection outcomes of HF-PEF orthogonal intersections. Under anisotropic stress conditions, the change in HF propagation direction upon intersecting the PEF associates with an increase in the magnitude of the compressive stresses acting on the HF walls. Thus, higher injection pressure is required to continue driving the HF past the deflection point, which creates pressure bumping patterns in the treatment pressure profiles.
4. Complex HF propagation such as the branch-out deflection patterns resulting from some HF-PEF intersections shows a higher average value of the fracture closure pressure than HFs with planar-like propagations. Moreover, branching-out HFs may exhibit indications of multiple closure pressures. Such HF complexity comes from having multiple fracture segments of different orientations. Thus, in anisotropic rock layers, the compressive stresses acting on each segment may differ in magnitude based on the magnitudes of the respective remote and local stresses per fracture orientation and region. Therefore, each fracture segment may close at a different pressure in response to the net compressive stresses acting on its walls.
5. In the cases of branching-out, deflected HF propagation, multiple HF closures could contribute to the issues of partial recovery of injected fluids during flowbacks. Having the middle fracture segments close before the far-end segments entraps some fluid volumes inside the far-end segments and leave them unrecovered.
6. Proppant transportability down HFs could be compromised in deflected HFs. Sudden propagation turns observed in deflected HFs provides regions of potential proppant bridging which would lead to premature screenouts.
7. The type of the PEF cement-fill relative to the type of the host rock has a dominant role in controlling the cohesion (S_0) and the internal friction coefficient (μ_0) of the

discontinuity interface between the PEF and the rock. Mineral precipitations and other geological processes often control the type of cementation inside PEFs. Cement-fills that are strongly bonded to the host rock increase the interfaces' S_0 and μ_0 values, which enhances the tendency of HF crossing the PEFs.

8. HF-PEF intersection mode seems to be insensitive of the PEF aperture.
9. The height of the HF relative to the height of the intersected PEF plays an important role in determining the intersection outcomes. Higher HF-to-PEF height ratio at the intersection region enhances HF crossing the PEF interface. HF height growth along the intersection vertical plane, and perhaps even height bypass, increases the stress intensity loading across the discontinuity interface, which ultimately could lead to its cracking, which allows HF to transmit across the interface. However, the effectiveness of this process is limited when the tensile strength of the cemented PEF is much larger than the host rock as suggested by the work of Bahorich (2012).
10. Numerical simulation models of HF-PEF intersections could enhance their crossing criteria by including the effect of relative height in addition to cohesion and friction.
11. Deflected HF into the direction of orthogonal PEF may exhibit mixed-mode-I-III propagation behaviors especially in the cases of non-cemented PEFs. Although tearing-mode forces may be ten times lower than opening-mode forces, their concurrent acts cause the creation of en-echelon cracks along the propagation direction.
12. At the side edges of orthogonal PEFs, deflected HFs kink off and branch out exhibiting mixed-mode-I-II behaviors.
13. Achieving equal fracturing injection and propagation for simultaneous multiple hydraulic fractures is operationally challenging. Laboratory experiments show

repeated tendency for having one dominant hydraulic fracture initiated from a fracturing source while other sources yield traces of smaller fractures.

14. The fracture initiation pressure tends to increase as the number of the simultaneous HFs increases. As more HFs attempt to simultaneously initiate, higher compressive stresses are induced on each fracturing source from neighboring sources, which require higher injection pressure to counteract them.
15. In a fracturing stage, perforation clusters located in the middle of the stage tend to exhibit the most inhibited HF propagation while perforation clusters located at the sides tend to yield larger HFs. Compressive stress interference is magnified on the middle region of the fracturing stage due to its relative closeness to other fracturing sources on both sides.
16. In a fracturing stage, outer HFs tend to curve outwardly in propagation while middle HFs tend to be more aligned into the direction of the maximum horizontal stress. Also, initial deviation angle away from the maximum horizontal stress seems to increase as the number of simultaneous hydraulic fractures per fracturing stage increases.
17. Some degrees of asymmetry and non-planarity in hydraulic fracture propagation are commonly observed even when the rock heterogeneity is considerably small.

Glossary

- α = Hydraulic fracture mixed mode rotation angle (degrees)
- BHP = Bottomhole pressure (a unit of force per area)
- C = perforation coefficient (0.95 for round perforation holes)
- D = wellbore diameter (a unit of length)
- ΔP = Pressure differential or pressure drop (a unit of force per area)
- $\frac{\partial u}{\partial y}$ = Fluid Shear Rate (a unit of 1/time)
- E = Young's modulus (a unit of force per area)
- ϵ = Relative roughness
- f_f = Friction factor
- $g(t_D)$ = Average decline rate function
- $G(t_D, t_D^*)$ = Dimensionless difference known as the G-function
- HF = Hydraulic fracture
- ISIP = Instantaneous Shut-In Pressure (a unit of force per area)
- K_I = Opening mode stress intensity (a unit of force per length$^{1.5}$)
- K_{II} = Sliding mode stress intensity (a unit of force per length$^{1.5}$)
- K_{III} = Tearing mode stress intensity (a unit of force per length$^{1.5}$)
- K_{IC} = Fracture toughness (a unit of force per length$^{1.5}$)
- K_v = Fluid viscosity constant (a unit of mass per length per time^{n-2})
- μ = Coefficient of friction
- μ_0 = Internal friction coefficient
- μ_v = Fluid viscosity (a unit of mass per length per time)
- n = Fluid-behavior power component

- N_{Re} = Reynold’s number
- ν = Poisson’s Ratio
- P = hydraulic fracture pressure (a unit of force per area)
- P_b = Formation breakdown pressure (a unit of force per area)
- PEF = Pre-existing fracture
- P_p = Pore pressure (a unit of force per area)
- p’ = The G-function’s pressure derivative (a unit of force per area)
- q = Injection flow rate (a unit of volume per time)
- Q = Total injection flow rate (a unit of volume per time)
- r = wellbore radius (a unit of length)
- R = stress ratio
- ρ = density (a unit of mass per volume)
- S_0 = Cohesion (a unit of force per area)
- $S_{h\,max}$ = Maximum horizontal stress (a unit of force per area)
- $S_{h\,min}$ = Minimum horizontal stress (a unit of force per area)
- σ_{xx}^{r} = Remote principle stress acting parallel to fracture-propagation direction (a unit of force per area)
- σ_{yy}^{r}= Remote principle stress acting perpendicular to fracture-propagation direction (a unit of force per area)
- t = Injection time (a unit of time)
- T = Tensile strength (a unit of force per area)
- t_D = Dimensionless shut-in time
- t_D^* = Reference time since shut-in ($t_D^* = 0$)
- t_{ISIP} = Time at Instantaneous Shut-In Pressure (a unit of time)
- u = flow velocity (a unit of length per time)

- UCS = Unconfined compressive strength (a unit of force per area)

References

1. Abass, H. H., Hedayati, S., and Meadows, D. L., 1996, Nonplanar Fracture Propagation From a Horizontal Wellbore: Experimental Study, SPE 24823, SPE Production & Facilities, Augus, Pages 133-137.
2. Bahorich, B. L., 2012, Examining the Effect of Cemented Natural Fractures on Hydraulic Fracture Propagation in Hydrostone Block Experiments, Master's Thesis at the University of Texas at Austin.
3. Blanton, T. L., 1982, An Experimental Study of Interaction Between Hydraulically Induced and Pre-Existing Fractures, SPE 10847, SPE/DOE Unconventional Gas Recovery Symposium, Pittsburgh, PA, May 16-18.
4. Brumley, J. L., and Abass, H. H., 1996, Hydraulic Fracturing of Deviated Wells: Interpretation of Breakdown and Initial Fracture Opening Pressure, SPE 37363, the Eastern Regional Meeting, Columbus, Ohio, October 23-25.
5. Bunger, A. P., Zhang, X., and Jeffrey, R. G., 2012, Parameters Affecting the Interaction Among Closely Spaced Hydraulic Fractures, SPE 140426, SPE Journal, March, Pages 292-306.
6. Castillo, J. L., 1987, Modified Fracture Pressure Decline Analysis Including Pressure-Dependent Leakoff, SPE 16417, the SPE/DOE Low Permeability Reservoirs Symposium, Denver, CO, USA, May 18-19.
7. Chang, F. F., Bartko, K., Dyer, S., Aidagulov, G., Suarez-Rivera, R., and Lund, J., 2014, Multi Fracture Initiation in Openhole without Mechanical Isolation: First Step to Fulfill an Ambition, SPE 168638, the SPE Hydraulic Fracturing Technology Conference, The Woodlands, TX, USA, February 4-6.
8. Chen, N. H., 1979, An Explicit Equation for Friction Factor in Pipe, Ind. Eng. Chem. Fund., 18: 296.
9. Darby, R., 2001, Chemical Engineering Fluid Mechanics, 2nd Edition, CRC Press, Page 64.
10. Economides, M. J., Hill, A. D., and Ehlig-Economides, C., 1994, Petroleum Production Systems, Prentice Hall, PTR, Pages 134, 140, 142, 207.
11. El Rabaa, W., 1989, Experimental Study of Hydraulic Fracture Geometry Initiated From Horizontal Wells, SPE 19720, the 64th Annual Technical Conference and Exhibiton of the Society of Petroleum Engineers, San Antonio, TX, USA, October 8-11.
12. Fisher, M. K., Harris, C. D., Davidson, B. M., Wright, C. A., and Dunn, K. P., 2004, Optimizing Horizontal Completion Techniques in the Barnett Shale Using

Microseismic Fracture Mapping, SPE 90051, the SPE Annual Technical Conference and Exhibition, Houston, TX, USA, September 26-29.

13. Fu, P., Johnson, S. M., and Carrigan, C. R., 2012, An explicitly coupled hydro-geomechanical model for simulating hydraulic fracturing in arbitrary descrete fracture networks, International Journal for Numerical and Analytical Methods in Geomechanics, August 23, Pages 2278-2300.
14. Geertsma, J., and de Klerk, F., 1969, A rapid method of Predicting Width and Extent of Hydraulically Induced Fractures. J. Pet. Tech. 21:1571–1581.
15. Gil, I., Nagel, N., and Sanchez-Nagel, M., 2011, The Effect of Operational Parameters on Hydraulic Fracture Propagation in Naturally Fractured Reservoirs – Getting Control of the Fracture Optimization Process, The 45th US Rock Mechanics/ Geomechanics Symposium, San Francisco, CA, USA, June 26-29.
16. Gu, H., and Weng, X., 2010, Criterion for Fractures Crossing Frictional Interfaces at Non-Orthogonal Angles, ARMA 10-198, the 44th US Rock Mechanics Symposium and 5th U.S.-Canada Rock Mechanics Symposium, Salt Lake City, UT, USA, June 27-30.
17. Gu, H., Weng, X., Lund, J., Mack, M., Ganguly, U., and Suarez-Rivera, R., 2012, Hydraulic Fracture Crossing Natural Fracture at Nonorthogonal Angles: A Criterion and Its Validation, SPE 139987, the SPE Hydraulic Fracturing Technology Conference, The Woodlands, TX, USA, January 24-26.
18. Hanson, M. E., Shaffer, R. J., and Anderson, G. D., 1981, Effects of Various Parameters on Hydraulic Fracturing Geometry, SPE Journal, August, Pages 435-443.
19. Holditch, S. A., 2014, Taking Unconventional Outside of North America—Where are the Barriers?, the SPE Hydraulic Fracturing Technology Conference, The Woodlands, TX, USA, February 4-6.
20. Holley, E. H., Zimmer, U., Mayerhofer, M. J., and Samson, E., 2010, Integrated Analysis Combining Microseismic Mapping and Fiber-Optic Distributed Temperature Sensing (DTS), CSUG/SPE 136565, the Canadian Unconventional Resources and International Petroleum Conference, Calgary, Alberta, Canada, October 19-21.
21. Hosseini, S. M., 2012, Hydraulic Fracture Mechanism in Unconsolidated Formations, Master's Thesis at the University of Texas at Austin.
22. Jennings, A. R., 2008, Comments Concerning Limited Entry Treatment Applications, Enhanced Well Stimulation, Inc.
23. Ketter, A. A., Daniels, J. L., Heinze, J. R., and Waters, G., 2006, A Field Study Optimizing Completion Strategies for Fracture Initiation in Barnett Shale Horizontal Wells, SPE 103232, the SPE Annual Technical Conference and Exhibition, San Antonio, TX, USA, September 24-27.

24. Khristianovic, S. A., and Zheltov, Y. P., 1955, Formation of Vertical Fractures by Means of Highly Viscous Fuids, the 4th World Petroleum Congress, Rome, Italy, 2, pp. 579–586.
25. Koskella, D., 2014, Observations from an Underground Laboratory: An Integrated Diagnostic Approach to Unlocking Performance in the Niobrara, Keynote Speech, the SPE Hydraulic Fracturing Technology Conference, The Woodlands, TX, USA, February 4-6.
26. Kresse, O., and Weng, X., 2013, Hydraulic Fracturing in Formations with Permeable Natural Fractures, INTECH, http://dx.doi.org/10.5772/56446.
27. Kresse, O., Weng, X., and Chuprakov, D., 2013, Effect of Flow Rate and Viscosity on Complex Fracture Development in UFM Model, INTECH, http://dx.doi.org/10.5772/56406.
28. Lolon, E. P., Cipolla, C. L., Weijers, L., Hesketh, R. E., and Grigg, M. W., 2009, Evaluating Horizontal Well Placement and Hydraulic Fracture Spacing/Conductivity in the Bakken Formation, North Dakota, SPE 124905, the 2009 SPE Annual Technical Conference and Exhibition, New Orleans, LA, USA, October 4-7.
29. Miller, C., Waters, G., and Rylander, E., 2011, Evaluation of Production Log Data from Horizontal Wells Drilled in Organic Shales, SPE 144326, the SPE North American Unconventional Gas Conference and Exhibition, The Woodlands, TX, USA, February 14-16.
30. Molenaar, M. M., Fidan, E., and Hill, D. J., 2012, Real-Time Downhole Monitoring of Hydraulic Fracturing Treatments Using Fiber Optic Distributed Temperature and Acoustic Sensing, SPE 152981, the SPE/EAGE European Unconventional Resources Conference and Exhibition, Vienna, Austria, March 20-22.
31. Morrell, R. S., and de Waele, A., 1920, Rubber, Resins, Paints, and Vanishes, Van Nostrand Company.
32. Nagel, N., Gil, I., Sanchez-Nagel, M., and Damjanac, B., Simulating Hydraulic Fracturing in Real Fractured Rock – Overcoming the Limits of Pseudo 3D Models, SPE 140480, the SPE Hydraulic Fracturing Technology Conference, The Woodlands, TX, USA, January 24-26.
33. Nagel, N., Sheibani, F., Lee, B., Agharazi, A., and Zhang, F., 2014, Fully-Coupled Numerical Evaluations of Multiwell Completion Schemes: The Critical Role of In-Situ Pressure Changes and Well Configuration, SPE 168581, the SPE Hydraulic Fracturing Technology Conference, The Woodlands, TX, USA, February 4-6.
34. Nolte, K. G., 1979, Determination of Fracture Parameters From Fracturing Pressure Decline, SPE 8341, the 54th Annual Fall Technical Conference and Exhibition of the Society of Petroleum Engineers of AIME, Las Vegas, NV, USA, September 23-26.

35. Nordgren, R. P., 1972, Propagation of a Vertical Hydraulic Fracture. Soc. Pet. Eng. J. 12:306–314.

36. Olson, J. E., 2008, Multi-Fracture Propagation Modeling: Applications to Hydraulic Fracturing in Shales and Tight Gas Sands, ARMA 08-327, the 42nd US Rock Mechanics Symposium and 2nd US-Canada Rock Mechanics Symposium, San Francisco, CA, USA, June 29-July 2.

37. Olson, J. E., Bahorich, B., and Holder, J., 2012, Examining Hydraulic Fracture – Natural Fracture Interaction in Hydrostone Block Experiments, SPE 152618, the SPE Hydraulic Fracturing Technology Conference, The Woodlands, TX, USA, February 6-8.

38. Olson, J. E., and Wu, K., 2012, Sequential Versus Simultaneous Multi-Zone Fracturing in Horizontal Wells: Insights from a Non-Planar, Multi-Frac Numerical Model, SPE 152602, the SPE Hydraulic Fracturing Technology Conference, The Woodlands, TX, USA, February 6-8.

39. Perkins, T. K., and Kern, L. R., 1961, Widths of Hydraulic Fractures. J. Pet. Tech. 13:937–949.

40. Pollard, D. D., Segall, P., and Delaney, P. T., 1982, Formation and Interpretation of Dilatant Echelon Cracks, Geological Society of America Bulletin, December, Pages 1291-1303.

41. Renshaw, C. E., and Pollard, D. D., 1995, An Experimentally Verified Criterion for Propagation Across Unbounded Frictional Interfaces in Brittle, Linear Elastic Materials, Int. J. Roch Mech. Min. Sci. & Geomech. Abstr., Vol. 32, No. 3, Pages 237-249.

42. Shin, D. H., and Sharma, M. M., 2014, Factors Controlling the Simultaneous Propagation of Multiple Competing Fractures in a Horizontal Well, SPE 168599, the SPE Hydraulic Fracturing Technology Conference, The Woodlands, TX, USA, February 4-6.

43. Soliman, M. Y., East, L., and Adams, D., 2004, GeoMechanics Aspects of Multiple Fracturing of Horizontal and Vertical Wells, SPE 86992, the SPE International Thermal Operations and Heavy Oil Symposium and Western Regional Meeting, Bakersfield, CA, USA, March 16-18.

44. Taleghani, A. D., 2009, Analysis of Hydraulic Fracture Propagation in Fractured Reservoirs: An Improved Model for the Interaction Between Induced and Natural Fractures, PhD Dissertation at the University of Texas at Austin.

45. Taleghani, A. D., and Olson, J. E., 2013,How Natural Fractures Could Affect Hydraulic-Fracture Geometry, SPE 167608, SPE Journal, June 12.

46. Valko, P., and Economides, M. J., 1995, Hydraulic Fracture Mechanics, John Wiley & Sons Ltd, Page 19.

47. Veeken, C. A. M., Davies, D. R., and Walters, J. V., 1989, Limited Communication Between Hydraulic Fracture and (Deviated) Wellbore, SPE 18982, the SPE Joint Rocky Mountain Regional Low Permeability Reservoirs Symposium and Exhibition, Denver, CO, USA, March 6-8.

48. Wang, W., Olson, J. E., and Prodanović, M., 2013, Natural and Hydraulic Fracture Interaction Study Based on Semi-Circular Bending Experiments, SPE 168714, Unconventional Resources Technology Conference, Denver, CO, USA, August 12-14.

49. Warpinski N. R., and Teufel, L. W., 1987, Influence of Geologic Discontinuities on Hydraulic Fracture Propagation, SPE Journal of Petroleum Technology, February 1987, Pages 209-220.

50. Warpinski, N. R., and Teufel, L. W., 1991, In Situ Stress Measurements at Rainier Mesa, Nevada Test Site—Influence of Topography and Lithology on the Stress State in Tuff, Int. J. Rock Mech. Min. Sci. & Geomech. Abstr. Vol. 28, No. 2 3, Pages 143-161.

51. Weng, X., Kresse, O., Cohen, C., Wu, R., and Gu, H., 2011, Modeling of Hydraulic-Fracture-Network Propagation in Naturally Fractured Formation, SPE Production & Operations Journal, November 2011, Pages 368-380.

52. Wu, K., and Olson, J. E., 2014, Fully Coupled Fluid Flow and Mechanics Modeling of Multi-Fracture Propagation in Naturally Fractured Formations, The University of Texas at Austin.

53. Zoback, M. D., 2007, Reservoir Geomechanics, Cambridge University Press, Pages 8-9, 220.